Proceedings of the

U.S. - Japan Workshop on

Very High Temperature Structural Materials

December 9 - 11, 1998
Turtle Bay, Hawaii

REPORT DOCUMENTATION PAGE

AFRL-SR-BL-TR-99-

0166

1. AGENCY USE ONLY *(Leave blank)*	2. REPORT DATE	3. REPORT TYPE AND DATES COVERED
	Dec 1998	FINAL TECHNICAL REPORT 1 Dec 98 - 31 May 99

4. TITLE AND SUBTITLE
U.S. - JAPAN WORKSHOP ON VERY HIGH TEMPERATURE STRUCTURAL MATERIALS

5. FUNDING NUMBERS
F49620-99-1-0046

61102F
2306/AX

6. AUTHOR(S)
TRESA M. POLLOCK

7. PERFORMING ORGANIZATION NAME(S) AND ADDRESS(ES)
CARNEGIE-MELLON UNIVERSITY
DEPT OF MATERIALS SCIENCE AND ENGINEERING
PITTSBURGH PA 15213

8. PERFORMING ORGANIZATION REPORT NUMBER

9. SPONSORING/MONITORING AGENCY NAME(S) AND ADDRESS(ES)
AIR FORCE OFFICE OF SCIENTIFIC RESEARCH (AFOSR)
801 N. RANDOLPH STREET, ROOM 732
ARLINGTON, VA 22203-1977

10. SPONSORING/MONITORING AGENCY REPORT NUMBER

11. SUPPLEMENTARY NOTES

12a. DISTRIBUTION AVAILABILITY STATEMENT
APPROVED FOR PUBLIC RELEASE, DISTRIBUTION UNLIMITED

12b. DISTRIBUTION CODE

13. ABSTRACT *(Maximum 200 words)*

The U.S. - Japan Workshop on Very High Temperature Structural Materials (VHTSM) was held on December 9 - 11, 1998 at Turtle Bay, HI. The objective of this workshop was to exchange information on the current state of research, development and application of very high temperature structural intermetallics and refractory compounds. For the purposes of this meeting, "very high temperature" structural materials were defined as systems with the potential to operate at temperatures in excess of 1200oC. A second workshop objective was to identify key areas of common interest where collaborations could significantly advance the state of these materials. Finally, participate identified critical engineering challenges and scientific issues likely to limit the understanding development and implementation of this class of very high temperature materials into structural engineering systems. Contained in this volume are extended abstracts that cover the topics addressed by each speaker. Classes of materials discussed in the workshop included refractory metal silicides, Nb based compounds (including Laves phases) and higher temperature B2 and L12 aluminides. A number of speakers also addressed fundamental problems common to these systems, including prediction of crystal structures, modeling of physical properties and defect structures, solid solution strengthening, effects of microstructural scale and architecture on fatigue and fracture and potential limitations of toughening mechanisms under cyclic loading conditions. Much of the research aimed at this class of very high temperature structural materials, though detailed in individual investigations, could be characterized as exploratory compared to breadth of potential alloying opportunities.

14. SUBJECT TERMS	15. NUMBER OF PAGES
	144
	16. PRICE CODE

17. SECURITY CLASSIFICATION OF REPORT	18. SECURITY CLASSIFICATION OF THIS PAGE	19. SECURITY CLASSIFICATION OF ABSTRACT	20. LIMITATION OF ABSTRACT
UNCLASSIFIED	UNCLASSIFIED	UNCLASSIFIED	

U.S. - Japan Workshop on
Very High Temperature Structural Materials
December 9-11, 1998
Turtle Bay, Hawaii

Table of Contents

Preface

The U.S. - Japan Workshop on Very High Temperature Structural Materials (VHTSM) was held on December 9 - 11, 1998 at Turtle Bay, HI. The objective of this workshop was to exchange information on the current state of research, development and application of very high temperature structural intermetallics and refractory compounds. For the purposes of this meeting, "very high temperature" structural materials were defined as systems with the potential to operate at temperatures in excess of 1200°C. A second workshop objective was to identify key areas of common interest where collaborations could significantly advance the state of these materials. Finally, participants identified critical engineering challenges and scientific issues likely to limit the understanding, development and implementation of this class of very high temperature materials into structural engineering systems.

Contained in this volume are extended abstracts that cover the topics addressed by each speaker. Classes of materials discussed in the workshop included refractory metal silicides, Nb based compounds (including Laves phases) and higher temperature B2 and $L1_2$ aluminides. A number of speakers also addressed fundamental problems common to these systems, including prediction of crystal structures, modeling of physical properties and defect structures, solid solution strengthening, effects of microstructural scale and architecture on fatigue and fracture and potential limitations of toughening mechanisms under cyclic loading conditions. A substantial amount of time within the workshop was devoted to discussion, since there has been much recent progress in understanding these systems.

Much of the research aimed at this class of very high temperature structural materials, though detailed in individual investigations, could be characterized as exploratory compared to breadth of potential alloying opportunities. As candidate systems, the Mo-Si and Nb-Si systems received the most attention; several speakers addressed different compositional and microstructural variants of these systems. Issues of greatest concern included oxidation, coatings, phase equilibria, ductility, toughness, creep and cyclic properties. In addition to the refractory silicides, a number of single phase or multiphase Laves, B2 or $L1_2$ systems were also shown to exhibit some interesting properties, but remain in need of broader investigations of composition and mechanical / physical properties. The need for advancements in the area of processing of these high melting point compounds was highlighted a number of times during discussion sessions. Finally, there has been progress in the area of modeling of material properties; discussions indicated that further developments in this area could significantly aid the process of designing new alloys.

In summary, this workshop demonstrated that these very high temperature materials systems display some very promising properties needed for the ultimate goal of 1200°C applications. Challenges remain with regard to understanding fundamental aspects of phase equilibria, microstructure development, oxidation and mechanical and physical properties. The exchange of ideas and information at the workshop clarified some goals and strategies for future activities in these areas. Importantly, further collaborative efforts are needed to determine if a balanced set of properties within the individual systems can be achieved.

The organizers would like acknowledge the financial support of AFOSR and the efforts of Dr. Spencer Wu and Dr. Julian Tishkoff. Additionally, we are grateful to Renee Madden of DTI Associates for assistance with organizing the meeting and for outstanding on-site support.

Professor Masaharu Yamaguchi
Kyoto University
Kyoto, Japan

Professor Tresa Pollock
Carnegie Mellon University
Pittsburgh, PA USA

VHTSM Workshop Program

Alloy Design - Wed AM — Session Chair: Masaharu Yamaguchi

8:00 - 8:10
Opening Remarks
Tresa Pollock, Carnegie Mellon University

8:10 - 8:50
Dennis Dimiduk, Air Force Research Laboratory
High Temperature Structural Materials: The Competition, Challenges, and Development Necessities

8:50 - 9:30
John Petrovic, Los Alamos National Laboratory
Recent Developments in High Temperature Structural Silicides

9:30 - 10:10
Bernard Bewlay, General Electric Corporate Research and Development
Niobium Silicide-Based In-Situ Composites: Process-Structure-Property Relationships

10:10 - 10:30
Break

10:30 - 11:10
Masahiko Morinaga, Nagoya University
New Crystal Structure Maps for Transition Metal Silicides and Aluminides

11:10 - 11:50
Doug Berczik, Pratt and Whitney Aircraft
The Development of Mo-Si-B Alloys for Aerospace Applications

11:50 - 12:10
General Discussion

12:10 - 1:30
Lunch

Nb-Si Alloys - Wed PM — Session Chair: John Perepezko

1:30 - 2:10
P.R. Subramanian, Air Force Research Laboratory / Universal Energy Systems
Progress in the Development of High Temperature Refractory Metal-Based Intermetallic Systems

2:10 - 2:50
John J. Lewandowski, Case Western Reserve University
Fracture and Fatigue of Refractory Metal-Silicide Composites

2:50 - 3:10
Break

3:10- 3:50
Mel Jackson, General Electric Corporate Research and Development
Niobium Silicide-Based In-Situ Composites: Oxidation Behavior

3:50 - 4:30
Timothy Weihs, Johns Hopkins University
Metal/Silicide Microlaminates: Stress, Strength and Stability

4:30 - 5:15
General Discussion

$MoSi_2$ Alloys - Thurs AM — Session Chair: Dan Miracle

8:00 - 8:40
Toshio Maruyama, Tokyo Institute of Technology
High Temperature Oxidation of $Mo(Si,Al)_2$ and Low Temperature Synthesis of Related High Temperature Intermetallics by Solid/Liquid Reaction

8:40 - 9:20
Haruyuki Inui, Kyoto University
Effects of Alloying Elements on Plastic Deformation of Single Crystals of $MoSi_2$

9:20 - 10:00
Open Discussion Session

10:00 - 10:20
Break

10:20 - 11:00
Katsushi Tanaka, Kyoto University
Elastic Constants and Electron Distribution in Transition Metal DiSilicides

11:00 - 11:40
Kazuhiro Ito, Kyoto University
Experiments and Recent Computer Simulation Studies on the Deformation Behavior of $MoSi_2$ Single Crystals

11:40 - 12:00
General Discussion

Mo and Nb Based Alloys - Thurs PM — Session Chair: Shuji Hanada

---

7:00 - 7:40
John Perepezko, University of Wisconsin
Phase Stability and Microstructure Control in High Temperature Mo-Si-B Alloys

7:40 - 8:20
Joachiem Schneibel, Oak Ridge National Lab
Processing and Mechanical Properties of Ultra-High Temperature Mo-Si-B Intermetallics

8:20 - 8:40
Break

8:40 - 9:20
Yoshinao Mishima, Tokyo Institute of Technology
Alloy design of multi-phase alloys based on $MoSi_2$ in various Mo-Si-X ternary systems

9:20 - 10:00
Masaharu Yamaguchi, Kyoto University
Mechanical Properties of Spark Plasma Sintered Nb-Al-N and Nb-Si-B Compacts and Creep of [001] Oriented $MoSi_2$ Single Crystals

10:00 - 10:20
General Discussion

Nb-based Intermetallics and Composites - Friday AM — Session Chair: John Lewandowski

---

8:00 - 8:40
Shuji Hanada, Institute for Materials Research, Tohoku University
Synthesis and Mechanical Properties of Nb matrix In-situ Composites

8:40 - 9:20
Dan Thoma, Los Alamos National Laboratory
Alloy Design of Laves Phase Systems

9:20 - 10:00
Dave Davidson, Southwest Research Institute
Investigation of the fracture resistance defecit of Nb-Cr-Ti-Al alloys and in-situ composites at ambient temperature

10:00 - 10:20
Break

10:20 - 11:00
Kwai Chan, Southwest Research Institute
Effects of Alloying Addition on Fatigue and Fracture of Nb-based Alloys and In-situ Composites

11:00 - 12:00
General Discussion

12:00 - 1:30
Lunch

Other Intermetallics - Friday PM — Session Chair: Dennis Dimiduk

1:30 - 2:10
Hiroshi Harada, National Institute for Research in Metals
Design of Refractory Superalloys Based on Ir and Rh

2:10 - 2:50
Chris Woodward, Air Force Research Laboratory / Universal Energy Systems
Modeling Solid Solution Effects in High Temperature Structural Intermetallics

2:50 - 3:30
Tresa Pollock, Carnegie Mellon University
Plasticity of RuAl and Related B2 Aluminides

3:30 - 3:50
Break

3:50 - 4:30
Yasuharu Shirai, Osaka University
Constitutional and/or Thermal Vacancies in some B2 Intermetallic Compounds Studied by Positron Lifetime Spectrometry

4:30 - 5:10
Robert Ritchie, University of California, Berkeley
Development of Fatigue and Fracture Resistance in High Temperature Intermetallic Materials

5:10 - 5:30
General Discussion

7:30
Conference Banquet

HIGH TEMPERATURE STRUCTURAL MATERIALS: THE COMPETITION, PROGRESS, AND DEVELOPMENT CHALLENGES

D. M. DIMIDUK

Air Force Research Laboratory, Materials and Manufacturing Directorate, AFRL/MLLM, Bldg. 655, 2230 10th Street, Wright-Patterson AFB, OH 45433-7817, USA

Research Objectives and Approach

The history of the turbine engine is shows an evolution of progressively increasing core horsepower or thrust, together with increasing turbine inlet temperature. Throughout this history improvements have occurred by simultaneous improvements in the temperature capability of materials and cooling effectiveness of the mechanical design of turbine airfoils. However, recent increases in turbine inlet temperatures are obtained through only slight improvements in cooling effectiveness together with increases the total amount of cooling air used in the turbine, rather than through improvements in the operating temperature of the materials. Such a trend will lead to rapid stagnation of the performance growth in advanced propulsion. Thus, a primary objective is to continue to provide increases in the temperature capability of structural materials. The success of the modern turbine engine blade relies upon successes in three intimately coupled factors: advanced materials, improved manufacturing methods, and progressively improved engineering design. Only the combination of such factors, integrated in a systems approach led to successful advancement of turbine airfoil technology. This is a powerful message regarding advanced materials development—namely, alloys, processes, and design must work hand-in-hand to lead to successful new technologies.

Selected intermetallic alloys exhibit a combination of thermophysical properties, thermochemical properties, and some structural or mechanical properties which make them candidates for high-temperature structural applications. Success in developing an aerospace materials technology around the gamma titanium-aluminide alloys illustrates some of the potential for intermetallics in the structural materials area. Research illustrates that unique chemical bonding in intermetallics relative to common metals leads to a balance of properties which is quite different than for common structural alloys. Consequently, the development paths and windows of opportunity for using them must be selected carefully. The extended challenge for the high-temperature materials community is in using the extremely large group of compounds which have melting points in excess of 1400°C and, complex crystal structures such as the Laves, sigma and Nowotny phases found in so many of the refractory metal, aluminide, and silicide systems. For the advanced intermetallics the alloy development strategies were recently grouped into four broad approaches [1]:

I. Ductile Systems: Within this category AIM systems consist of the advanced refractory metal beta-phase compositions based on the Nb-Ti-Al system, and ductile-wire reinforced versions of these alloys. These systems offer a composition base from which a new class of refractory metal ordered alloys could offer near-term competition to high-temperature low-strength sheet superalloys.

II. Ductile-Brittle Systems: This group is represented by alloy development approaches wherein a ductile metallic matrix is reinforced with brittle particles or fibers. This includes dispersion hardened systems. The alloy class listed in *I* above is the only identified ductile alloy system having both sufficiently high oxidation resistance for service above 1000°C, and a melting point which significantly exceeds that of the Ni alloys (~1400°C).

III. Brittle-Ductile Systems: The alloy families falling within this category represent one of the potentially revolutionary classes of materials which are receiving evaluation for service at temperatures exceeding 1400°C. The prototypical material in this category is a ductile-phase toughened system based on an intermetallic and a refractory metal beta-phase (ordered or disordered) alloy. A number of potentially viable systems exist in this class. Examples of this approach are the high-temperature eutectic and peritectic systems existing between intermetallic phases and refractory metal solid solutions. The systems treated most extensively to date, and which are discussed further are alloys based on Nb-Ti-Si, and Nb-Cr, and Mo-Si-B.

Alternatively, synthetic or engineered composites are also being pursued. Typically these efforts build from a relatively oxidation-resistant base material with ductile phase additions for toughness improvements. An example of this is the effort underway for improving the mechanical behavior of $MoSi_2$ alloys containing ductile reinforcements of Nb, W, Mo, or Ta. Many of these are thermochemically unstable systems, which adds complexity in both processing and composition selection since kinetic barriers to the reactions occurring between the constituents are required.

IV. Brittle-Brittle Systems: A final category of intermetallic alloy development approaches is similar to the toughening approaches being developed for ceramic composites. $MoSi_2$ with ceramic particulate and/or fiber reinforcements of SiC, Al_2O_3 and ZrO_2 are the principal systems being explored in this class. Such systems are highly restricted in the balance of properties that have been attained. Without a doubt, the greatest understanding of the known and projected performance of such systems comes from the ceramic-composites community. However, unlike the ceramic-matrix systems, the intermetallic-matrix systems may offer higher thermal conductivity and simplified processing.

Progress and Highlights

A model system, chosen to represent the class of ductile-phase toughened alloys, is the Nb-Si binary (Nb)/Nb_5Si_3 in situ intermetallic composite system. Numerous other systems may be identified that parallel this systems. The Nb-Si phase diagram indicates the existence of a wide Nb_5Si_3+(Nb) two-phase field which is kinetically stable up to 1660°C. The melting points and densities of the terminal Nb_5Si_3 and (Nb) phases are 2484° and 2469°C and 7.09 and 8.57 gm/cm^3, respectively. The compound Nb_5Si_3 is essentially a line compound. The terminal (Nb) phase has a low Si solubility which varies slightly with temperature up to 1500°C. The two-phase Nb_5Si_3+(Nb) field has a composition range from ~0.6-37.5 at.% Si; this wide range permits high flexibility in obtaining (Nb)/Nb_5Si_3 composites with a wide range of volume fractions of the phases. Other potential inherently thermochemically stable brittle/ductile systems which are currently being explored are (Nb)/Cr_2Nb and (Nb)/$(Nb,Ti)_3Al$. These materials are being fabricated mainly by solidification processing, although research has just begun on other processes such as PVD to produce layered structures. In hypoeutectic compositions, large primary (Nb) dendrites solidify first during cooling of the melt. In certain thermomechanical conditions, it has been shown that these large primary (Nb) particles are responsible for providing a high degree of low temperature toughening. The eutectic/eutectoid microstructure consists of almost equal amounts of continuous (Nb) and Nb_5Si_3 phases.

The composite toughness exhibits a strong dependence on composition and thermomechanical treatment. In the cast and heat treated condition the Nb-10Si alloy exhibited a room-temperature toughness of ~9 MPa$\sqrt{m}$, and predominantly cleavage-like fracture of the primary-Nb phase. In the extruded condition, the same alloy, however,

showed a high toughness of ~21 MPa$\sqrt{m}$ with some interface debonding and extensive plastic stretching of the (Nb) phase before final rupture. This enhancement of fracture behavior was attributed to bridging of cracks by constrained ductile-phase particles.

Following the path of the model Nb-Si system, there are quaternary and higher- order composition systems which show good promise for building on the model system behavior while improving environmental resistance. The Nb-Ti-Al-Si system shown is one of those. Several types of microstructures are possible in the system, and we have been exploring these. More recently, an approach toward improving the oxidation resistance of Mo-based alloys has been reported by Berczik, et. al. Coincidentally, the approach can lead to similar microstructures as those found in the Nb-based ductile-phase toughened alloys. For this system, boron additions have a potent influence on the nature of oxide-scale formation. As one contemplates the vast alloy chemistry space that remains to be explored for the high-temperature intermetallic systems, the obvious question arises as to the role that theory may play in helping to isolate the appropriate chemistry regimes. While theory alone may be inadequate for developing materials, in the field of phase diagrams there is strong evidence to suggests that coupling computational methods to experiment may lead to fewer mistakes and a more insightful path toward understanding the phase equilibria and transformation paths for new alloy systems.

Reviewing properties, the modulus versus yield-strength properties of the intermetallics are unremarkable relative to steel, titanium, and nickel alloys. However, multiphase intermetallics such as the Nb/Nb-silicide alloys have an elastic modulus which varies widely with the volume fraction of phases present, just as for composite materials. Such a property may be useful in attempting to achieve a specific balance of properties.

From the perspective of strength properties, the intermetallics typically exhibit values which are less than or equal to those available in titanium and nickel alloys. Their strength properties only become interesting relative to other structural metals when the density of the material is important. The aluminides typically define a regime of yield strength-density which is less than that of nickel alloys, or in the case of gamma titanium aluminides, even less than titanium alloys. However, the Nb-silicide materials offer only a slight density benefit relative to their competition, the nickel-based superalloys.

Density-related properties are best compared by examining the density normalized properties of strength and Young's modulus, or specific strength and modulus, respectively. The specific-modulus and specific-strength variations with temperature illustrate the remarkable opportunities for structural design available through technology development based on the aluminides. Gamma titanium aluminides have a specific modulus which is 50 to 70 percent greater than that for titanium alloys and retain their stiffness to higher temperatures. The Nb-based intermetallics do no offer such a dramatic benefit as the gamma alloys, but still offer some advantage over the Ti- and Ni-alloy bases.

The specific strengths of gamma alloys exceed those of polycrystalline nickel alloys at all temperatures and even those for titanium alloys at temperatures greater than ~500 K. However, the upper use temperature of the gamma alloys also defines a barrier for all known structural materials at about 1200 K and above. This temperature sets a limit in oxidation performance, creep-strength performance, or durability performance for all materials. That is, in order to operate above this temperature, the requirements for one or more of these vital structural materials properties must be relaxed. The refractory metals perform well, provided coatings can be used or inert environments are controlled. Similarly, there are opportunities for ceramic materials above this temperature; however, for this entire class of materials the durability properties are greatly diminished and consequently manufacturing costs are typically prohibitively high even when structural

properties are achieved. Other metals which exhibit good oxidation resistance, such as the superalloys, simply run out of strength at high temperatures.

On the basis of specific modulus versus specific strength, the aluminides equal or exceed all structural alloys with the single exception of beryllium-based alloys. The entirely new regime of density-normalized properties for metallic alloys offered by the gamma titanium aluminides continues to be the driving force behind advanced development efforts for this system. While not quite to the performance level of the gamma alloys, the Nb-base intermetallics may offer a difficult to attain benefit by this measure.

Modern mechanical design demands control of fracture properties for structural materials used under both static and cyclic conditions. These properties directly set the limitations that can be considered in design with the material, even more so than the uniaxial yield strength. For intermetallics and other high-specific-strength materials the question of establishing lower limits for such properties continues to be a part of research and development. For example, most engineering ceramic systems exhibit fracture-toughness values in the range of 3-7 MPa$\sqrt{m}$. Mechanical design experience has shown that such low values set severe limitations on engineering use. Low toughness values, together with virtually no ability to diminish local stress concentrations through plastic flow, continue to pace the evolution of ceramic materials in engineering systems. Additionally by way of examples, for NiAl alloys and for TiAl alloys, fracture toughness typically ranges from 5-25 MPa$\sqrt{m}$—only slightly beyond those of ceramics and well below those of titanium alloys. More importantly however, both of the aluminide-alloy classes exhibit the ability to deform plastically at room temperature (between 1 and 4% ductility) unlike ceramic materials, thus enabling the possibility for reducing local stress concentrations. Even such modest ductility levels are shown to be quite important in structural design.

Considering ductility and toughness properties even further, the two aluminide classes perform slightly differently under mixed mode loading and with variations in strain rate; that is, their responses to impact loading are rather different, though not completely understood and quantified. Both toughness and impact properties will limit their implementation. The 'accumulated learning' from using structural alloys suggests that a fracture toughness of about 20 MPa$\sqrt{m}$ is near a lower limit for broad engineering implementation of a structural material. The limits for impact resistance are far more application specific and still evolving in the design experience base. As engineering experience progresses with gamma alloys, there is a strong likelihood that the lower limits of fracture-toughness and ductility combinations will be more clearly established, thereby expanding opportunities for implementing other brittle materials.

As revealed by the room-temperature-toughness versus modulus relationships, both NiAl alloys and gamma alloys exhibit properties somewhat similar to cast irons, while the iron aluminides are both stiffer and tougher, approaching the properties of some steels. The Nb-silicides appear to offer toughness levels which exceed even that of the gamma alloys and which are known to be relatively strain-rate insensitive. Additional comparison to Ti and Ni-based alloys, which are the most important competitors to intermetallics, shows that none of the intermetallics will exhibit toughness levels close to those of titanium alloys, and only approach the lower range of nickel alloys. This situation changes more favorably toward the intermetallics as temperatures increase.

When toughness and density are compared, gamma alloys, NiAl and FeAl offer distinct advantages over cast iron, steels and nickel alloys. Once again this illustrates the distinct advantage offered by selected aluminides when minimum-weight structures are desired. The Nb-silicides have toughness which exceed that of cast iron and overlap with some steels, at about the same density.

With a toughness and strength comparison, a further distinction can be made amongst the intermetallics. Alloys of NiAl are no better than cast irons, while the iron aluminides have low-temperature properties which are intermediate between aluminum alloys on the low end and steel alloys on the upper end. However, the gamma alloys offer a new regime of properties with strengths equal to or greater than many aluminum, and nickel alloys and fracture-toughness values which are competitive at the low end of the range. The Nb-silicides are quite competitive to nickel-based alloys.

Recent research on aluminide systems recognizes the low but significant toughness levels for the aluminides relative to ceramic systems, and has investigated the role of toughness on ductility. These investigations now show that the dominant intrinsic factor controlling ductility is post-yield cleavage crack nucleation, and a small but finite crack propagation strain which scales with the fracture toughness of the material. The crack nucleation strain scales with grain size, and is relatively unaffected by alloy chemistry. For gamma alloys toughening involves two distinct aspects. Crack bridging mechanisms and tortuousity are clearly associated with long crack propagation, while dislocation mechanisms and plastic flow are associated with crack-initiation. These findings illustrate another important factor in the development of other intermetallics. Ductility must be understood mechanistically. Once the mechanisms of ductility were established for gamma alloys, the development path changed. The prospects for improving ductility through chemistry selection were diminished, while those for improvements through microstructural control were enhanced. Immediately the development paths were altered and more successful. Similar levels of understanding are only just emerging for other intermetallic systems.

For intermetallic alloys, especially gamma alloys, current research seeks to build the knowledge of durability and life-limiting behavior under fatigue conditions, and to establish design approaches based on such knowledge. The intrinsic fatigue resistance of gamma alloys exceeds that of nickel and titanium alloys when viewed as normalized by the ultimate strength of the material. This finding suggests that the intrinsic fatigue capability or resistance to crack initiation via intrinsic processes of the material is quite high. However, for some structural designs the magnitude of tolerable cyclic-stress levels may be greater for other alloys because their failure strengths are greater. This property had a strong influence on the design approaches used for implementing gamma alloys. However, similar properties are essentially unmeasured for other intermetallics. The community must discontinue the common view that fatigue is a "second tier" property. In modern structural design, fatigue life is often among the primary design constraints.

For materials such as the aluminides which exhibit steep crack-growth curves as a function of cyclic stress-intensity range, studies must focus on understanding the microstructural and metallurgical aspects of long-crack growth thresholds. Further, provided that cyclic-stress amplitudes are low enough, and material quality is high enough to avoid early crack growth, then the behavior of short-cracks having lengths below or comparable to the grain size under high-cycle fatigue environments becomes important. Crack-growth thresholds, as measured from long-crack arrest methods, are also good for the aluminides in general, ranging from 10-20 $MPa\sqrt{m}$ for iron aluminides down to 6-10 $MPa\sqrt{m}$ for gamma alloys. These are within or better than the behavior of aerospace titanium and nickel alloys. Knowing these, however, is not enough. The measured performance of the materials must be brought together in a suitable mechanical design and life-management system which permits the designer to have full confidence in introducing a new material. This is one of the limiting factors to the introduction of gamma alloys, and will be no less of a factor for any other intermetallic. Fortunately, the gamma alloys should set new views and methods in place which could facilitate introduction of other limited-ductility materials.

Some early data on fatigue-crack-growth rates in the Nb-Si based alloys have been obtained at Case Western Reserve University. Fortunately, these data indicate that ductile-phase toughening can contribute to damage tolerance, even under cyclic conditions, provided that suitable reinforcement phases are present. Significant further study is required to fully explore the suitability of such an approach to damage tolerance.

A comparison is made for stress-to-rupture properties between a wide set of structural materials. Clearly, the Nb-silicide system opens a materials behavior regime which has never been available before. The potential exists for refractory intermetallics to significantly advance the barriers to high-temperature materials use. However, the focus of development must remain on achieving balanced properties with specific designs in view. Secondary-creep rates, for selected Nb-based materials, at 1200°C have also been examined. Data for monolithic Nb_5Si_3 and pure Nb define limits for the alloy class. The Nb-based alloys have been tested in an inert environment. Monolithic Nb_5Si_3 is seen to be highly creep resistant. The simple (Nb)/Nb_5Si_3 in situ composite system has desirably low creep rates, even though there has been no effort to specifically develop or improve the creep performance of the system.

Recession-rate data for selected high-temperature alloy systems were compared. In high-pressure turbine engines, a service temperature is typically kept below the temperature for which the alloy system in question undergoes less than 250μm of recession after exposure to an oxidizing atmosphere for 100 h. While still insufficient for structural applications, the oxidation response of some of the beta + silicide systems show a substantial improvement over the base Nb-Si binary system and Nb alloys. Early data indicates that the Mo-Si-B system may achieve design goals at quite high temperatures. Closer inspection of the Mo-Si-B system indicates that deficiencies in environmental resistance may exist at low temperatures, even though the material performs well at high temperatures. Weight-change data at 800°C indicate that the rate of metals loss is much greater for a Mo-11Si-11B alloy than it is at even 1300°C. Such date serves to illustrate the demand for mechanistic understanding of environmental degradation, and the need to incorporate such knowledge into the development approach. For eventual application in oxidizing environments, oxidation-protective coatings will have to be employed. However, in the event of a coating failure, the improved alloys are predicted to have adequate environmental tolerance to prevent catastrophic failure.

Critical Engineering Issues in the Evolution of Structural Materials Technologies

Once the capability offered by a material is considered, a large number of issues pertaining to cost, reliability, and availability of the technology enter into the materials selection and technology maturation. Within these factors, existing materials having a historical knowledge and production base behind them will always win in competition over a new materials technology. Likewise, provided that an enabling capability does exist with a new material system, development times should be reduced by early attention being given to issues associated with cost, production base and reliability of the technology.

Typically an 'S-curve' of materials readiness indicators plotted against time generically tracks the stages of technology maturity. An historical problem in the materials development community is that a huge, open ended gap exists between the traditional regime of academic research on the far left of such a curve, and the domain called 'proof of feasibility' which is the typical start of corporate investments in the modern era. The gap is spanned by the search and discovery of inventions which could lead to an improved technology. Too often academic research does not seek out all of the necessary inventions required for a new material to be successful. There are several examples of this within the intermetallics field. The historical lack of integrating or coupling design and materials

engineering in a systems approach too often results in lost focus in materials/system development efforts, expanding them in time.

The earliest stages of alloy development seek three principle requirements: identifying a "windows of opportunity" or specific components which could benefit from new alloy technology, defining suitable alloy compositions, and gaining control of a synthesis or process route for them. These three requirements form a general basis for alloy development strategies, although more detailed aspects may be defined. For example, early in the our intermetallics development effort, we observed that one can engineer flaw tolerance or toughness into ceramic materials without ever achieving crystal plasticity or ductility. This suggested that, even if the causes for brittleness can not be overcome through process or composition control, composite engineering concepts can be employed to achieve damage tolerance. This key idea was a basis for the chosen alloy development strategy for Nb-Si alloys, and formed the focus for composition selection and processing investigations. Other strategies may be required for other design needs; however, keeping sight of the design goals, processing and manufacturing constraints, and alloy development strategies can facilitate more rapid progress toward them.

In order for a technology to achieve demonstration status and production readiness, numerous engineering technologies must be established. Alloys do not in themselves compete or exhibit readiness; rather, a materials technology for a given product exhibits readiness and competes against other materials and design solutions for a similar end product capability. Thus, for engineering technologies to mature, the alloy composition, general process method, and desired part geometry must be identified as inputs.

Synthesis and processing development seeks to define composition specifications and methods for producing shapes with controlled microstructures. Composition specification has been difficult for gamma alloys since compound chemical reference standards do not exist. For high-temperature structural alloys, compositions are still not known of fixed, even as classes.

Structure-properties research has spurred the improvements in gamma alloy technology over the last ten years. Such research is being applied to the technologies of fabrication, joining and repair, surface treatments and properties, environmental protection technologies, machining and finishing technologies, and in providing a statistically relevant data base for selected alloys. Such topics fall outside the mainstream of structure-properties research but are essential. These topics are not yet opened for most other potential high-temperature materials.

Finally, design methods must continue to evolve. For this, the relationships between laboratory 'test coupon' behavior and component performance require mapping into a design-analysis system. Gamma alloys are likely to require a departure from some of the design allowables used with other structural materials, simply because the balance of properties is so different. Research into design and life-prediction methods continues pace full exploitation of advanced intermetallics.

Summary

Marked progress in demonstrating a potentially useful balance of properties in some intermetallics has been achieved during the last few years. The future of these alloys as viable engineering materials largely depends on how rapidly and cost effectively the total technology of composition-process-structure-properties can be developed. The fundamental understanding of gamma alloys has progressed dramatically over the last decade, and together with this the engineering technologies matured sufficiently to make

gamma alloys viable competitors as structural materials. This material sets a new benchmark for using limited ductility materials—other intermetallics must build from this. Further, some aspects of maturing alloy technologies were highlighted, illustrating the difficult path for introducing new alloy systems in the business world. Extensive additional research efforts on alloy modification, developing innovative thermal and thermomechanical treatments to control microstructures, and precise understanding of microstructure-property relationships will be pivotal in advancing these alloys into service in the near term. A systems engineering approach, which simultaneously develops the mechanical design, alloy composition, and manufacturing processes is likely to be far more successful than isolated academic investigation.

References

1. "Advanced Intermetallic Alloys—Beyond Gamma Titanium Aluminides," P.R. Subramanian, M.G. Mendiratta, D.M. Dimiduk, and M.A. Stucke, *Mat. Sci. & Engr. A*, A239-240 (1997) pp. 1-13.

2. "The Development of Nb-Based Advanced Intermetallic Alloys for Structural Applications," P.R. Subramanian, M.G. Mendiratta, and D.M. Dimiduk, *JOM*, 48 (1996) pp. 33-38.

3. "Exploration of Nb-Based Advanced Intermetallic Materials," (Invited Paper) D.M. Dimiduk, P.R. Subramanian, and M.G. Mendiratta, *Acta Metall. Sinica (English Edition)*, 8 (4-6), (1995) pp. 519-30.

4. "Compressive Creep Behavior of Nb_5Si_3," P.R. Subramanian, T.A. Parthasarathy, M.G. Mendiratta, and D.M. Dimiduk, *Scripta Mettal.*, 32 (1995) pp. 1227-32.

5. "Unconstrained and Constrained Tensile Flow and Fracture Behavior of an Nb-1.24 at. pct. Si Alloy," M.G. Mendiratta, R. Goetz, D.M. Dimiduk, and J.J. Lewandowski, *Met. Trans. A*, 26A (1994) pp. 1767-76.

6. "Microstructures and Mechanical Behavior of Nb-Ti Base Beta + Silicide Alloys," P.R. Subramanian, M.G. Mendiratta, and D.M. Dimiduk, in *High-Temperature Silicides and Refractory Alloys*, eds., C.L. Briant, J.J. Petrovic, B.P. Bewlay, A.K. Vasudevan, and H.A. Lipsitt, MRS, Pittsburgh, PA, 322 (1994) pp. 491-502.

7. "Development Approaches for Advanced Intermetallic Materials - Historical Perspective and Selected Successes," D.M. Dimiduk, M.G. Mendiratta, and P.R. Subramanian, in *Strucutral Intermetallics*, R. Darolia, J.J. Lewandowski, C.T. Liu, P.L. Martin, D.B. Miracle, and M.V. Nathal, eds., TMS, Warrendale, PA (1993) pp. 619-30.

8. "Ductile Phase Toughening of Nb / Nb Silicide In Situ Composites," M. Mendiratta, J.J. Lewandowski and D.M. Dimiduk, *Metall. Trans. A*, 22A (1991) pp. 1573-83.

9. "Strength and Ductile-Phase Toughening in the Two-Phase Nb/Nb_5Si_3 Alloys," M. Mendiratta, J.J. Lewandowski and D.M. Dimiduk, *Metall. Trans. A*, 22A (1991) pp. 1573-83.

Recent Developments in High Temperature Structural Silicides

John J. Petrovic
Materials Science and Technology Division
Los Alamos National Laboratory
Los Alamos, New Mexico 87545

Extended Abstract:

The intent of the presentation was to highlight important recent developments in high temperature structural silicides. Most of the material was drawn from the Proceedings of the Engineering Foundation High Temperature Structural Silicides Conference, which was held 25-29 May 1998 in Hyannis, Massachusetts. These Proceedings will shortly be published (March 1999) in Reference 1. The interested reader should refer to Reference 1 for more detailed information and individual references on topical areas.

The presentation was directed at the following topical areas: 1) $MoSi_2$ single crystals, modeling, and alloying; 2) Mo-Si-B and other silicides; 3) $MoSi_2$ diffusion and creep; 4) $MoSi_2$-based composites; 5) Silicide applications. These areas are summarized briefly below.

$MoSi_2$ single crystals, modeling and alloying:

$MoSi_2$ single crystals exhibit macroscopic compressive deformation in some orientations at temperatures as low as –100 °C. Experimental observations suggest that alloying to alter dislocation slip behavior may improve the low temperature ductility of $MoSi_2$. Theoretical alloying studies have suggested that Mg, V, Nb, Tc, and Al may enhance the low temperature ductility of $MoSi_2$, while Ge, P, and Re are not expected to. Experimental observations indicate that Al alloying influences low temperature plastic deformation in $MoSi_2$, while Re alloying does not, in agreement with the theoretical predictions. Atomistic potentials for the Mo-Si system have recently been developed, which may lead to improved understanding of dislocation core effects.

Mo-Si-B and other silicides:

Boron additions significantly improve the oxidation resistance of Mo_5Si_3, through borosilicate glass formation. Oxidation-resistant Mo-Si-B alloys are under development. These materials are multi-phase in makeup. Carbon, boron, and oxygen additions significantly improve the oxidation resistance of Ti_5Si_3.

$MoSi_2$ diffusion and creep:

Diffusion studies suggest a small range of stoichiometry in $MoSi_2$. The creep rate of polycrystalline $MoSi_2$ is highly grain size dependent in both the newtonian ($n = 1$) and power-law ($n = 4$) creep ranges, and strain history-dependent grain size effects on power-law creep have also been observed.

$MoSi_2$-based composites:

Si_3N_4 composite reinforcement additions to the $MoSi_2$ matrix completely eliminate the $MoSi_2$ 500 °C oxidation pest behavior. $MoSi_2$ matrix-Si_3N_4 reinforced composites with room temperature fracture toughness values as high as 15 MPa $m^{1/2}$ have been developed. Si_3N_4 matrix-$MoSi_2$ reinforced composites have significantly improved fracture toughness while retaining creep resistance, and can be electro-discharge machined.

Silicide applications:

The corrosion of $MoSi_2$ materials above and in molten glass is similar to the ceramic refractory material AZCS, which is currently widely used in the glass industry. $MoSi_2$ has the following advantages over AZCS: It is electrically conductive, mechanically stronger, and does not contain chromium. Maximum glass corrosion rates of $MoSi_2$ occur at the glass-air interface.

$MoSi_2$-Si_3N_4 composites may have significant potential for wear-related applications, particularly at elevated temperatures. A $MoSi_2$-Si_3N_4 diesel engine glow plug has been developed which has a long lifetime and faster engine starting.

Hybrid composites of $MoSi_2$-Si_3N_4 and SiC continuous fibers have been developed with high fracture toughness and impact resistance, for potential aircraft engine applications as blade outer air seals.

Reference:

1. Materials Science and Engineering A, A261, 1-308 (1999).

Creep Mechanisms in High-Temperature In-Situ Composites

B.P. Bewlay[1], M.R. Jackson[1], J.A. Sutliff[1], C.L. Briant[2],
[1]GE Corporate Research and Development,
Schenectady, NY 12301, USA.
[2]Division of Engineering, Brown University,
Providence, RI 02912, USA.

1.0. Objectives and Approach

The objective of the present research is to investigate high-temperature creep and low-temperature toughening mechanisms in directionally solidified in-situ composites with melting temperatures above 1700°C. The composites under investigation consist of Nb-based silicides, such as Nb_3Si and Nb_5Si_3, that are toughened by a Nb-based solid solution [1-5]. The approach for investigation of creep mechanisms is separated into two stages : first compression creep tests are performed, and second, in those composites that show promising properties, tensile creep tests are performed.

2.0. Research Progress and Highlights

In the present section recent results of studies of fracture toughness, creep, and phase stability will be described.

2.1 Fracture Toughness Measurements

Effect of Hf:Ti Ratio on Fracture Toughness

Room temperature fracture toughness measurements are shown in Table 1 below for Hf compositions of 7.5-12.5 and Ti compositions of 21-33% (all compositions are given in atom percent throughout the present report).

Table 1 : Fracture toughness of Nb-16Si composites modified with Hf and Ti.

Composition	Fracture Toughness (MPa$\sqrt{m}$)
Nb-7.5Hf-21Ti-16Si	12.2
Nb-10Hf-21Ti-16Si	11.9
Nb-12.5Hf-21Ti-16Si	12.1
Nb-21Ti-16Si	11.6
Nb-7.5Hf-33Ti-16Si	12.6
Nb-10Hf-33Ti-16Si	13.3
Nb-12.5Hf-33Ti-16Si	14.0
Nb-33Ti-16Si	11.1

Room temperature fracture toughness was relatively insensitive to Hf: Ti composition ratios in the range 0.2-0.6. However, Ti additions appear to have a stronger effect on

toughness than Hf additions. The room temperature fracture toughness of composites with 33Ti were generally higher than those at 21Ti.

Fracture Toughness in Complex Alloy Composites

Table 2 shows a range of alloys derived from the base MASC composition [1, 2] (last row of the table below).

Table 2 : Fracture toughness of Nb-16Si composites modified with Hf, Ti, Cr and Al.

Composition	**Fracture Toughness** ($MPa\sqrt{m}$)
Nb-20Ti-8Hf-2Al-2Cr-16Si	21.0
Nb-30Ti-8Hf-2Al-2Cr-16Si	19.3
Nb-24.6Ti-11Hf-2Al-2Cr-16Si	21.8
Nb-23.6Ti-14Hf-2Al-2Cr-16Si	18.2
Nb- 25Ti-8Hf-2Al-2Cr-18Si	20.0
Nb-26.5Ti-8Hf-2Al-10Cr-16Si	18.7
Nb-24.7Ti-8.2Hf-2.0Cr-1.9Al-16.0Si	23.3

These data indicate that for Ti concentrations in the range 20-30%, there is little effect on toughness. The above data also indicate that the Si concentration of the MASC can be increased to 18% without compromising composite toughness. It can also be seen that increasing Hf from 8 to 14%, or increasing the Cr concentration up to 10% leads to a reduction in toughness. Higher Cr levels are important for oxidation resistance.

2.2 Creep Mechanisms

The effects of Ti, Hf and Mo additions on the secondary creep rate have been studied and the findings will be described in the following section.

Nb-Ti-Hf-Si In-Situ Composites

Creep tests were performed for a series of quaternary Nb-Hf-Ti-Si alloys at a temperature of 1200°C and at stress levels in the range 140-280 MPa. These data are shown in Table 3 and Figure 1. Data for the Nb-7.5Hf-16Si ternary alloy are also included. Hf concentrations in the range 7.5-12.5 and Ti concentrations in the range 21-33 were examined, providing Ti:Hf ratios in the range 1.7 to 4.4.

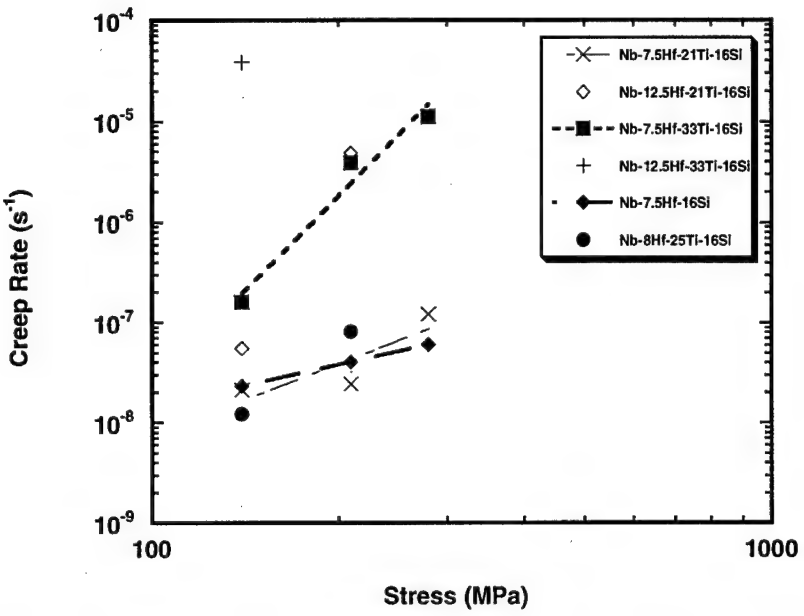

Figure 1 Secondary creep rates at 1200°C for a range of quaternary Nb-Hf-Ti-Si alloys.

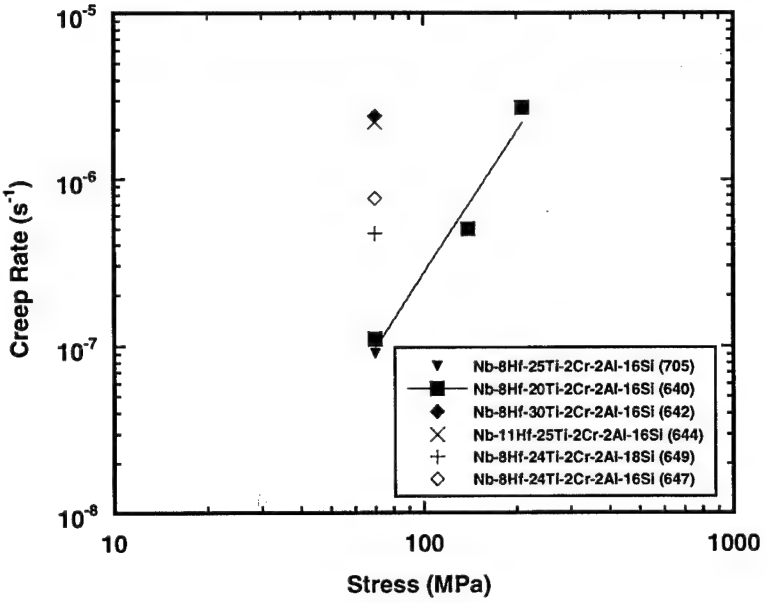

Figure 2 Secondary creep rates at 1200°C for a range of Nb-Hf-Ti-Si-Cr-Al alloys.

Table 3 : Secondary creep rates at 1200°C for a range of Nb-Hf-Ti-Si alloys.

Composition	**Constituent Phases**	**140 MPa Creep Rate (s^{-1})**	**210 MPa Creep Rate (s^{-1})**	**280 MPa Creep Rate (s^{-1})**
Nb-7.5Hf-16Si	(Nb), Nb_3Si	$2.3x10^{-8}$	$4.0x10^{-8}$	$4.8x10^{-8}$
Nb-7.5Hf-21Ti-16Si	(Nb), Nb_3Si	$2.1x10^{-8}$	$3.2x10^{-8}$	$1.2x10^{-7}$
Nb-7.5Hf-33Ti-16Si	(Nb), Nb_3Si, $(Ti,Hf)_5Si_3$	$1.6x10^{-7}$	$3.9x10^{-6}$	$1.1x10^{-5}$
Nb-12.5Hf-21Ti-16Si	(Nb), Nb_3Si, $(Ti,Hf)_5Si_3$	$5.5x10^{-8}$	$4.8x10^{-6}$	Failed
Nb-12.5Hf-33Ti-16Si	(Nb), Nb_3Si, $(Ti,Hf)_5Si_3$	$3.8x10^{-5}$	Failed	--
Nb-16Si	(Nb), Nb_3Si	$1.5x10^{-8}$	$4.9x10^{-8}$	--

The creep data indicate that the Nb-7.5Hf-16Si and the Nb-16Si composites possessed the lowest creep rates, and that at any selected stress level and Hf concentration the creep rate increased with increasing Ti concentration. Thus, Ti and Hf additions can have a significant effect on the creep performance. For example, at 7.5Hf increasing the Ti concentration from 21 to 33% increased the creep rate from $2.1x10^{-8}s^{-1}$ to $1.6x10^{-7}s^{-1}$ at 140MPa. At stress levels of 210MPa and below there is little difference between the secondary creep rates of the Nb-16Si, the Nb-7.5Hf-16Si and the Nb-7.5Hf-21Ti-16Si compositions. At higher stress levels the Ti additions have a detrimental effect on creep performance. Similarly, at Hf concentrations of 12.5 and stress levels of 140MPa, increasing the Ti concentration from 21 to 33% increases the creep rate from $5.5x10^{-8}s^{-1}$ to $3.8x10^{-5}s^{-1}$. At higher stress levels the effect of increasing the Ti concentration led to premature failure.

At any selected stress level, increasing the Hf concentration leads to an increase in the creep rate. For example, at a stress level of 140 MPa and Ti concentration of 21%, increasing the Hf concentration from 7.5 to 12.5% increases the creep rate from $2.1x10^{-8}s^{-1}$ to $5.5x10^{-8}s^{-1}$, but there is a strong stress sensitivity of this effect, so that at 210MPa the creep rates are $3.2x10^{-8}s^{-1}$ and $4.8x10^{-6}s^{-1}$, i.e. Hf concentrations higher than 7.5% provide a strong sensitivity of the secondary creep rate to stress.

These creep data suggest that the Ti:Hf ratio should be maintained at a level less than 3 and the Ti concentration should be kept below 21%. The mechanisms that lead to increased creep rates at higher Ti, higher Hf, or higher (Hf+Ti) concentrations are still under investigation. One of the effects that is significant is that at high (Ti+Hf) concentrations the hP16 Ti_5Si_3 type silicide is stabilized in preference to the tI32 Nb_5Si_3 type or tP32 Nb_3Si type silicides [6, 7]. Thus the creep performance is modified by changes in the constituent phases rather than the intrinsic performance of the silicide [6] or the (Nb). It appears that the $(Ti,Hf)_5Si_3$ is highly detrimental to creep performance. For example, at 280MPa failure of the composites was observed to occur by shear band formation in the large-scale $(Ti,Hf)_5Si_3$ dendrites. There is a suggestion that this behavior is controlled by the crystal structure and texture of the the hP16 relative to the loading axis because the melting temperature of Hf_5Si_3 is close to that of Nb_5Si_3 [7, 8].

Six Element Alloy Composites

Secondary creep rates are shown at 1200 °C and stress levels in the range 70-280 MPa in Figure 2 for a range of composites derived from Nb-Hf-Ti-Cr-Al-Si alloys. Some important trends can be seen in these data. First, the creep rate increased with increasing Ti concentration from 20 to 30%. This may have been due in part to the larger volume fraction of Hf_5Si_3 type phase in the composite, as well as the lower melting temperature of the metallic phase.

The creep data also indicate that increasing the Si concentration from 16% to 18% (substituting Si for Nb) led to a slight reduction on creep rate at 1200 °C and 70MPa from $7.6x10^{-7}s^{-1}$ to $4.7x10^{-7}s^{-1}$. Lastly, substituting Hf for Nb appears to have a detrimental effect on the secondary creep rate; increasing the Hf concentration from 8 to 11% led to a change in the creep rate from $7.6x10^{-7}s^{-1}$ to $2.2x10^{-6}s^{-1}$ at 70MPa and 1200 °C. This was probably due to the reduction in the volume fraction of Nb_5Si_3 type and the increased volume fraction of Hf_5Si_3 type silicides. These observations regarding the effects of Ti and Hf in these complex alloy composites are all consistent with those that were reported for the quaternary Nb-Hf-Ti-Si alloys.

2.3 Phase Stability Investigations

Several investigations of phase stability have been performed, including determination of solid-state phase equilibria in Nb-Ti-Si alloys, definition of silicide stability in the binary Hf-Si system, and definition of the Nb-Hf-Si liquidus surface [1, 5, 7].

Nb-Hf-Si Ternary Phase Stability

Hf is an important alloying addition to niobium silicide in-situ composites because it improves oxidation resistance and strength. Figure 3 is the Nb-Hf-Si liquidus projection.

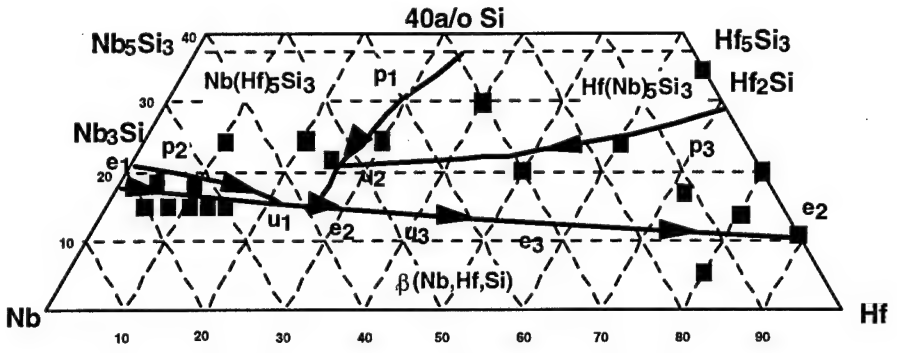

Figure 3 Diagram showing the projection of the Nb-Hf-Si liquidus surface, including the peritectic ridges, p_1, p_2, p_3, the eutectic valleys, e_1, e_2, e_3, and the invariant reactions, U_1, U_2, U_3. The compositions investigated are also shown.

At the metal-rich end of the Nb-Hf-Si ternary phase diagram there is a eutectic trough between the two binary eutectics [8]. However, because of the different binary eutectic reactions there is a change in the nature of the liquidus surface, with decreasing Nb and increasing Hf concentration. The resulting transition reactions are shown below:

U_1 $\quad L + Nb(Hf)_5Si_3 \rightarrow Nb(Hf)_3Si + \beta(Nb,Hf,Si)$

U_2 $\quad L + Hf(Nb)_5Si_3 \rightarrow Nb(Hf)_5Si_3 + Hf(Nb)_2Si$

U_3 $\quad L + Nb(Hf)_5Si_3 \rightarrow \beta(Nb,Hf,Si) + Hf(Nb)_2Si$

The first of these transition reactions occurs at a composition of Nb-21Hf-16Si, and at a temperature between ~1850°C. The second of these transition reactions occurs at a composition of Nb-27Hf-22Si, and a temperature of ~2040°C. The third transition reaction occurs at a composition of Nb-26Hf-14Si, and a temperature of ~1840°C. This work has been prepared for publication in Zeitschrift für Metallkunde. Several examples of the compositions examined are shown below.

The typical microstructure of the DS Nb-15Hf-16Si is shown in Figure 4. There is a small volume fraction of primary β(Nb,Hf,Si) dendrites, which are the dark grey phase in the BSE micrograph, together with an interdendritic $Nb(Hf)_3Si$-β(Nb,Hf,Si) cellular eutectic. The Nb-15Hf-16Si also contained a small volume fraction of intercellular eutectic of $Nb(Hf)_5Si_3$ and β(Nb,Hf,Si), which suggests that the liquid composition passed through the invariant reaction U_1.

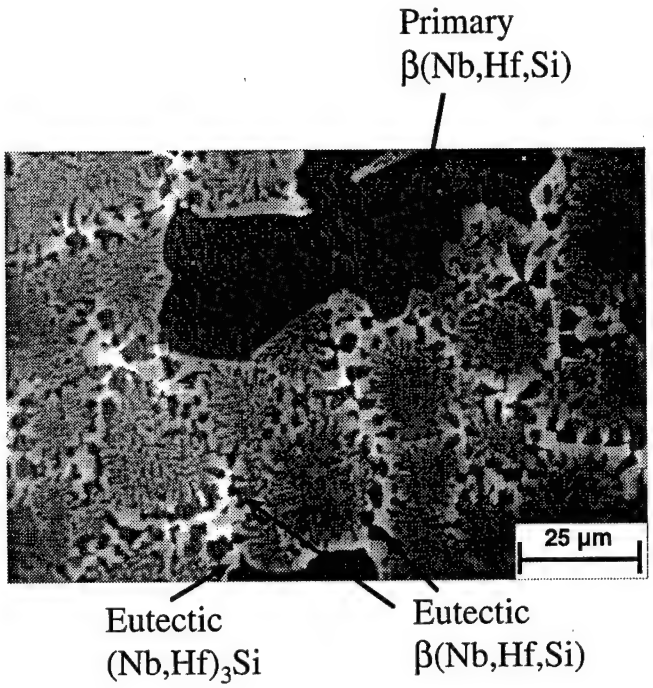

Figure 4 Typical microstructure of the transverse section of DS Nb-15Hf-16Si.

The microstructure of the transverse section of the DS Nb-10Hf-25Si alloy is shown in Figure 5. The large black phase is $Nb(Hf)_5Si_3$, and it is surrounded by dark grey peritectic $Nb(Hf)_3Si$. This composition has experienced the peritectic reaction, L + $Nb(Hf)_5Si_3$ --> $Nb(Hf)_3Si$. Hf partitioning between the $Nb(Hf)_3Si$ and β(Nb,Hf,Si) was such that there was little contrast between these two phases.

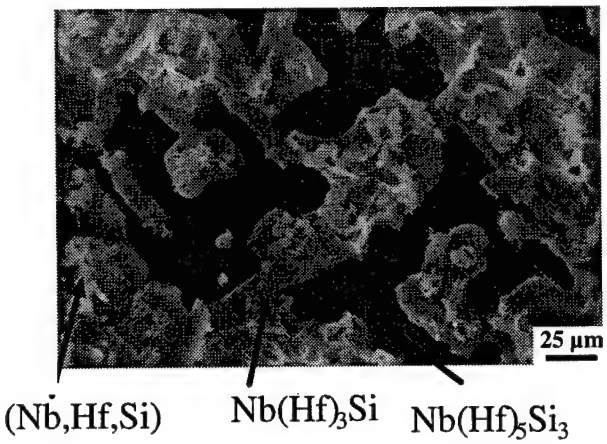

Figure 5 Typical microstructure of the transverse section of DS Nb-10Hf-25Si.

3.0 Summary

The addition of Ti, Hf and Mo have significant effects on composite room temperature fracture toughness and secondary creep rates. The threshold Hf, Ti and Mo concentrations above which the creep performance degenerates beyond that of the Nb-16Si composite have been defined, together with the appropriate stress levels for possible component operations. For example, the creep data indicate that the creep performance of the Nb-8Hf-25Ti-16Si is compatible with the creep goals at temperatures up to 1200 °C. Above these Ti and Hf compositions the creep rates are not acceptable. In addition, the initial Nb, Hf, Ti, Mo and Si composition ranges within which the room temperature fracture toughness can be maintained above 20 MPa$\sqrt{m}$ have been identified.

4.0 Acknowledgments

The authors would like to thank D.J. Dalpe for the directional solidification, and C. Bull for assistance with creep testing. This research was sponsored by AFOSR under contract #F49620-96-C-0022 with Major C.H. Ward and Dr. S. Wu as Program Managers.

5.0 References

[1] B.P. Bewlay, M.R. Jackson, W.J. Reeder, and H.A. Lipsitt, MRS Proceedings on High Temperature Ordered Intermetallic Alloys VI, 1994, Vol. 364, pp. 943-948.

[2] B.P. Bewlay, M.R. Jackson and H.A. Lipsitt, *Metall. and Mater. Trans.*, 1996, Vol 279, pp. 3801-3808.

[3] M.G. Mendiratta, J.J. Lewandowski and D.M. Dimiduk, *Metall. Trans. 22A* (1991), pp. 1573-1581.

[4] M.R. Jackson, B.P. Bewlay, R.G. Rowe, D.W. Skelly, and H.A. Lipsitt, J. of Metals 48 (1), (1996), pp. 38-44.

[5] P.R. Subramanian, M.G. Mendiratta and D.M. Dimiduk, *Mat. Res. Soc. Symp. Proc.*, 322 (1994), pp. 491-502.

[6] P.R. Subramanian, T.A. Parthasarathy, and M.G. Mendiratta, Scripta Met. and Mater., Vol. 32(8), pp. 39-54.

[7] B.P. Bewlay, M.R. Jackson and H.A. Lipsitt, *Journal of Phase Equilibria*, Vol 18(3), 1997, pp. 264-278.

[8] B.P. Bewlay, R.R. Bishop and M.R. Jackson, submitted Zeitschrift für Metallkunde, 1998.

New Crystal Structure Maps for Transition Metal Silicides and Aluminides

Masahiko Morinaga * and Yoshihisa Harada**

* Department of Materials Science and Engineering, Graduate School of Engineering, Nagoya University, Furo-cho, Chikusa-ku, Nagoya, Aichi, 464-8603, Japan.

** Department of Materials Science and Engineering,MLSB,Northwestern University, Evanston, Illinois 60208,USA

1. Introduction

The physical and chemical properties of intermetallic compounds depend strongly on the crystal structures. Many investigators have attempted to put in order crystal structural data on the two or three dimensional structure maps employing a variety of parameters such as the electronegativity, the pseudopotential radius and the Mendeleev number. However, despite great effort to predict the crystal structures of the compounds, there are still some difficulties in these previous approaches.

In this study, two electronic parameters which represent the nature of the chemical bond between atoms in intermetallic compounds, have been calculated by the DV-Xα molecular orbital method. Employing these electronic parameters, new crystal structure maps have been proposed for silicides and aluminides[1].

2. DV-Xα molecular orbital calculation

The DV-Xα molecular orbital method is based on the Hartree-Fock-Slater approximation. The detailed explanation of this method is given elsewhere[2].

The selection of the cluster model is most crucial in the present calculation. In this study, an octahedral model is chosen in order to express atomic interactions as simply as possible and also to increase the applicability of the results to a variety of crystal structures of intermetallic compounds. The actual cluster model used is shown in Fig.1(a). Such an octahedron ,M_2X_4, is often seen in the structures of many compounds as shown in Fig.1(b-d).

For aluminides, as shown in Fig.1(a), Al is set on X, and a M_2Al_4 cluster is used in the calculation, where M's are transition metals. The a-axial length is fixed at 0.2864 nm, twice as large as the aluminum atomic radius, and the c-axial length is varied following the atomic radius of M so that the M atom sphere contacts with the Al atom sphere as if they are rigid-body spheres. For silicides, a similar cluster model, M_2Si_4, is employed except for the a-axial length of 0.2638 nm, twice as large as the silicon atomic radius.

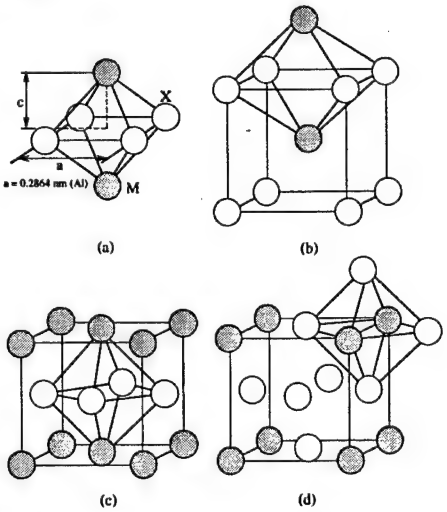

Fig.1 (a) Octahedral cluster model, M_2X_4, and typical crystal structures containing octahedral cluster, (b) B2-type, (c) $L1_0$-type and (d) $L1_2$-type structures.

3. Electronic parameters used for structure maps

Two electronic parameters are obtained from the calculation and used for constructing structure maps. One is the bond order, Bo, which is a measure of the covalent bond strength between atoms. When X is a non-transition metal and M is a transition metal, the p-d interaction is most dominant between X and M atoms. So, the bond order is estimated from the overlap population between X-p electrons and M-d electrons. The another parameter is the d-orbital energy level of

transition element, Md. This parameter is associated with two classical parameters, the electronegativity and the atomic radius of element, M. The electronegativity is concerned with the charge transfer between atoms, and hence this parameter is a sort of measure to show the ionic interaction between atoms. Also, as the Md parameter is related closely to the atomic size, the use of this parameter may guarantee the structural classification even for the size-controlling compounds like the Laves phases.

Thus, the concept of the covalent bonding, ionic bonding and atomic size, all of which are important factors in determining crystal structures, is involved in the two calculated parameters, the bond order, Bo, and the d-orbital energy level, Md. Furthermore, both of them change following the position of elements in the periodic table. This is very important since the crystal structures of compounds also change following the periodic table. In fact, the same or similar crystal structure appears in the same group or its neighborhood in the periodic table. In this sense, these Bo and Md are indeed suitable parameters for constructing structure maps.

4. Structure maps

4.1 Aluminides

The structure maps are shown in Fig.2 for aluminides ; (a) MAl, (b) M_3Al and (c) MAl_3. The crystal structure data of intermetallic compounds are taken from the Pearson's Handbook [3]. Each crystal structure is distinguished from the others using different symbols on the map. In addition to binary compounds, ternary compounds, for example, $(M_{1-x}Y_x)Al$; No.1~No.6 shown in Fig.2(a), are also located on the map, simply by taking the compositional average of the Bo and the Md parameters. Namely,

$$Bo=(1-x)\cdot(Bo)_M+x\cdot(Bo)_Y,$$
$$Md=(1-x)\cdot(Md)_M+x\cdot(Md)_Y.$$

The crystal structures are well separated in each map. For example, for the MAl map, TiAl with the $L1_0$-type structure is located between the B33-type and the B2-type compounds on the map. PtAl and PdAl take the B20-type structure at low temperatures and the B2-type structure at high temperatures. In response to this, the B20-type region lies at the edge of the B2-type region. For the M_3Al map shown in Fig.2(b), the A15-type region is located in a high Bo region on the map. The $D0_{19}$-type region lies between the A15-type and the $L1_2$-type regions. Ternary compounds of No.1~19 have either the $D0_3$-type or the $L2_1$-type structure. Here, the $D0_3$ and the $L2_1$-type structures resemble each other as shown in Fig.2(b-1) and (b-2), respectively, and hence their regions are nearly overlapped on the map. For the MAl_3 map shown in Fig.2(c), there is the $D0_{22}$-type region near the $D0_{23}$-type region, because of the structural resemblance between them. In fact, $HfAl_3$ takes both the $D0_{22}$-type and the $D0_{23}$-type tructures, varying with the temperature.

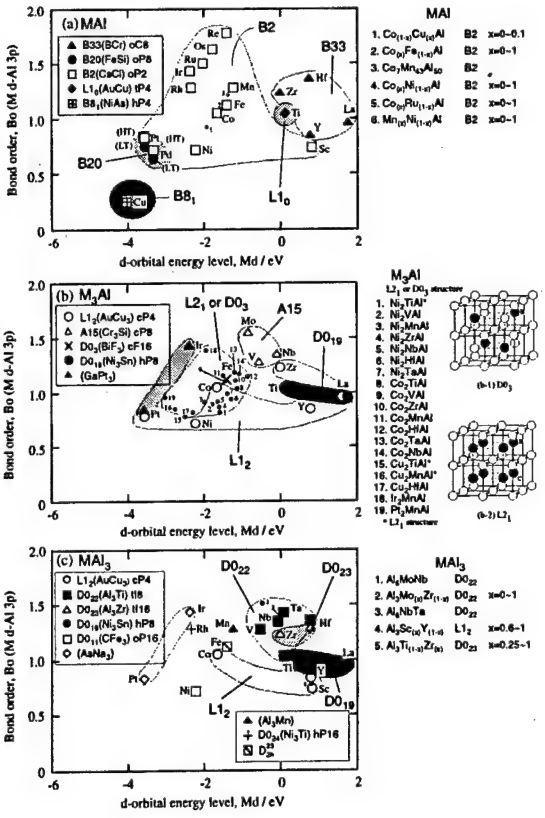

Fig.2 Structure maps for (a) MAl, (b) M_3Al and (c) MAl_3 compounds. Crystal structures are denoted using the Structurbericht symbol or the Pearson's symbol.

4.2 Silicides

The structure maps for silicides are shown in Fig.3; (a) MSi, (b) M_3Si and (c) MSi_2. In each map, there is a good separation of the crystal structures. For example, as shown in Fig3(c), the $C11_b$-type region of $MoSi_2$ is located in a high Bo region, and adjacent to the C40-type region on the map. This is reasonable since even for pure $MoSi_2$ the C40-type structure is found when it is rapidly quenched from the melt, even though this may be a metastable phase. It is also known that if a (110) stacking fault is introduced into the $C11_b$-type structure, the crystal structure becomes identical with the C40-type structure. Also, as shown in Fig.3(b), the A15-type region is close to the PTi_3 region, since both of them appear, for example, in Nb_3Si.

5. Comparison with other structure maps

5.1 Miedema's electronegativity and electron density at Wigner-Seitz atomic cell boundary

Miedema has proposed two parameters to estimate the heat of formation of intermetallic compounds [4]. One is the electronegativity, ϕ^*, and the other is the electron density at the boundary of the Wigner-Seitz atomic cell, n_{ws}. The structure map for M_3Al is made using these parameters and the result is shown in Fig.4(a). The regions of the $D0_{19}$-type, the $L2_1$-type, the $D0_3$-type and the $L1_2$-type structures are mixed together on the map. It is evident that this map shows a poorer separation of crystal structures, as compared to the map shown in Fig.2(b).

5.2 Zunger's pseudopotential radius

Zunger has calculated the pseudopotential radii of s electrons, rs, and also of p electrons, rp [5]. Using these rs and rp, dual parameters are obtained for the AB compound as,

$$R_\sigma^{AB}=|(rs^A+rp^A)+(rs^B+rp^B)|,$$
$$R_\pi^{AB}=|(rs^A-rp^A)+(rs^B-rp^B)|.$$

The structure map for MAl made of these parameters is shown in Fig.4(b). The B2-type region is very broad and it is overlapped with both the B20-type and the B33-type regions. Thus, the separation of the crystal structure seems poorer in this map than the map shown in Fig.2(a).

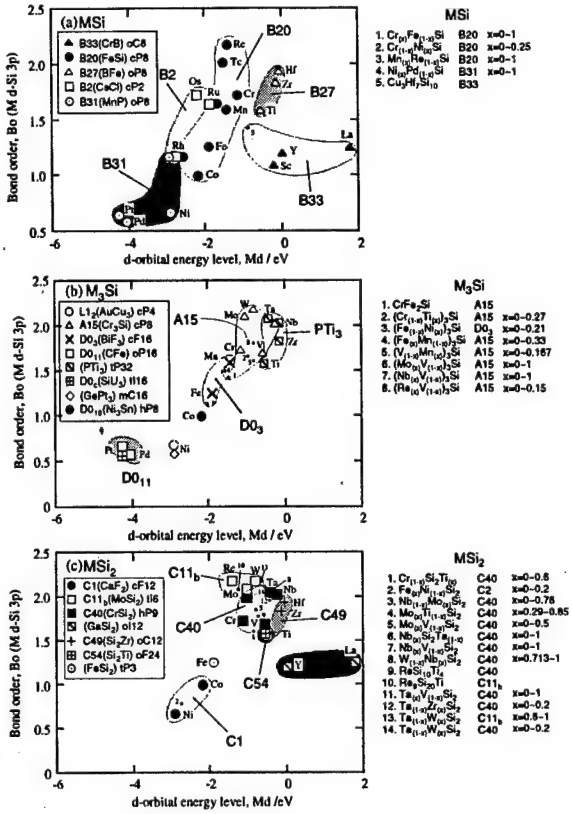

Fig.3 Structure maps for (a) MSi, (b) M_3Si and (c) MSi_2 compounds.

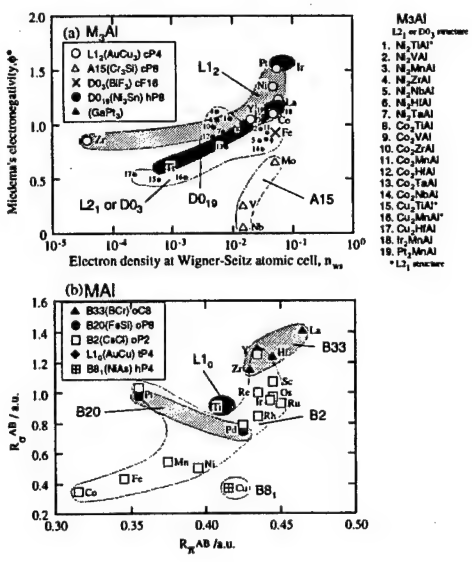

Fig.4 Structure maps for (a) M_3Al compounds with the Miedema's parameters and (b) MAl compounds with the Zunger's parameters.

5.3 The Mendeleev number

Pettifor has proposed the usefulness of the Mendeleev number for the structural classification of intermetallic compounds [6]. The magnitude of the Mendeleev number for each element changes in the way as if it forms an one-dimensional chain lying on the periodic table. For the binary A_mB_n compound, the structure map is constructed using two Mendeleev numbers (M_A, M_B). For example, the AB_3 structure map is shown in Fig.5 for aluminides and silicides containing transition metals. However, the accuracy of prediction is still poor in this case. For example, as shown in Fig.5, either the $L1_2$-type or the $D0_{19}$-type region is separated into two different regions on the map. A ternary Pt_2MnAl has the $D0_3$-type structure, but this is located in the $L1_2$-type region on the map. A main reason for these discrepancies is probably due to the missing of two-dimensional periodicity in the single Mendeleev parameter, despite the fact that any compounds having the same crystal structure tend to appear in the same group or near the group in the two-dimensional periodic table. On the other hand, there are no such discrepancies on the Bo-Md structure map shown in Fig.2(b). For example, Pt_2MnAl of No.19 is positioned in the $D0_3$ (or $L2_1$)-type region, consistent with the experiment.

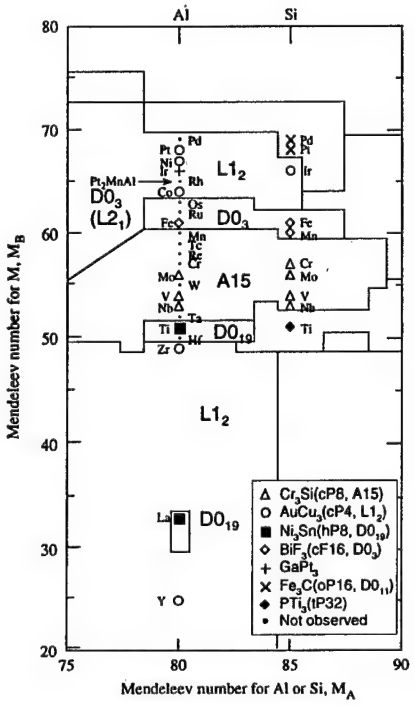

Fig.5 AB_3 structure map of using the Mendeleev number for aluminides and silicides containing transition metals.

6. Conclusion

New crystal structure maps for transition metal silicides and aluminides are constructed on the basis of the DV-Xα molecular orbital calculations of electronic structures. There is a clear separation of the crystal structures on the maps. These maps are applicable to the prediction of crystal structures not only for binary compounds but also for ternary compounds.

Acknowledgments

The authors acknowledge the Computer Center, the Institute for Molecular Science, Okazaki National Institutes for the use of the NEC SX-3 model 34R super computer. This research is supported in part by a Grant-in-Aid for Scientific Research from the Ministry of Education, Science, Sports and Culture of Japan.

References

[1] Harada Y, Morinaga M, Saito J and Takagi Y 1997 J. Phys.:Condens. Matter **9** 8011

[2] Morinaga M, Yukawa N, Adachi H and Mura T 1987 J. Phys.F:Met. Phys. **17** 2147

[3] Villars P and Calvert L D 1985 Pearson's Handbook of Crystallographic Data for Intermetallic Phases vols 1-3 (Metal Park,OH:ASM)

[4] Miedema A E 1973 J. Less-Common Met. **32** 6439

[5] Zunger A 1980 Phys. Rev. B **22** 5839

[6] Pettifor D G 1986 J. Phys. C:Solid State Phys. **19** 285

The Development of Mo-Si-B Alloys for Aerospace Applications

Douglas M Berczik, Mark V. Garguilo
United Technologies-Pratt and Whitney
MS 707-26
P.O. Box 109600
West Palm Beach, Fl 33410-9600
Phone: 561.796.6442 -- Fax: 561.796.7454
E-mail: berczik@pwfl.com

From the first jet engines developed during WWII to the high performance military engine that will power the Air Force's frontline fighters of the 21st Century, the efficiency of all jet engines is almost directly proportional to the temperature at which the hot section of the engine can be run. Nowhere else are high temperature materials as

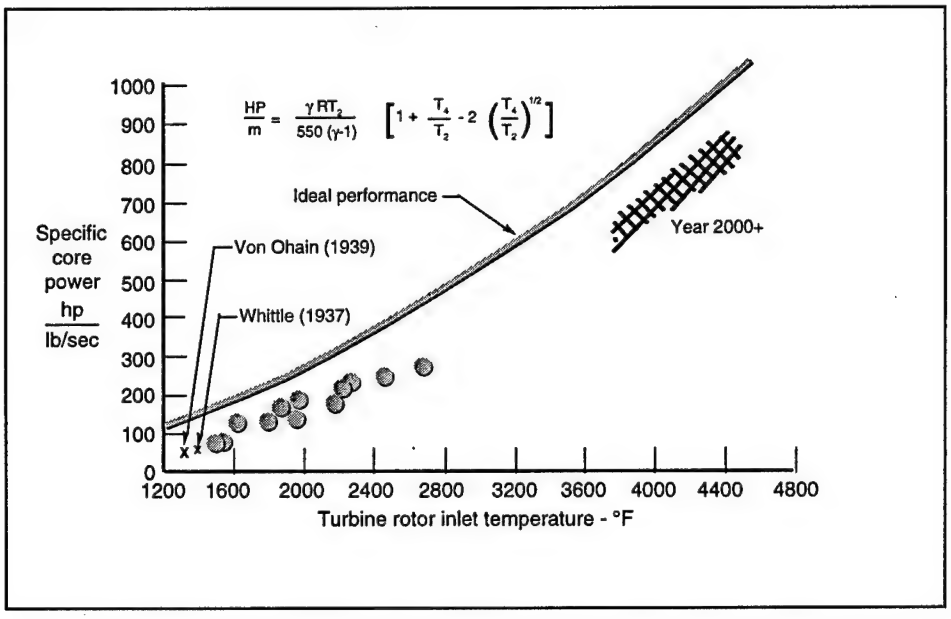

Engine Efficiency as a function of Turbine Inlet Temperature

important as in the components that are exposed to the gases in the turbine section. This list of components includes the airfoils, rotating and non-rotating, the seals, and the combuster. As can be seen in the previous chart, the switch from the heat resistant stainless steels of the 40's to the nickel based superalloys and the advanced cooling schemes of the present day has led to an increase of over 500% in the efficiency of jet engines. Current day turbine airfoils operate at temperatures up to 100 degrees below their incipient melt point. While advanced cooling schemes have extended gas path temperatures to well beyond the melting points of these materials it has been at a price, that of system complexity and cost. In order to realize the still existing increases in performance, a new higher melting point class of alloys is needed.

Refractory alloys based on molybdenum and niobium exist that would meet the melting point and mechanical requirements of the future generation of jet engines were it not for their inherently poor environmental resistance.

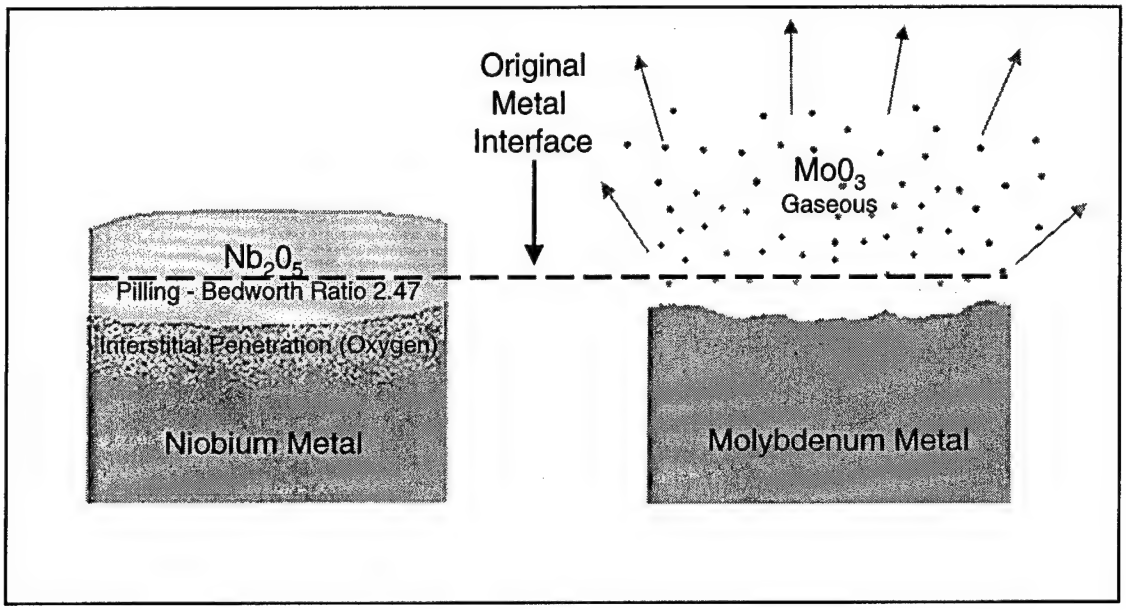

Oxidation Mechanism comparison for Niobium and Molybdenum

Conversely, refractory metal intermetallics based on silicon (notable among them $MoSi_2$) exist that have the necessary environmental resistance but do not have the combination of mechanical properties and fabricability to allow them to be used as critical components. After years of research into this area, only multiple phase systems that contain intermetallics for environmental resistance and a non-ordered refractory metal phase either as a continuous matrix or as a reinforcing phase appear to offer the possibility of the needed balance of properties.

At Pratt &Whitney, research since 1990 has concentrated on alloys in the Molybdenum-Silicon-Boron system. This system contains the prerequisite two-phase region of refractory metal (Mo) in equilibrium with an oxidation resistant intermetallic (Mo_5SiB_2).

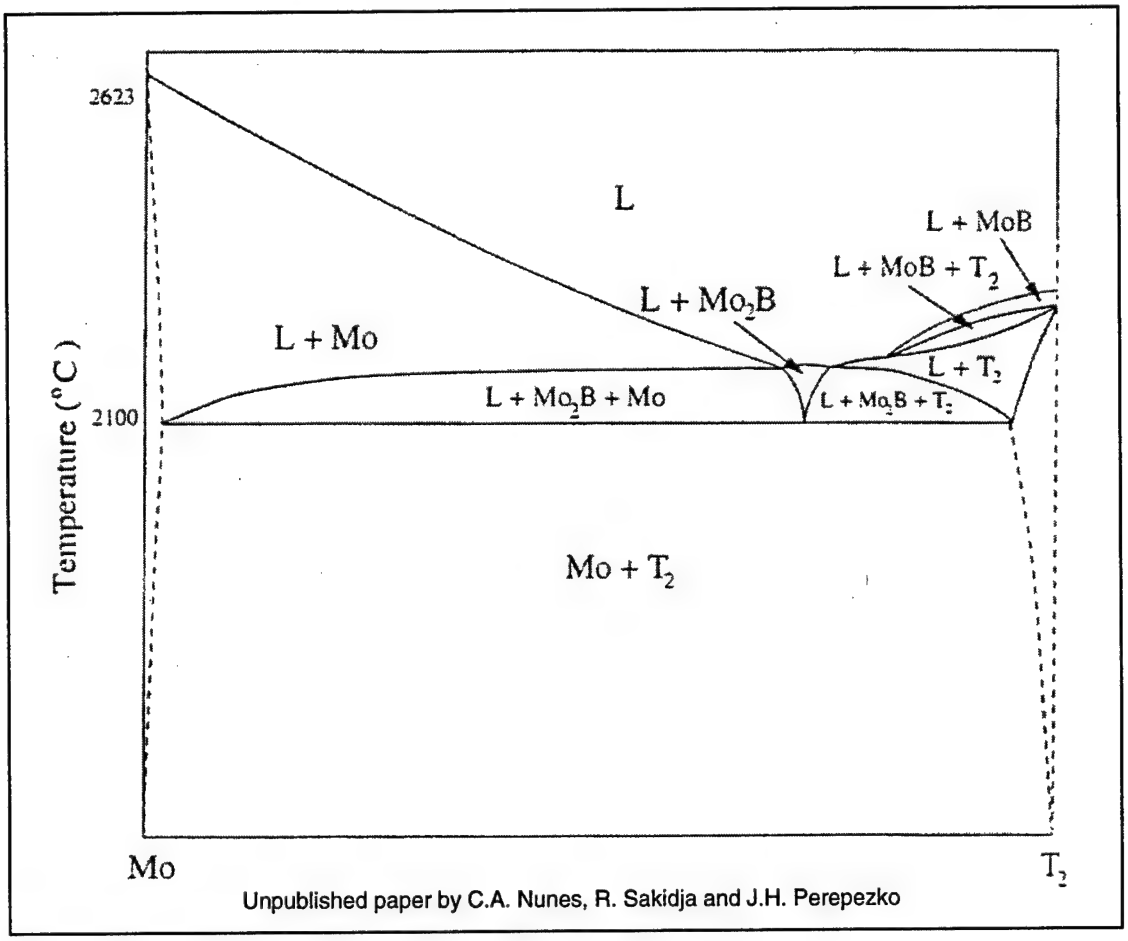

Early in the effort alloys were developed that demonstrated enhanced oxidation resistance and the ability to be fabricated into standard test specimens, an achievement in an area of research were the reporting of the compressive properties of round cylinders of material is common.

Temperature	Yield Strength	Ultimate Strength	Percent Elongation	% Reduction in Area
RT	794.4	797.2	0.2	0
540 C	775.1	966.0	2.5	0.8
825 C	712.4	1019.7	2.6	1.6
1093 C	471.3	530.5	21.5	29.4
1260 C	250.1	298.3	28.2	36
1370 C	169.5	203.3	31.6	39.8

Tensile Strength of Mo-2.0Si-1.0B-.3Hf

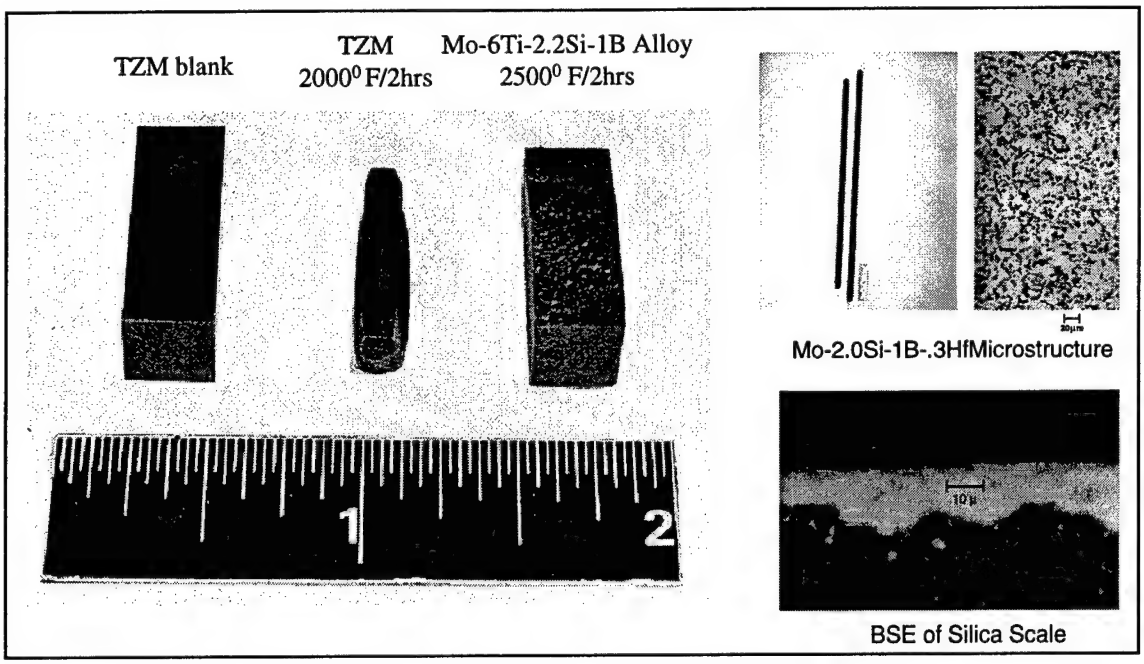

Oxidation Resistance of Mo-Si-B based Alloys

While this combination of environmental resistance and mechanical properties was promising, further improvements were deemed necessary. During the Aerospace downturn of the mid 90's the research was carried on under a caretaker status.

As the conceptual designs were completed on the Phase III IHPTET engine, the need for a new generation of blade materials resurfaced across the propulsion industry. Under ONR/NAWC funding, efforts at further improving the environmental resistance of the Mo-Si-B alloys and at exposing them for the first time to the engine environment have been proceeding. The effort to date has established a range of compositions with increased oxidation resistances that are still within the processable range of the 3 phase Mo-Mo_5SiB_2-Mo_3Si field. The remainder of the Navy funded effort will concentrate on the production of material for property characterization and the design, manufacturing, and testing of a cooled turbine exit guide vane in a demonstrator bed of an IHPTET Phase III demonstrator core.

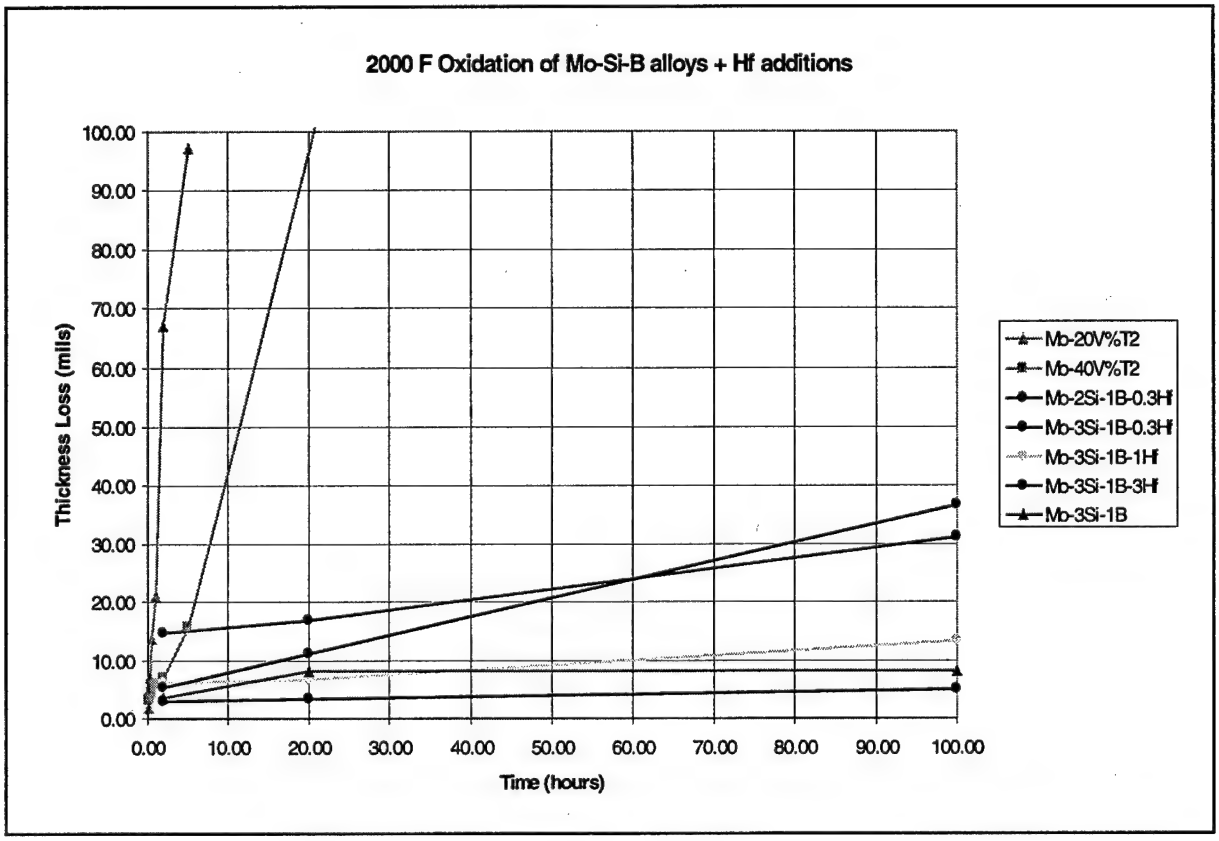

Oxidation Resistance at 2000 F of Mo-Si-B-Hf Alloys

Future efforts in this system will continue to concentrate on identifying oxidation resistant chemistries within either the 2 phase Mo-Mo_5SiB_2 field or the 3 phase Mo-Mo_5SiB_2-Mo_3Si field. Establishing the eventual tradeoffs between environmental resistance, processablity and mechanical properties will be the prime area of research for some time to come. In particular, the environmental resistance of the material across the entire range of use temperatures must be considered in these systems. Historically it has not been uncommon for alloys of this type to demonstrate better high temperature than low temperature oxidation resistance.

The alloying for environmental resistance will then have to be balanced against the physical demands of turbine airfoils. Given the complex failure modes that occur in these components, the up-front development of an integrated materials/design system will be vital for the success of the effort.

OBSERVATIONS AND CHALLENGES IN DEVELOPING REFRACTORY METAL-SILICIDE MULTIPHASE SYSTEMS

P. R. SUBRAMANIAN*, M. G. MENDIRATTA*, AND D. M. DIMIDUK
AIR FORCE RESEARCH LABORATORY, AFRL/MLLM
WRIGHT-PATTERSON AFB, OH.

***UES, INC., DAYTON, OH.**

Research Objectives and Approach

Recent studies have shown that Nb-base refractory intermetallic materials may be viable for service at temperatures that compete with the nickel-based superalloys in structural applications. While advanced intermetallics in monolithic form have limited prospects for providing the required balance of properties for use at high operating temperatures, two-phase or multiphase intermetallic systems composed of a ductile, Nb-base refractory phase in equilibrium with one or more silicide intermetallics show promise for further development as structural materials. Such alloy systems offer a potential advantage over the beta alloys in that the introduction of the intermetallic phases can result in reasonable high-temperature properties, while the ductile constituent can impart good low-temperature toughness. Two-phase Nb/Nb_5Si_3 alloys represent a model material system in this class. Extensive microstructure-processing-property relationship studies performed on Nb/Nb_5Si_3 alloys have shown that these alloys possess a useful range of mechanical properties, such as low-temperature toughness as well reasonable high-temperature strength and creep resistance. However, one major impediment to the development of the Nb-Nb_5Si_3 alloys for high-temperature applications is their catastrophic oxidation behavior. Alloy studies were initiated on the model Nb-Nb_5Si_3 system in an effort toward obtaining material systems with improved environmental resistance while retaining the structural properties achieved to date. Exploratory efforts on these systems have indicated that damage tolerance, creep resistance and oxidation tolerance may be obtained and controlled simultaneously.

This presentation will highlight research progress in multicomponent Nb-base system with focus on alloying strategies, microstructural development, and oxidation behavior. The influence of processing on microstructure and selected properties will be discussed briefly. Finally, the presentation will close with discussions of critical issues and future directions in this area.

Research Progress and Highlights

Alloying pathways have resulted in a progressive transition from the model Nb/ Nb_5Si_3 system to a multiphase, multicomponent system of Nb-Ti-Hf-Cr-Al-Si-X with the microstructure still consisting of a refractory solid solution and one or more silicide intermetallics as well as Laves phase existing in equilibrium. A key component of this research was the exploration of the role of chemistry on microstructural evolution. The Cr concentration appeared to play a critical role in phase distribution. At a Cr concentration to ~ 10 at.%, a continuous beta phase with a distribution of blocky M_3Si or M_5Si_3 phases was observed. The observations thus far indicate that, in the NbTiCrAlSi alloys, a continuous beta phase is responsible for poor high T strength and creep resistance. Typically, the Cr &/or Al content has to be lowered to ~ 2-5%, if the silicide phase has to be made continuous. In contrast, increasing the Cr content has important implications with regard to oxidation resistance. Addition of "beta" formers such as Mo and Ta appear to be beneficial in creating a co-continuous microstructure of beta and M_5Si_3 phases. These additions, in turn, allowed an increase in the Cr concentration in these alloys to ~ 15 at.% while still maintaining the desirable co-continuous microstructure. In an attempt to understand the microstructural evolution as a function of chemistry, efforts have been initiated toward calculating solidification

pathways in these complex alloys, using THERMOCALC (collaborative research with Y. A. Chang, Computherm, LLC).

The alloying modifications in the Nb-Ti-Hf-Cr-Al-Si-X alloys have a significant influence on the oxidation response, which has been characterized in terms of both metal recession under static and cyclic exposures as well as oxygen penetration within the beta phase as a function of depth. Progressive improvements have been noted in the oxidation behavior, although the advances are still short of the goal for structural applications. Of the various chemistries, Cr additions have been found to be most beneficial in terms of metal recession rates. Examination of the oxide scales on the alloys indicate a stratified morphology consisting of multiple oxides, with CrO_2 and TiO_2 as the primary scale constituents.

A systematic study of the effect of different processing routes on structure-properties of specific alloy chemistries is lacking, although some general trends have been observed. As an example, in selected Nb-Ti-Hf-Cr-Al-Si alloys, the metastable M_3Si phase persists even after extended heat treatments at elevated temperatures. In this instance, thermomechanical treatments have been found to be essential for accelerating the decomposition of these phases into equilibrium beta and M_5Si_3 phases. Another observation on the influence of processing is that, in general, directionally solidified alloys appear to be stronger at high temperatures and more creep resistant, presumably from directional alignment of the silicide dendrites. Such interrelationships between chemistry-processing-microstructure-properties have to be investigated in much greater detail.

Issues and Challenges

The present study essentially constitutes the exploratory stages of alloy development in the Nb-base beta + silicide class of materials, with the alloying efforts focused on defining alloy compositions and microstructures, followed by screening studies. A major challenge in designing a multiphase, multicomponent system is understanding the role of diverse alloying elements in creating desirable microstructures and/or phase distribution. In this instance, a co-continuous distribution of beta and intermetallic phases or a microstructure consisting of one or more intermetallic phases reinforced by a distribution of ductile beta particles appear to be most favorable for obtaining a desirable balance of mechanical properties. While the trends indicate that a useful balance of low-temperature and high-temperature properties may be obtained through appropriate alloying, processing, and microstructural control, the alloy development efforts are still in the exploratory stage. There is a definite need for further research on microstructural control, composition modifications, and understanding of structure-property relationships before these alloy systems can be considered for service. A more sustained effort is required toward generating a database of engineering properties, such as fracture toughness, fatigue-crack growth, temperature dependence of tensile strength, and creep as well as stress rupture on selected alloy compositions. Further, processing methods for these advanced alloy systems have not been sufficiently explored. Ingot processing of the multicomponent, multiphase alloys pose serious technical challenges. Alternate processing techniques, such as vapor deposition, have to be explored for good composition and microstructural control. Finally, this research was aimed at potential applications at temperatures over 1200°C. There may be a number of competitive applications in the 800-1200°C temperature regime, where these alloys may provide incremental improvement over Ni-base alloys, especially, in terms of density, cost, and mechanical performance. Additional research efforts should focus on this temperature regime.

The oxidation improvements shown by some of the advanced alloys are still short of the goals. Even if the oxidation goals are realized through alloying efforts, the materials will require oxidation-protective coatings for any long-term use in the temperature range of proposed service (1200-1400°C). Coating development for the advanced Nb-base alloys will require further research on new coating compositions as well as coating techniques. At the fundamental level, continuing needs exist in terms of quantification of short-term parabolic oxidation behavior and a

mechanistic understanding of scale evolution as a function of alloy chemistry. In essence, the challenge in developing these oxidation-tolerant alloys is to identify means to extend the oxidative lifetime and guarantee scale stability under cyclic conditions, while maintaining the microstructure and mechanical properties achieved to date.

Selected Publications

1. "Development Approaches for Advanced Intermetallic Materials - Historical Perspective and Selected Successes," D. M. Dimiduk, M. G. Mendiratta, and P. R. Subramanian, in Structural Intermetallics, eds., R. Darolia, J. J. Lewandowski, C. T. Liu, P. L. Martin, D. B. Miracle, and M. V. Nathal, TMS, Warrendale, PA, 1993, pp. 619-630.

2. "Microstructures and Mechanical Behavior of Nb-Ti Base Beta + Silicide Alloys" P. R. Subramanian, M. G. Mendiratta, and D. M. Dimiduk, in High-Temperature Silicides and Refractory Alloys, eds., C. L. Briant, J. J. Petrovic, B. P. Bewlay, A. K. Vasudevan, and H. A. Lipsitt, MRS, Pittsburgh, PA, 1994, pp. 491-502.

3. "Compressive Creep Behavior of Nb_5Si_3," P. R. Subramanian, T. A. Parthasarathy, M. G. Mendiratta, and D. M. Dimiduk, Scripta Met. et. Mater., 32(8), (1995), pp. 1227-1232.

4. "Simulations of Creep in Ductile-Phase Toughened Nb_5Si_3/Nb In-Situ Composites," G. A. Henshall, M. J. Strum, P. R. Subramanian, and M. G. Mendiratta in High-Temperature Ordered Intermetallic Alloys VI, eds., J. A, Horton, I. Baker, S. Hanada, R. D. Noebe, and D. S. Schwartz, MRS Symp. Proc., 364, Pittsburgh, PA, 1995, pp. 937-942.

5. "Exploration of Nb-Based Advanced Intermetallic Materials," (Invited Paper), D. M. Dimiduk, P. R. Subramanian, and M. G. Mendiratta, Acta Metall. Sinica (English Edition), 8 (4-6) (1995) pp. 519-530.

6. "The Development of Nb-Based Advanced Intermetallic Alloys for Structural Applications," P. R. Subramanian, M. G. Mendiratta, and D. M. Dimiduk, Journal of Metals, 48(1), (1996) pp. 33-38.

7. "Continuum Predictions of Deformation in Composites with Two Creeping Phases -II. Nb_5Si_3/Nb Composites," G. A. Henshall, P. R. Subramanian, M. J. Strum, and M. G. Mendiratta, Acta Mater., 45(8), (1997) pp. 3135-3142.

8. "Advanced Intermetallic Alloys-Beyond Gamma Titanium Aluminides," P. R. Subramanian, M. G. Mendiratta, D. M. Dimiduk, and M. A. Stucke, Materials Sci. Engg., Vol. A239-240, 1-13 (1997)

Acknowledgments

The authors acknowledge the support from the Air Force Office of Scientific Research (AFOSR) through exploratory research funds. Two of the authors, P.R.S and M.G.M, acknowledge partial financial support from the Air Force Research Laboratory, Materials & Manufacturing Directorate under Contract Nos. F33615-91-C-5663 & F33615-96-C-5258. The authors also acknowledge the collaborations and contributions of Ms. Monica Stucke of AFRL/MLLM, Prof. J. J. Lewandowski of Case-Western Reserve University, Prof. Austin Chang of University of Wisconsin-Madison, and Drs. Mel Jackson and Bernard Bewlay of General Electric CR&D Center.

1.Fracture and Fatigue Behavior of Refractory Metals, Metal-Intermetallic (Nb-Si) Composites

F49620-96-1-0164

John J. Lewandowski
Department of Materials Science and Engineering
Case Western Reserve University
Cleveland, OH 44106

2a. Research Objectives:

The main focus in the present work has been on determining the fundamental mechanisms controlling the fracture and fatigue behavior of material toughened with ductile/tough phases. This research is utilizing materials processed at WPAFB from the binary Nb-Si system and alloy variants, as well as recently developed directionally solidified (DS) Nb-Ti-Hf-Si-Al-Cr (i.e. at GE CRD) base materials in order to determine the factors controlling the mechanical behavior under both monotonic and cyclic loading conditions. Considerable work has already demonstrated the positive effects of compositing Nb_5Si_3 with Nb on the toughness of such materials. However, relatively little is known regarding the monotonic fracture and cyclic fatigue behavior of the materials obtained from the binary Nb-Si systems as well as those obtained via alloying of both monolithic and composite Nb alloys.

2b. Research Approach:

This research is focusing on the following areas of Nb-based tough(ened) alloys/composites:

1. Determining the microstructural factors controlling the fracture and fatigue behavior of the individual constituent phases which comprise toughened materials. The features (i.e. microstructural, stress state) controlling the ductility, cleavage fracture stress, and fracture toughness of pure Nb and solid solution strengthened Nb-Zr and Nb-Si alloys were determined over a range of test temperatures. One desire was to determine whether cleavage fracture in such materials obeys a critical tensile stress criterion, in addition to determining the level of toughness possible when failure occurs via cleavage fracture.

2. Investigate the fatigue behavior of monolithic Nb alloys and Nb toughened silicides. Despite the great benefits afforded via the incorporation of ductile/tough Nb phases into brittle materials such as Nb_5Si_3, the behavior of such systems under cyclic conditions has only recently begun to be explored and very limited data exists. Fatigue tests have been conducted under a variety of conditions in order to determine the dependence of fatigue crack growth rate on ΔK for both the monolithic Nb alloys and Nb silicide composites. All relevant portions of the fatigue crack growth curve have been developed including the threshold regime, the Paris Law regime, and the region of overload failure. Both rising ΔK and falling ΔK tests have been conducted over a range of frequencies and R-ratios in order to also determine the effects of changes in the fatigue conditions on the subsequent crack growth behavior and fractographic observations. In addition, the effects of changes in the size and spacing of the toughening constituents on the subsequent fatigue behavior are being determined. I*n-situ* monitoring of crack growth has been used in some cases to delineate the mechanisms of crack growth.

3. Comparison of the fatigue behavior of the monolithic constituents to that of processed composites over a range of ΔK levels are being conducted. In particular, it is being determined if the mechanisms which contribute to high toughness in static tests are compromised when testing is conducted under cyclic loading conditions. This is being accomplished by determining the fatigue threshold, ΔK_{th}; Paris law exponents, m; and catastrophic overload stress intensity, K_c; over a range of R ratios and fatigue test conditions.

In all cases, close contact has been maintained with researchers at WPAFB, UES, Inc., and General Electric Corporate Research and Development (CE CRD), where complementary studies are being conducted on the creep and oxidation resistance of materials processed via vacuum arc-casting/extrusion, vapor deposition, and directional solidification. Recent contact with design engineers has also been initiated to delineate possible applications for such materials. The processing forms provide a range of microstructures and composite architectures for analysis.

3. Research Progress and Highlights:

I. Flow, Fracture, and Fatigue of Nb, Nb-Zr, Nb-Si Monolithic Materials

a) Flow Behavior

Fracture of any material is controlled by the competition between flow and fracture. In polycrystalline single phase metals, the dependence of flow stress on microstructural parameters is usually well predicted by the Hall-Petch equation:

$$\sigma_y = \sigma_o + k_y d^{-1/2}$$

which consists of a friction stress term, σ_o, in addition to a term that combines grain size, d, with a factor k_y which represents the effectiveness of grain boundaries as barriers to slip. The present work has demonstrated that pure Nb, Nb-1wt% Zr, and perhaps Nb-Si appear to exhibit a very low Hall-Petch slope, k_y, over the range of grain sizes spanning 25 μm – 165 μm (1-3). In these cases, the 0.2% offset yield strength was relatively insensitive to changes in grain size(1-3), consistent with previous work on pure Nb (4). Most polycrystalline metals (including other refractory metals) exhibit a much larger Hall-Petch slope, k_y, the magnitude of which is very sensitive to both interstitial and substitutional alloying elements. Preliminary work on polycrystalline Mo (5) reveals a somewhat higher Hall-Petch slope, while this value for Mo may be very interstitial content dependent.

b) Fracture Behavior

While the flow behavior of the Nb based systems described above appears to be well described by the Hall-Petch equation, the cleavage fracture stress of identical materials has been determined using techniques successfully used in evaluating similar parameters in structural steels (6,7). The concept of a cleavage fracture stress which was proposed independently by Orowan and Davidenkov to be temperature independent, requires the presence of a tensile stress controlled fracture mechanism. The presence of such a tensile stress controlled fracture mechanism has been determined by utilizing techniques successfully utilized for structural steels (6,7). The present work (1-3) on pure Nb, Nb-1 wt% Zr, and Nb-Si has indicated that cleavage fracture in these materials is temperature independent over the range 77K to as high as 298K, while fractographic observations of broken notched specimens revealed that cleavage fracture was tensile stress

controlled. The magnitude of the cleavage fracture stress was shown (1,2) to depend primarily on changes in grain size over the range 25 μm – 165 μm, with reductions in the grain size producing an increase in the cleavage fracture stress. Little effect of solid solution additions of Zr or Si (over the range indicated) on the magnitude of the cleavage fracture stress were obtained. Such information was successfully used to model the fracture morphology of laminated Nb_5Si_3/Nb (9,10) as well as in-situ composites based on the Nb-10 Si system (3).

The fracture toughness of identical materials was determined over a similar temperature range (2). Nb and Nb-Zr materials exhibited fracture toughness in excess of 40 MPa-m $^{1/2}$ at temperatures as low as 77-150K, while examination of the fracture surfaces revealed that tensile stress controlled cleavage fracture was exhibited over that range of test temperatures. Fracture toughness of the Nb-Si solid solution material was shown to exceed 25 MPa-m $^{1/2}$ at room temperature. Such values are clearly important to determine since the fracture toughness of any composite which utilizes Nb as the toughening phase will predominantly rely on the toughness of that phase to provide the majority of the toughening. These observations also indicate that such materials can exhibit significant toughness despite the appearance of 100% cleavage fracture on the fracture surface. The fracture toughness values obtained were successfully predicted (2) using the crack tip stress analyses by Hutchinson, Rice and Rosengren (11,12) in combination with the cleavage fracture stress data obtained presently (1,2).

c) Fatigue Behavior

Fatigue tests were conducted on bend bar specimens in a closed loop MTS servo-hydraulic machine at 20 Hz at R ratios of 0.1 and 0.4. Table I summarizes the data on monolithic Nb (13,14) which shows a negligible effect of grain size (over the range examined) on the threshold for fatigue crack growth in the Nb and Nb-Zr systems. An improvement in the threshold and fatigue behavior at higher ΔK was exhibited by the Nb-Si solid solution material. The Paris law exponents for all of the monolithic Nb alloys were in the range 2-5, consistent with much previous work on metallic materials, although little information on the fatigue behavior of Nb exists in the literature.

II. Fracture and Fatigue of Nb-Si In-situ Composite Materials

a) Fracture Behavior of Nb-Si Composite Materials

The fracture behavior of a model Nb-10 at% Si composite material was determined (3,15) over a range of loading rates and test temperatures in order to provide baseline data for comparison to subsequent work. Temperatures ranging from 77K to 773K were utilized to characterize the fracture behavior, while loading rates were varied over 6 orders of magnitude. Figure 1 demonstrates that the fracture toughness is relatively insensitive to changes in both loading rate and test temperature, over the range tested, while the magnitude of fracture toughness measured was in excess of 24 MPa-m $^{1/2}$. Such observations are consistent with the high values for toughness measured over a range of temperatures on the pure Nb, Nb-Zr, and Nb-Si materials reviewed above. The fracture toughness measured at 773K (15) was not significantly different than that measured at 77K.

b) Fatigue Behavior of Nb-Si Composite Materials

Continuing work has focused on determining the effects of cyclic loading on the fatigue crack growth behavior of both monolithic Nb and Nb alloys (13,14,16,17), as well as toughened

composites. Some additional *in-situ* composite materials prepared by directional solidification and arc casting/extrusion have been obtained from GE CRD and WPAFB, respectively.

The fatigue tests were conducted on bend bar specimens in a closed loop MTS servo-hydraulic machine at a variety of test frequencies (with most at 20 Hz) at R ratios including 0.05, 0.1, 0.4, 0.6 and 0.8. Table I summarizes the data obtained on the composites in comparison to the monolithic alloys reported above (13,14,16,17). Although the composites exhibit a somewhat reduced threshold for fatigue in comparison to that of the monolithic alloys, the values are still in the range of those exhibited by metallic materials. As important, the values for the Paris law exponents, m, are also in the range of that exhibited by metallic materials, although in the range 5-6.6 for the tests conducted at R=0.1 (13,14,16,17). The fatigue performance of the presently tested materials are significantly better than that obtained on other intermetallics toughened with Nb/Nb alloys, where the fatigue performance of the composite was often not better than that of the semi-brittle intermetallic. The possible reasons for such differences are discussed elsewhere (13,14).

Extensive fractographic analyses have revealed that for a given R ratio, increasing the level of ΔK produces a transition in fracture mode to increasing amounts of transgranular cleavagelike fracture of the primary Nb (16,17). The fractographic features are consistent with that of cleavage fracture, although a few additional tests are being conducted in order to conclusively determine the type of fracture being exhibited. Such an effect has been observed at all of the R ratios listed above, while the quantification of the amount of cleavagelike fracture present at each level of ΔK is provided in Figure 2 (17). The appearance of transgranular cleavagelike fracture in the primary Nb is possibly due to the intervention of static modes of fracture at increasing values of ΔK (and K_{max}). The data in Figure 2 is replotted in Figure 3 using K_{max} as the normalizing parameter, and this appears to collapse the data into a narrower band, suggesting that K_{max} is the appropriate normalizing parameter. Including data obtained over a wider range of R ratios supports this view (13,14).

A possible rationale for the increase in % transgranular cleavagelike fracture vs K_{max} is presented elsewhere (17) and relates to the size of the plastic zone in relation to the microstructure size scale. At low values of K_{max} regardless of the R ratio, the amount of primary Nb sampled by the plastic zone is insufficient to permit transgranular cleavagelike fracture to occur. As K_{max} increases, the stress distribution ahead of the fatigue crack broadens and more Nb is sampled, facilitating transgranular cleavagelike fracture in the primary Nb.

In addition to the binary Nb-10Si composites, a number of higher alloyed DS composites prepared by GE CRD have been tested. Preliminary work summarized in Table I indicates that the fatigue performance of the DS composite is similar to that of the cast/extruded materials, although much additional work must be conducted in order to determine the mechanisms controlling fatigue because of the significantly different microstructures present in such materials.

4. Potential Structural Applications and Engineering Issues:

The combinations of mechanical properties presently exhibited suggest that a variety of potential high temperature applications could be envisioned, provided that a number of related engineering issues are addressed. Potential engine applications include airfoils as well as exhaust nozzle applications. In addition, various engine components on hypersonic vehicles could benefit from the high specific strength at high temperature afforded by such materials. Engineering issues

related to such materials include: issues related to scale up of materials and resulting properties; improved oxidation resistance via alloying; ensuring/investigating whether alloying additions for improved oxidation resistance do not compromise mechanical properties of interest to application (e.g. ductility, fracture toughness, fatigue behavior); coatings for oxidation protection; secondary processing (e.g. extrusion, rolling) of such materials to produce the desired size and shape. It will be particularly important to determine if the heterogeneity of the microstructure in such materials produces any problems in the mechanical performance under the variety of conditions that might be expected in service or during inspection at ambient conditions. The effects of changes in grain size and alloy content (of any constituent) on the resulting mechanical performance (i.e. strength, toughness, fatigue) are critical engineering questions that must be addressed/evaluated if these materials are to be manufactured in the quantities required for engineering applications. In particular, the short fatigue crack growth behavior has not been characterized in such materials. Due to the high volume fraction of brittle intermetallic present in such materials, short fatigue cracks are likely to initiate and grow in such regions and thereby produce significantly different fatigue crack growth in comparison to that generated presently.

5. Critical Scientific Issues and Challenges:

A number of critical scientific issues have been identified during the duration of the present grant period on both refractory metal based alloys and composites. These include the following:

A. Monotonic Deformation and Fracture Issues:
   1. Source(s) of the low Hall-Petch slope in Nb and whether the Hall-Petch slope in advanced Nb alloys and composites is significantly affected by either interstitial or substitutional atoms.
   2. Effects of alloying elements and microstructural variables on the cleavage fracture stress in higher alloy variants of Nb and Nb composites and other refractory based systems. Will cleavage fracture continue to be tensile stress controlled in higher alloy variants/other systems?
   3. How does cleavage fracture nucleate in refractory systems – stress state effects?
   4. In laminated/layered systems, can cleavage fracture of both the refractory metal and refractory metal silicide be prevented via refinement of their size and spacing – is this beneficial and can this be predicted? Does an optimum size exist?

B. Cyclic Deformation and Fracture Issues:
   1. What controls the crack growth of short fatigue cracks in such materials?
   2. Is the appearance of cleavagelike fracture in fatigue indicative of the intervention of static modes of fracture? What controls such behavior microstructurally and which fatigue parameters (e.g. K, ΔK) appear to describe the intervention of such features. How to improve it?
   3. In metallic materials, the Paris law slopes are relatively unaffected by changes in R ratio, while in the present Nb-Si composites changes in R ratio may significantly affect the Paris law slopes – Why?
   4. How does composite architecture control fatigue and fracture in such materials?

References:

1. Samant, A., and Lewandowski, J.J. (1997). "Effects of Grain Size and Alloy Content on the Cleavage Fracture Stress of Nb", Metall. Trans. A., 28A, pp. 389-399.
2. Samant, A., and Lewandowski, J.J. (1997). "Effects of Test Temperature, Grain Size and

Alloy Additions on the Low Temperature Fracture Toughness of Polycrystalline Nb", Metall. Trans. A, 28A, pp. 2297-2307.
3. Rigney, J.D., and Lewandowski, J.J. (1996). "Loading Rate and Test Temperature Effects on Fracture of Nb_5Si_3/Nb *In-situ* Composites", Metall. Trans. A., 27A, pp. 3292-3306.
4.Adams, M.A., Roberts, A.C., and Smallman, R.E. (1960). Acta Metall., 8, pp. 328-337.
5. Zwonitzer, S.A., Rozak, G. and Lewandowski, J.J. (1998) "Effects of Rolling Temperature and Reduction on Microstructure and Tensile Properties of Thick Plate, P/M Mo", In Mo and Mo Alloys, (A. Crowson, J.A. Shields, P.R. Subramainan and E.S. Chen, eds.) TMS-AIME,Warrendale,PA,in press.
6. Lewandowski, J.J., and Thompson, A.W. (1986) Metall. Trans. A, 17A, pp. 1769-1786.
7. Lewandowski, J.J., and Thompson, A.W.,(1987) Acta Metall., 35, pp. 1453-1462.
8. Mendiratta, M.G., Goetz, R., Dimiduk, D.M., and Lewandowski, J.J. (1995). "Unconstrained and Constrained Tensile Flow and Fracture Behavior of an Nb-1.24 at. Pct. Si Alloy", Metall. Trans. A, 26A, pp. 1767-1777.
9. Kajuch, J., Rigney, J.D., and Lewandowski, J.J. (1992). "Processing and Properties of Tough Laminated Nb Silicides", Materials Science and Eng., A155, pp. 59-65.
10. Kajuch, J., Short, J.W., and Lewandowski, J.J. (1995). "Effects of Constraint and Test Temperature on Toughness of Nb_5Si_3/Nb Laminates", Acta Metall., 43, pp. 1955-1967.
11.Hutchinson, J.W. (1968). J. Mech. Physics Solids, 16, pp. 13-31.
12.Rice, J.R. and Rosengren, G.R. (1968). J. Mech. Physics Solids, 16, pp. 1-12.
13. Lewandowski, J.J. (1998). "Effects of the Addition of Toughening Ligaments on the Fatigue of Composites", in Fatigue '99, (X.R. Wu and Z.G. Zhang, eds.) EMAS, 1998, in press.
14. Zinsser, W.A., Solov'yev, S. and Lewandowski, J.J. (1998) "Fracture and Fatigue of Refractory Metal Intermetallic Composites", in Intermetallics VIII, Vol. 552, (E. George, M. Yamaguchi, and M. Mills, eds.), MRS, Pittsburgh, PA, 1998, in press.
15. Lewandowski, J.J., Dimiduk, D., and Mendiratta, M. (1988). "Fracture of Nb-Nb-Silicide Composites", Proc. Mater. Res. Symp.-High Temperature Composites, (S. Fishman, F. Lemkey, A.G. Evans, eds.), Pergamon, Vol. 20, pp. 103-109.
16. Lewandowski, J.J. and Zinsser, W., (1998). "Effects of R-ratio on Fatigue Crack Growth on Nb-Si (ss) and Nb-10Si *In-situ* Composites", Metall. Trans. A., 29A, pp. 1749-1757.
17. Zinsser, W. and Lewandowski, J.J. (1998). "Fatigue Crack Growth in Nb-10Si Composites", Scripta Metall. 28, 12, pp. 1775-1780.
18. Fariabi, S., Collins, A.L.W., and Salama, K. (1983). Metall. Trans. A, 14A, pp. 701-707.

6a. Publications Acknowledging AFOSR Support:

BOOKS

1. Structural Intermetallics I-ISSI (R. Darolia, J.J. Lewandowski, C.T. Liu, P.L. Martin, D.B. Miracle and M.V. Nathal, eds.), TMS, Warrendale, PA, 1993.
2. Intermetallic Matrix Composites III, (J.A. Graves, R.R. Bowman, and J.J. Lewandowski, eds.),MRS, Vol. 350, Pittsburgh, PA, 1994.
3. Intrinsic and Extrinsic Fracture Mechanisms in Inorganic Composites, (J.J. Lewandowski and W.H. Hunt, Jr., eds.), TMS, Warrendale, PA, 1995.
4. Layered Materials for Structural Applications-I, (J.J. Lewandowski, C.H. Ward, M.R. Jackson and W.H. Hunt, Jr., eds.), MRS, Pittsburgh, PA, 1996.

PAPERS ON Nb, Nb SILICIDE

1. Lewandowski, J.J., Dimiduk, D., and Mendiratta, M. (1988). "Fracture of Nb-Nb-Silicide Composites", Proc. Mater. Res. Symp.-High Temperature Composites, (S. Fishman, F. Lemkey, A.G. Evans, eds.), Pergamon, Vol. 20, pp. 103-109.
2. Rigney, J.D., and Lewandowski, J.J. (1990). "*In-situ* Studies of Ductile Phase Toughening in Silicides", in Proc. Second Int'l. Ceramic Sci. and Tech. Congress,-Advanced Composite Materials, Westerville, OH., (M.D. Sacks, et. al. eds.), pp. 519-525.
3. Mendiratta, M., Lewandowski, J.J., and Dimiduk, D. (1991). "Ductile Phase Toughening in Two Phase Nb/Nb_5Si_3 Alloys", Metallurgical Transactions A, 22A, pp. 1573-84.
4. Rigney, J.D., Singh, P.M., and Lewandowski, J.J. (1992). "Environmental Effects on Ductile Phase Toughening in Nb_5Si_3-Nb Composites", JOM, August, 1992, pp. 36-41.
5. Kajuch, J., Rigney, J.D., and Lewandowski, J.J. (1992). "Processing and Properties of Toughened Silicides" Materials Science and Eng., A155, pp. 59-65.
6. Kajuch, J., Rigney, J.D., and Lewandowski, J.J. (1993). "The Kinetics of Formation of Nb_5Si_3", in Proc. Symposium on Mater. Research, (J.D. Whittenberger, M.H. Yoo, R. Darolia, and I. Baker, eds.), MRS, Pittsburgh, PA, Vol. 288, pp. 853-860.
7. Zhang, J., and Lewandowski, J.J. (1994). "An Indentation Technique to Evaluate Interface Toughness of Laminates", Journal of Materials Science, 29, pp. 4022-4026.
8. Lewandowski, J.J. (1994). "Mechanical Behavior of In-situ Composites", in *In-situ* Composites: Science and Technology, (M. Singh and D. Lewis, eds.), TMS, Warrendale, PA, pp. 159-167.
9. Short, J.W., Kajuch, J., and Lewandowski, J.J. (1994). "Processing and Properties of Nb_5Si_3/Nb Laminates", in Proc MRS Symposium-Intermetallic Matrix Composites III, (J.A. Graves, R.R. Bowman, and J.J. Lewandowski, eds.), MRS, Pittsburgh, PA, pp. 285-293.
10. Rigney, J.D., Singh, P.M., and Lewandowski, J.J. (1994). "Effects of Environmental Exposure on Ductile-Phase Toughening in Niobium Silicide-Niobium Composites", in MRS Proceedings-Vol 332, MRS, Pittsburgh, PA, pp. 503-509.
11. Kajuch, J., Short, J.W., and Lewandowski, J.J. (1995). "Effects of Constraint and Test Temperature on Toughness of Nb_5Si_3/Nb Laminates", Acta Metall., 43, pp. 1955-1967.
12. Mendiratta, M.G., Goetz, R., Dimiduk, D.M., and Lewandowski, J.J. (1995). "Unconstrained and Constrained Tensile Flow and Fracture Behavior of an Nb-1.24 at. Pct. Si Alloy", Metall. Trans. A, 26A, pp. 1767-1777.
13. Rigney, J.D., and Lewandowski, J.J. (1995). "Effects of Loading Rate and Test Temperature on the Toughness of *In-situ* Composites Based on Niobium Silicides", in Fatigue and Fracture of Ordered Intermetallic Materials II, (T.S. Srivatsan, W.O. Soboyejo, and R.O. Ritchie, eds.), TMS, Warrendale, PA, pp. 339-359.
14. Lewandowski, J.J. and Rigney, J.D. (1996). "Temperature and Loading Rate Effects on Toughness of *In-situ* Niobium Silicide-Niobium Composites", in Proc. NATO ASI-Mechanical Behavior of Materials at High Temperature, (C. Moura Branco, R.O. Ritchie, and V. Sklenicka, eds.), Kluwer Dordrecht, pp. 535-545.
15. Rigney, J.D., and Lewandowski, J.J. (1996). "Loading Rate and Test Temperature Effects on Fracture of Nb_5Si_3/Nb *In-situ* Composites", Metall. Trans. A., 27A, pp. 3292-3306.
16. Samant, A., and Lewandowski, J.J. (1997). "Effects of Grain Size and Alloy Content on the Cleavage Fracture Stress of Nb", Metall. Trans. A., 28A, pp. 389-399.
17. Samant, A., and Lewandowski, J.J. (1997). "Effects of Test Temperature, Grain Size and

Alloy Additions on the Low Temperature Fracture Toughness of Polycrystalline Nb", Metall. Trans. A, 28A, pp. 2297-2307.
18. Bewlay, B.P., Lewandowski, J.J., and Jackson, M.R. (1997). "Refractory Metal Intermetallic *In-Situ* Composites for Aircraft Engines", JOM, August, pp. 44-47.
19. Lewandowski, J.J. and Zinsser, W., (1998). "Effects of R-ratio on Fatigue Crack Growth on Nb-Si (ss) and Nb-10Si *In-situ* Composites", Metall. Trans. A., 29A, pp. 1749-1757.
20. Zinsser, W. and Lewandowski, J.J. (1998). "Fatigue Crack Growth in Nb-10Si Composites", Scripta Metall. 28, 12, pp. 1775-1780.
21. Lewandowski, J.J. (1998). "Effects of the Addition of Toughening Ligaments on the Fatigue of Composites", in Fatigue '99, (X.R. Wu and Z.G. Zhang, eds.) EMAS, 1998, in press.
22. Zinsser, W.A., Solov'yev, S. and Lewandowski, J.J. (1998) "Fracture and Fatigue of Refractory Metal Intermetallic Composites", in Intermetallics VIII, Vol. 552, (E. George, M. Yamaguchi, and M. Mills, eds.), MRS, Pittsburgh, PA, 1998, in press.
23. Lowhaphandu, P. and Lewandowski, J.J. (1998), Effects of Heat Treatment and Cu-Infiltration on Toughness and Fatigue Crack Growth of Porous Steels, *Metall. Trans. A.*, press.
24. Lowhaphandu, P. and Lewandowski, J.J. (1998), Fracture Toughness and Notch Toughness of Bulk Metallic Glass, *Scripta Metall*, **38**, 12, pp. 1811-1817.
25. Zwonitzer, S.A., Rozak, G. and Lewandowski, J.J. (1998) "Effects of Rolling Temperature and Reduction on Microstructure and Tensile Properties of Thick Plate, P/M Mo", In Mo and Mo Alloys, (A. Crowson, J.A. Shields, P.R. Subramainan and E.S. Chen, eds.) TMS-AIME, Warrendale, PA, in press.

6b.Acknowledgements

The author would like to acknowledge a number of students who have contributed to this work: J. Kajuch, J. Short, J.D. Rigney, W.A. Zinsser, S. Solv'vev, L. Leeson, P. Lowhaphandu. The refractory metal systems were supplied by Cabot, WPAFB, and General Electric CRD, with funding from AFOSR F-49620-96-1-0164 with Drs. C.H. Ward and S. Wu as contract monitors. Useful discussions and supply of some materials by M. Mendiratta, P.R. Subramanian, B.P. Bewlay, M.R. Jackson, and D. Dimiduk are also gratefully acknowledged.

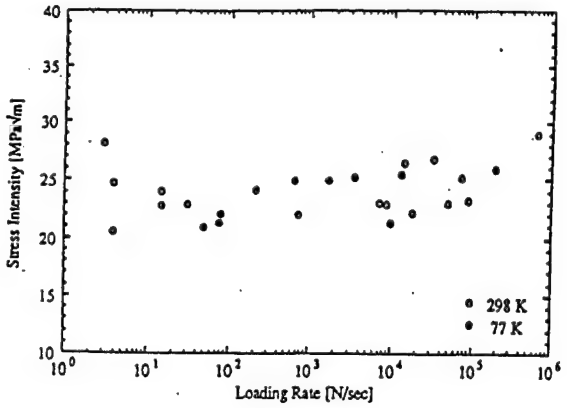

Figure 1. Effects of loading rate and test temperature on toughness of Nb-10Si (3).

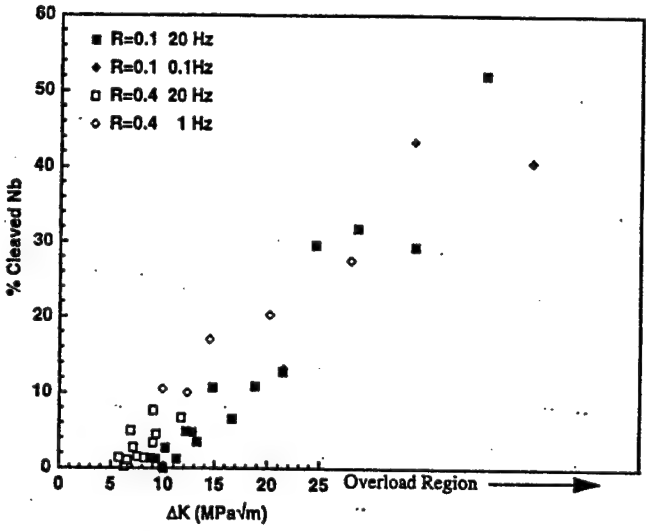

Figure 2. % Cleavage of Nb_p vs ΔK

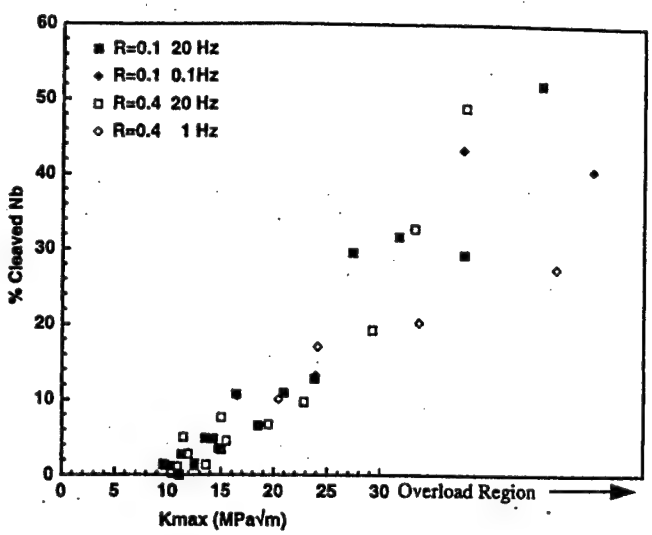

Figure 3. % Cleavage of Nb_p vs K_{max}

Material	Grain Size (μm)	R-ratio	ΔK_{th} (MPa$\sqrt{m}$)	Paris Law Exponent, m
Nb (pure)	15(18)	0.05(18)	10.1(18)	4.2(18)
	15(18)	0.4(18)	7.1(18)	6.6(18)
	63	0.1	10.7	2.9
	63	0.4	6.6	N/A
	135	0.1	10.2	2.8
Nb-1% Zr	66	0.1	11.8	4.9
	66	0.4	7.6	N/A
	165	0.1	12.3	3.4
	165	0.4	8.6	N/A
Nb-Si(ss)	135	0.1	12.9	2.3
	135	0.4	8.1	2.5
Nb-10Si		0.05	12.0	N/A
		0.1, 0.1, 0.1	9.0, 8.4, 9.7	5.3, 6.5, 6.6
		0.4	5.6	N/A
		0.6	6.5	N/A
		0.8	4.4	N/A
DS Nb-Si-Hf-Cr-Al-Ti		0.1	8.5	2.9

TABLE I – Fatigue Crack Growth Results for Nb, Nb Composites

Nb Silicide-Based *In Situ* Composites: Oxidation Behavior

Mel Jackson, Bernard Bewlay & Reed Corderman
GE Corporate Research & Development
Schenectady, NY 12301

1.0 Objectives and Approach

Nb-based silicide composites have been identified as potential high-temperature blade alloys, based on melting range, oxidation, toughness and strength. Although oxidation behavior of these alloys was substantially better than binary Nb-Si composites, they fall far short of superalloy behavior, considering this behavior must be achieved at much higher temperatures, approaching 2400F. The objective of the present effort is to determine if the oxidation resistance of silicide systems can be improved. The approach is an iterative one, with this being the first of four iterative stages, with the goal for each stage to improve behavior over the previous iteration. Goals for the iterations, starting from current behavior as baseline, are 3X baseline, 9X, 27X, and 81X baseline.

2.0 Research Progress and Highlights

Oxidation studies of Nb-based composite alloys modified with large concentrations of Ti and lesser concentrations of Hf were reported [1] for 1000, 1200 and 1400C exposures. The alloys containing aluminides had virtually no resistance at any temperature, but those with Laves phase (Cr_2M) were reasonably resistant, and those with silicide were within a factor of five of the Laves phase (Figure 1). To try to improve the resistance of the much stronger and tougher silicide systems, we added more Cr to develop some fraction of Laves phase in the metal-silicide structures.

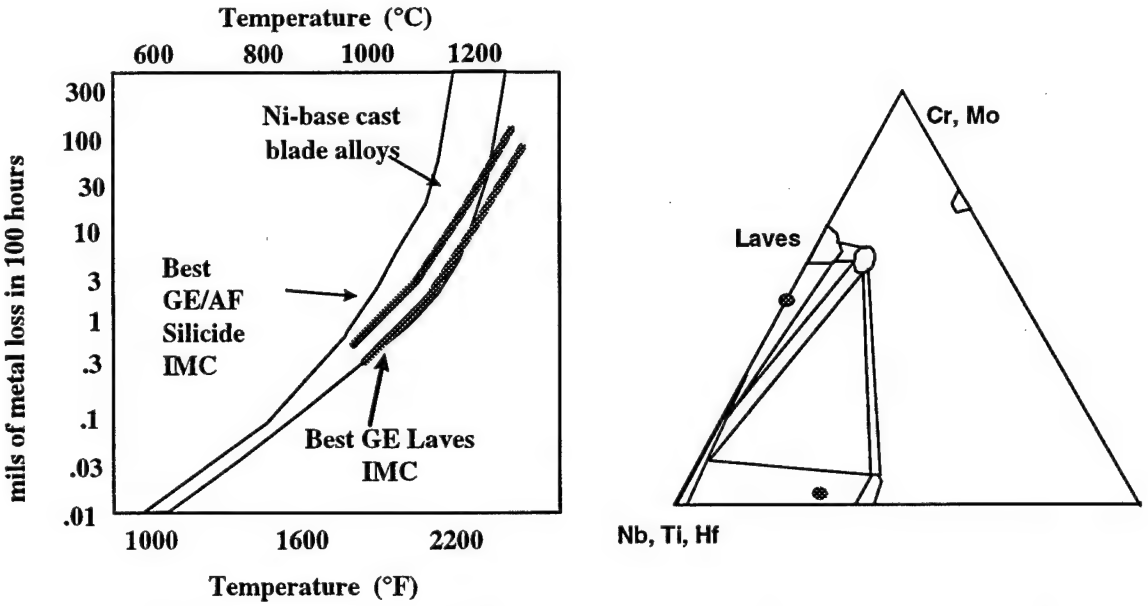

Figure 1: Earlier research showed that for Nb-based materials, the Laves composites were better in oxidation than the Silicide composites.

Oxidation testing of the Laves-containing metal-silicide alloy is shown in Figure 2 for exposures at 1204C and 1315C (2200F and 2400F), compared to a complex metal-silicide material [2]. To be useful at 1315C surface temperatures with the same robustness as superalloys at their current surface temperatures (~1150C), the oxidation behavior of the silicide alloy must be improved about 80-fold. The loss of material in 100 hours measured metallographically for the Laves-containing material was ~40 microns at 1204C and 425 microns at 1315C. These values represent improvements over the Figure 1 and 2 silicide examples of approximately 4X and 6X, at 1204 and 1315C, respectively. This is shown schematically in Figure 3. Another 16X improvement still remains.

However, the addition of Cr reduces the volume fraction of metal in the structure, and this is expected to reduce the fracture toughness of the material system. To develop a better understanding of the influence of all of the major elements, Nb, Ti, Hf, Cr, Al and Si, we developed a matrix of alloys for evaluation (a quarter factorial design of experiments). This would allow us to determine which elements and in what concentrations could be traded for Cr, without damaging oxidation behavior but retaining high fracture toughness.

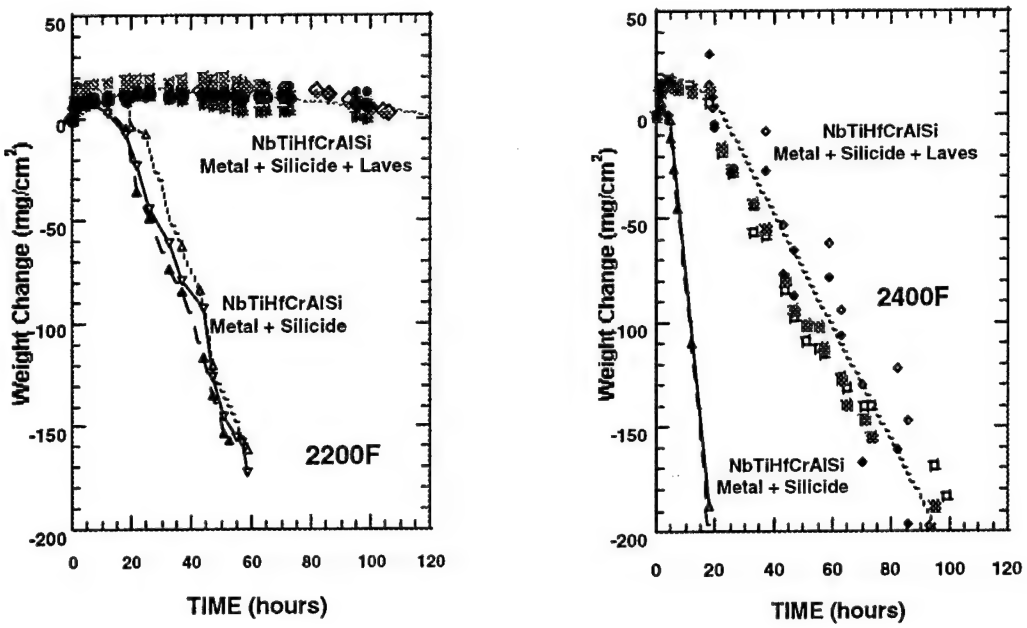

Figure 2: Comparison of 2200F and 2400F oxidation resistance of a high-Cr Nb-Ti-Hf-Cr-Al-Si composite to the baseline alloy behavior.

Figure 4 shows the results of statistical analysis of the oxidation testing at 1204C for the eight quarter-factorial DoE alloys. The largest positive effect came from increasing Si, while Cr and Ti had nearly equivalent effect, and Al had a still smaller effect. There was almost no influence of Hf on 1204C oxidation.

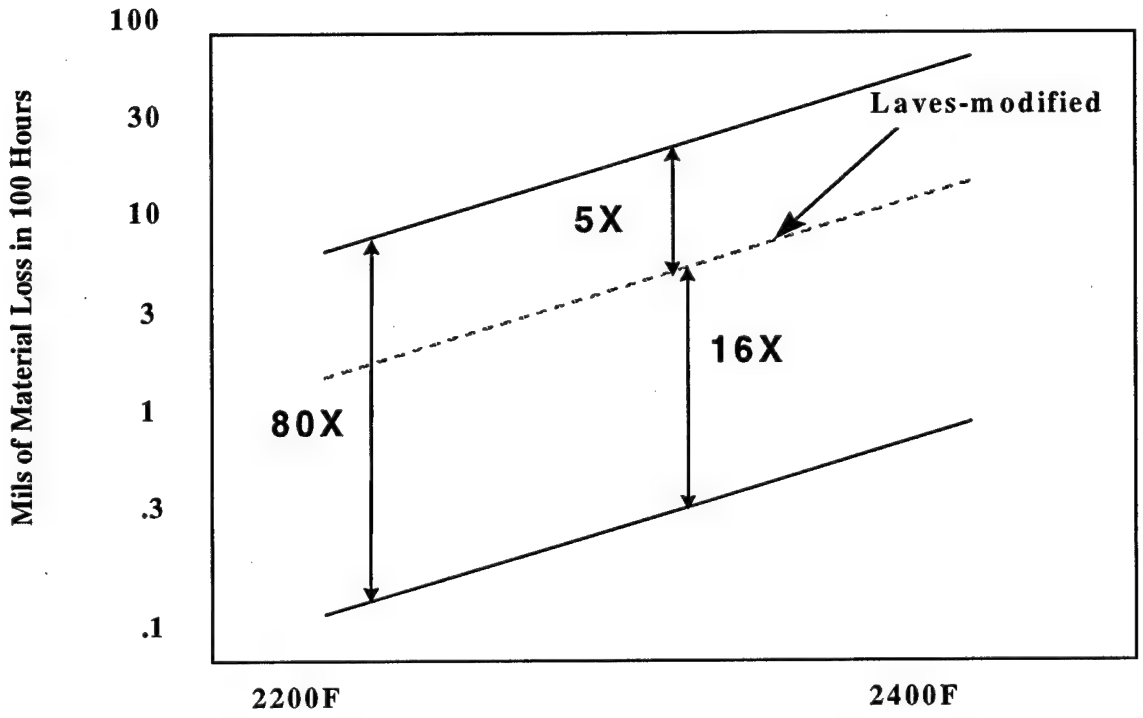

Figure 3: The improvement in oxidation behavior for the Laves-containing silicide composite leaves a further 16X improvement to be achieved.

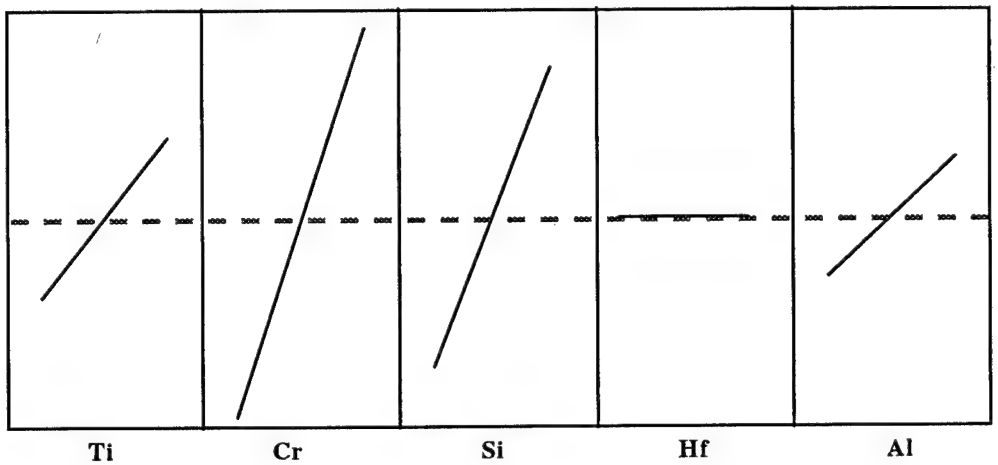

$$\Delta wt/A]\ 1204C = f\,(aTi + aCr + 1.5aSi + 0.5aAl)$$

Figure 4: The relative influence of the major alloying elements on 1204C oxidation behavior. Vertical axis is weight change per unit area.

A similar analysis was conducted for oxidation at 1315C, with the functionality that described the behavior being:

$$\Delta wt/A]\ 1315C = f(\ 0.8bTi + b(Cr + Si + Al) - b/3\ Hf\ ).$$

Here, Hf appeared to have a slightly negative influence on oxidation at 1315C.

The equations for 1204C and 1315C oxidation indicate that there should be compositional trades for Cr that will allow for the desired reduced oxidation degradation.

3.0 Critical Issues

Of course, as we have noted, achieving improved oxidation resistance is critical. However, this must be achieved without substantially degrading other properties, such as fracture toughness, creep resistance, and fatigue response. Producing materials with the required balance of properties remains a very difficult task. Another issue will be achieving stability in thin-walled airfoils, since the turbine blade designs currently envisioned have hot-wallthicknesses of 0.3-1.0mm. Within that thickness must fit not only the structural composite alloy, but also an internal and an external protective coating. We have been working with Movchan and Marinsky of the International Center for Electron Beam Technology (Kyiv) to begin developing some experience with deposition of such silicide composites and the coatings demanded by the service conditions. Figure 5 shows a four-element Nb-Ti-Hf-Si laminate composite fabricated at ICEBT. The possibility of tailoring the through-thickness chemistry to produce coatings, varying properties, etc., can be done directly by the EB processing.

Nb-Ti-Si-Hf Micro-laminate Made for GECRD by ICEBT

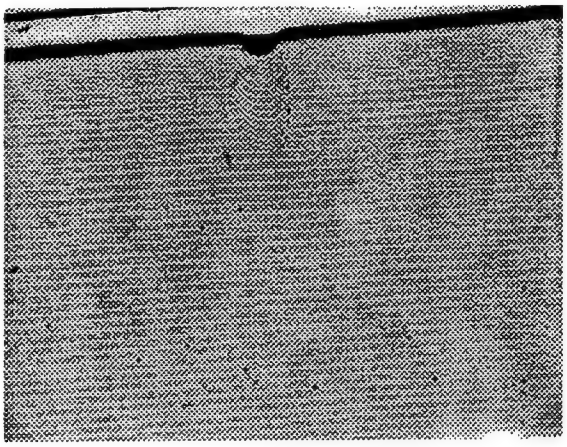

- **Graded Structures**
- **Single-Phase Surfaces (such as Laves)**
- **In situ coatings deposition**

Figure 5: An example of a Nb-Ti-Hf-Si microlaminate produced at ICEBT-Kyiv.

4.0 References

[1] M.R. Jackson, R.G. Rowe and D.W. Skelly, MRS Symp Proc 364, 1995, pp. 1339-1344.
[2] M.R. Jackson, B.P. Bewlay, R.G. Rowe, D.W. Skelly and H.A. Lipsitt, JOM 48-1, 1996, pp39-44.

1. METAL/SILICIDE MICROLAMINATES: STRESS, STRENGTH, AND STABILITY

T. P. Weihs, D. Van Heerden, A. J. Gavens, C.H. Shang, and T. Foecke*

Department of Materials Science and Engineering, The Johns Hopkins University, Baltimore, Maryland, 21218-2689
*Materials Science and Engineering Laboratory, National Institute of Standards and Technology, Gaithersburg, MD 20899

2. RESEARCH OBJECTIVES AND APPROACH

A number of metal-silicide alloys are currently being evaluated for use at high temperatures, beyond those presently attainable with nickel based superalloys. One such alloy, that holds considerable promise, consists of BCC Nb and the tetragonal line compound Nb_5Si_3. Both phases are chemically stable to temperatures exceeding 1660°C, and the Nb contains only a limited solubility of Si. In this binary alloy, the Nb phase provides room temperature toughness, and the Nb_5Si_3 phase provides high temperature strength and creep resistance.

Metal silicide alloys such as Nb/Nb_5Si_3 can be fabricated into several different composite geometries using casting, high temperature extrusion, or physical vapor deposition. This study focuses on microlaminated composites which have potential application in future turbine blades. Microlaminates have a number of advantages over other composite fabrication geometries, including the fact that they can be produced by physical vapor deposition and thus readily manufactured into complex, plate-like geometries. Furthermore, physical vapor deposition easily produces the very thin walls (2mm) that are desired in future turbine blades. The simple and controlled geometry of microlaminates also makes them an ideal model system for studying many structure-property relationships in metal/silicide composites.

Our initial goal with this study was to determine the microstructural and morphological stability of microlaminated Nb/Nb_5Si_3 materials at elevated temperatures. In order to do this we first developed a technique for preparing mechanically robust Nb/Nb_5Si_3 microlaminates. We then determined the mechanisms by which their microstructures (and hence properties) degrade at elevated temperatures by performing a series of extended anneals. As part of this study, we also investigated their room temperature mechanical properties, and are currently investigating their high temperature mechanical properties.

3. RESEARCH PROGRESS AND HIGHLIGHTS

3.1. Fabricating Nb/Nb_5Si_3 Microlaminates

Several different methods were investigated for fabricating Nb/Nb_5Si_3 microlaminates. In the first route we deposited thick layers of Nb and thin layers of Si, and then annealed the samples to form the silicide layer via diffusion. However, on annealing, gross delamination occurred due to the inter-layer stresses developed during the formation of the silicide. Thus we tried a more direct processing method in which we directly deposited layers of Nb and amorphous Nb-Si from either a composite target, or via co-deposition from a Nb and a Si target. The silicide layers then crystallized into the desired Nb_5Si_3 phase on annealing at 1200°C.

The microstructure of an annealed sample is shown in figure 1. The layers are continuous, and relatively flat with little evidence of grooving or roughness and no signs of growth defects.

Further, there is no silicide phase in the Nb grains. Both the Nb grains and the silicide grains are nearly equiaxed with the Nb grains spanning their full layer thickness and the Nb_5Si_3 grains roughly 300nm in diameter. As will be discussed later, annealing at or above 1500°C is required to significantly increase the grain size of the silicide phase.

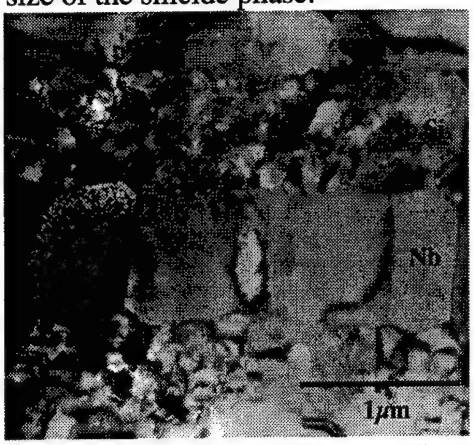

Figure 1: TEM cross-section of a Nb/Nb_5Si_3 microlaminate after annealing at 1200°C for 3 hours showing the discrete layering, sharp interfaces, and lack of second phase formation in the Nb layers.

3.2. High temperature microstructural stability

The Nb-Si equilibrium binary phase diagram shows that the Nb and Nb_5Si_3 phases should be chemically stable to a temperature of 1660°C. To determine the morphological stability of the laminates a series of anneals were performed at temperatures up to 1600°C.

The layering exhibited remarkable stability, with little evidence of breakdown after annealing at 1400°C for 100 hours (figure 2). Furthermore there was no evidence of significant grain boundary grooving. This grooving arises from imbalances in the interfacial versus grain boundary energies, and it can pinch-off grains, ultimately destroying phase continuity in the layers. The limited grooving that was present was more pronounced into the Nb layers (i.e. along the Nb grain boundaries) than into the silicide layers. This was expected based on bond enthalpies and is advantageous in that the more creep resistance silicide layers remain continuous. Annealing at 1500°C for 3 hours produced significant grain growth in the silicide, but still did not significantly alter the grooving into either layer.

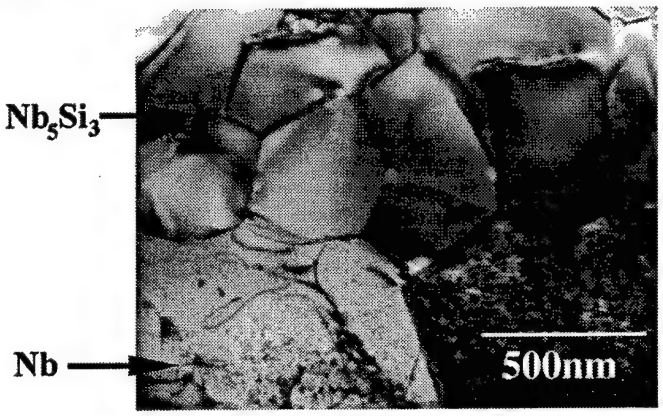

Figure 2: TEM cross-section of a Nb/Nb_5Si_3 interface in a microlaminate which was annealed at 1400°C for 100 hours. Notice the sharpness of the interface, and the lack of significant interfacial grooving.

Annealing at temperatures above 1200°C did, however, result in a loss of Si from the sample by sublimation. The loss of Si could be suppressed by annealing in a Si-rich environment at 1400°C,

but proved difficult to suppress at and above 1500°C. The loss of Si manifested itself in the thinning of the outermost silicide layer, in the formation of large pores in the inner silicide layers and, in extreme cases (at 1600°C), blistering of the sample surface. It should be noted, however, that all of our anneals were done in vacuum, and the kinetics of Si sublimation should be drastically reduced by annealing in an Ar atmosphere. Alternatively, surface alloying could be used to form a stable, non-volatile surface silicide.

3.3. Room temperature properties:

In order to determine the room temperature properties of the microlaminates tensile tests were performed on a series of the microlaminates. Two different alloy compositions, one with equal layer thicknesses, and another with 14 volume % Nb_5Si_3 were studied. The measured fracture strength of the laminates ranged from 563MPa to 972MPa, increasing with volume fraction of Nb (figure 3). Similar strengths and trends were reported previously for bulk Nb/Nb_5Si_3 alloys. Additional tests are underway.

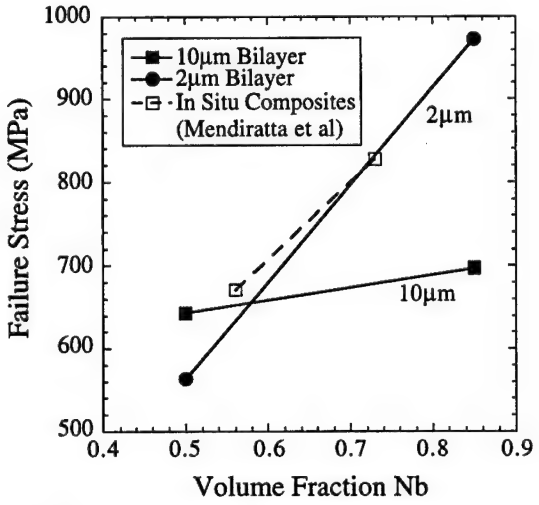

Figure 3: Failure Strength of Nb/Nb_5Si_3 microlaminates. Note that strength tends to increase with volume fraction of Nb.

Based on the coefficients of thermal expansion (CTE) for the two phases, it was suspected that substantial residual stresses would be present within the layers following high temperature anneals. It was also thought that these stresses might influenced the measured mechanical properties. The known CTE's suggest that on cooling from high temperatures the Nb layers will be in residual tension and the silicide layers in residual compression. As failure of the laminate is likely to be controlled by fracture of the silicide layers, higher residual compressive stresses in the silicide layers should raise the failure stress of the composite. The trend in figure 3 supports this hypothesis. The residual thermal stresses in our Nb/Nb_5Si_3 microlaminates were characterized using a $\sin^2(\psi)$ analysis and range in magnitude from 100 to 500MPa.

The stress-displacement curves for most of the microlaminates foils were linear to failure, suggesting limited plasticity. Examination of the fracture surfaces indicates that the Nb_5Si_3 layers fractured in a brittle manner for all of the foils. Interestingly, the fracture characteristics of the Nb layers depends on layer thickness. The Nb layers which were 1μm thick failed in a relatively ductile manner, while thicker Nb layers displayed a quasi-cleavage like failure with the fracture characteristics occurring primarily normal to the layering. The difference in fracture mode is

attributed to differences in the constraint of the Nb - plane stress for thin layers of Nb and plane strain for thick layers.

For all of the microlaminates, cracks observed in the Nb_5Si_3 did not propagate into the Nb and typically did not approach the interface of the Nb and Nb_5Si_3 layers. Cracks that did cross the interface were blunted upon entering the Nb layers. In addition, no interfacial delamination was observed in any of the specimens.

4. POTENTIAL STRUCTURAL APPLICATIONS AND ENGINEERING ISSUES

The major structural application envisaged for metal/silicide microlaminates is a thin plate, high temperature component such as the thin walls (2mm) of a turbine blade. These composite materials are also ideally suited for producing thick, structural coatings for other high temperature applications.

One of the major engineering challenges in the development of these microlaminates is alloy development. Alloying elements must be found that will suppress the sublimation of Si at elevated temperatures. One likely solution is the formation a stable, passivating outer coating on the microlaminate. Alloying will also be required to suppress oxidation of these Nb based systems at elevated temperatures.

Another engineering challenge is the high-rate deposition of microlaminates with complex geometries. The ability to control laminate uniformity over these geometries will be difficult but critical and the ability to vary composition and layering through the thickness of the laminate will also be desirable. Significant development work will be required. Furthermore, if the microlaminates are to be used as coatings, interfacial bonding to the substrate and thermal mismatch with the substrate will also present considerable engineering concerns.

5. CRITICAL SCIENTIFIC ISSUES AND CHALLENGES

There are several critical scientific issues associated with the development of metal/silicide microlaminates for high temperature, structural applications. One is the influence of alloying on the interfacial energies, and therefore the morphological stability of the phases and layering. Adding elements such as Hf or Ti to enhance oxidation resistance may result in interfacial or grain boundary energies that promote grain boundary grooving and layer pinch-off. Experimental investigations of layer breakdown will be necessary, and measurements and predictions of interfacial energies would be very useful.

Another important scientific aspect (currently being investigated) is the dependence of the creep resistance of the microlaminates on the layer thicknesses, grain sizes, and volume fractions of the metal and silicide phases. Little is know as to how each of these factors individually and collectively determine the creep rate of laminated composites. Basic creep studies that identify the critical and controlling mechanisms are necessary.

As discussed in section 3.3. the room temperature mechanical properties of the microlaminates can be strongly influenced by residual thermal stresses. In the Nb/Nb_5Si_3 system the mismatch in CTE's is advantageous in that the silicide is drawn into compression at room temperature, thereby raising the stresses that must be applied to fracture the silicide layers under tension. Since these stresses can be significant, in both Nb/Nb_5Si_3 microlaminates and in situ composites, they should be considered when modeling room temperature mechanical behavior. They should also be considered when alloying so as to enhance the CTE mismatch and not reduce it.

The fracture surfaces of the microlaminates clearly show a strong dependence of the metallic

phase's plasticity on its layer thickness. In simplest terms, the thin layers have less constraint and fail in ductile manner due to a plane stress loading. The thicker layers fail in a brittle manner due to more constraint and a plane strain loading. However, layer thickness also affects the strength of the layers with thinner layers have a greater resistance to dislocations motion. Furthermore, the ratio of layer thicknesses can alter the residual thermal stresses. Thus, a number of issues must be considered when trying to model or predict the plastic work of metallic laminates as they bridge crack faces during fracture. Since the plastic work involved in this failure process is critical to the toughening of these composites, a full understanding of the multiple issues is imperative.

Lastly, most of the scientific issues described above apply to in situ metal/silicide composites as well as microlaminates composites. And, since the microlaminates provide such a simple and well controlled sample geometry, they should be employed more routinely when investigating basic structure-property relationships in metal/silicide alloys.

6. PUBLICATIONS AND PRESENTATIONS:

Publications:

1. D. Van Heerden, A. J. Gavens, T. Foecke, and T. P. Weihs, "Evaluation of Vapor Deposited Nb/Nb_5Si_3 Microlaminates," Mater. Sci. & Eng. A, (in press).

2. D. Van Heerden, C.H. Shang, A. J. Gavens, and T. P. Weihs, "Characterization of Microstructure Property Relationships in Microlaminate Nb/Nb_5Si_3 Composites," in proceedings of The Fifth International Conference on Composites Engineering, Las Vegas, NV, July 5-11(1998) 909-910.

3. M. E. Reiss, C. M. Esber, D. Van Heerden, A. J. Gavens, M. E. Williams, and T. P. Weihs, "Self-Propagating Formation Reactions in Nb/Si Multilayers," Mater. Sci. & Eng. A, (in press).

4. A.J. Gavens, D. Van Heerden, T. Foecke, and T.P. Weihs, "Fabrication and Characterization of Nb/Nb_5Si_3 Microlaminates," submitted to Metall. Trans, (1998).

5. C.H. Shang, A. J. Gavens, D. Van Heerden, and T. P. Weihs, "Characterizing Residual Thermal Stresses and Bending Stresses in Nb/Nb_5Si_3 Microlaminate Composites," to be submitted to Acta Mater., in January 1999.

Presentations:

1. A.J. Gavens, D. van Heerden, and T.P. Weihs, *Formation of Nb/Nb_5Si_3 Microlaminates by Sputter Deposition of Nb and Amorphous Nb-Si*, presented at the 2nd International Symposium on Structural Intermetallics, Seven Springs, PA, September 21-25, 1997.

2. D. Van Heerden, A. J. Gavens, T. Foecke, and T. P. Weihs, *Evaluation of Vapor Deposited Nb/Nb_5Si_3 Microlaminates*, presented at the Engineering Foundation Conference on High Temperature Structural Silicides, Hyannis, MA, May 25-29, 1998.

3. D. Van Heerden, C.H. Shang, A. J. Gavens, and T. P. Weihs, *Characterization of Microstructure Property Relationships in Microlaminate Nb/Nb_5Si_3 Composites*, presented at the Fifth International Conference on Composites Engineering, Las Vegas, NV, July 5-11, 1998.

4. T. P. Weihs, *Stable Microlaminates and Reactive Nanolaminates: the Fabrication and Characterization of Layered Foils with Structural Applications,* presented at WPAFB, Materials Directorate, Dayton, OH, July 16, 1998.

5. M. E. Reiss, C. M. Esber, D. Van Heerden, A. J. Gavens, M. E. Williams, and T. P. Weihs, *Self-Propagating Formation Reactions in Nb/Si Multilayers*, presented at the Engineering Foundation Conference on High Temperature Structural Silicides, Hyannis, MA, May 25-29, 1998.

6. A. J. Gavens, D. Van Heerden, C.H. Shang, T. Foecke, and T. P. Weihs, *Nb/Nb_5Si_3 Microlaminates for High-Temperature Structural Applications,* Fall TMS Meeting, Chicago, IL, October 11-15, 1998.

HIGH TEMPERATURE OXIDATION OF $Mo(Si, Al)_2$ AND LOW TEMPERATURE SYNTHESIS OF RELATED HIGH TEMPERATURE INTERMETALLICS BY SOLID/LIQUID REACTION

Toshio MARUYAMA

Department of Metallurgical Engineering
Tokyo Institute of Technology
2-12-1, O-okayama, Meguro-ku, Tokyo 152, JAPAN

1. OBJECTIVES

Intermetallics of refractory metal silicides/aluminides exhibit very high melting temperature and are brittle in nature. These materials will be fabricated by powder metallurgical technique as same as for ceramic materials. The possibility of more economical fabrication of potential high temperature intermetallics is one of the issues to be considered in the alloy design. Incorporation of aluminium offers a low temperature fabrication of high temperature silicides because one can utilize the liquid aluminium as a reactant.

Molybdenum disilicide is a potential material with an excellent oxidation resistance at very high temperature. Substitution of aluminium for silicon in $MoSi_2$ ($C11_b$) gives $Mo(Si_{1-x}, Al_x)_2$ (C40). High temperature oxidation of $Mo(Si_{1-x}, Al_x)_2$ was studied up to 2000 K and the material degradation due to so called "pesting" was also examined around 800 K.

The phase diagram of Mo-Si-Al system shows the formation of $Mo(Si_{1-x}, Al_x)_2$ with a fixed composition if Mo is dipped in Si-saturated aluminium melt. The kinetics of growth rate of $Mo(Si_{1-x}, Al_x)_2$ on Mo and microstructure observation of the $Mo(Si_{1-x}, Al_x)_2$ layer indicates that Al-Si melt permeates the product layer through very thin channels between grains and thin layer of the melt contacts Mo. Mo dissolves into the melt and precipitates as $Mo(Si_{1-x}, Al_x)_2$.

In the case of Nb dipped in an Al-Si melt, the mechanism of the formation of intermetallics is basically as same as in the case of Mo. When Nb is dipped in Si-saturated aluminium melt, the product is $Nb(Si, Al)_2$ (C40). A particular composition of Al-Si melt presents the repeated layer growth of $Nb(Si, Al)_2$ (C40) and $Nb(Al, Si)_3$ ($D0_{22}$). The competition between supply of the Al-Si melt to the Nb surface and the rate of precipitation of the intermetallics gives the occirative layer structure.

The analysis of the reaction process gives useful information to design the low temperature fabrication of high temperature silicides/aluminides.

2. High temperature oxidation of $Mo(Si_{1-x}, Al_x)_2$.

High temperature oxidation of $Mo(Si_{1-x}, Al_x)_2$ ($0.14<x<0.37$) gave a protective Al_2O_3 scale at temperature below 1868 K of which is the eutectic temperature in the SiO_2-$3Al_2O_3 \cdot 2SiO_2$ system. Above the eutectic temperature, the scale was a liquid of SiO_2-Al_2O_3 with the Al_2O_3 content being richer than the eutectic composition. The cooling of the hypereutectic liquid scale suppresses the formation of β -

crystobalite and gives amorphous scale with an excellent adherence to intermetallics.

3. Pesting of $Mo(Si_{1-x}, Al_x)_2$.

The disintegration of $MoSi_2$ (pesting) due to oxidation is severe around 773 K. The addition of Al markedly reduces pesting. Amorphous Mo-Si-Al-O forms in initial cracks and voids. This amorphous oxide is probably more plastic than the amorphous Mo-Si-O formed on $MoSi_2$ and decreases the stress generation at the crack which leads to disintegration.

3. Dipping of Mo in Si-saturated Al melt at temperatures between 1000 and 1200 K

The phase diagram of Mo-Si-Al system shows the formation of $Mo(Si_{1-x}, Al_x)_2$ with a fixed composition if Mo is dipped in Si-saturated aluminium melt. The kinetics of growth of $Mo(Si_{1-x}, Al_x)_2$ on Mo obeyed a linear rate law and microstructure observation of the $Mo(Si_{1-x}, Al_x)_2$ layer indicates that Al-Si melt permeates the product layer through very thin channels between needle-like grains. $Mo(Si_{1-x}, Al_x)_2$ considered to form by dissolution of Mo into the melt and precipitate on $Mo(Si_{1-x}, Al_x)_2$. The layer formed around the corner of Mo plates with a large curvature has many cracks due to uni-directional formation of $Mo(Si_{1-x}, Al_x)_2$. In corporation of Cr in the melt gave the crack free product layer.

4. Dipping of Nb in Si-Al melt at 1025 K.

An Nb plate was dipped in Si-Al melts at 1025 K. The product layer in Si-saturated Al melt consisted of $Nb(Si_{0.9}, Al_{0.1})_2$ (C40) and that in Al rich melt (about 90 mol% Al) was a single phase of $Nb(Al_{0.98}Si_{0.02})_3$ ($D0_{22}$). A melt, whose composition was about 80mol%Al-20mol%Si, gave the repeated layered product of C40 and $D0_{22}$. This structure arises from the competition between the supply of the Al-Si melt to the Nb surface and the rate of precipitation of the intermetallics. The composition of the melt at the Nb/product interface changes because the supply of the Al-Si melt through the product layer is not rapid enough and the consumption of Al or Si is largely differnt whether C40 or $D0_{22}$ forms. This phenomenon offers a way to fabricate a composite intermetallics.

Effects of alloying elements on plastic deformation of single crystals of $MoSi_2$

H. Inui, K. Ishikawa and M. Yamaguchi

Department of Materials Science and Engineering, Kyoto University
Sakyo-ku, Kyoto 606-8501, Japan.

1. Introduction

There has been a growing interest in transition-metal disilicides as possible candidates for very-high-temperature structural applications because of their high melting temperatures, relatively low densities and good oxidation resistance. Of these disilicides, $MoSi_2$ with the $C11_b$ structure has been regarded as the most promising candidates for such applications [1-3]. However, monolithic $MoSi_2$ exhibits only a modest value of fracture toughness at low temperatures and inadequate strength at high temperature. As a natural consequence, many recent studies on the development of $MoSi_2$-based alloys have focused on the improvement of these poor mechanical properties through forming composites with ceramics and other silicides. Thus, $MoSi_2$-based alloys will be of multi-component and of multi-phase in their practical usage. From this perspective, it is important to investigate effects of alloying elements on the plastic behavior of $MoSi_2$.

In the present study, we have chosen V, Cr, Nb and Al that form a disilicide with the C40 structure and W and Re that form a disilicide with the $C11_b$ structure as alloying elements to $MoSi_2$, and investigated the deformation behavior of single crystals of $MoSi_2$ containing these elements. The crystal orientations investigated were the [0 15 1] orientation, in which slip on {110)<111] is operative, and the [001] orientation, in which the highest strength is obtained.

2. Alloying strategy and specimens

The atomic arrangements on (110) for the $C11_b$ structure is shown in Fig. 1. In this (pseudo-) hexagonally-arranged $TMSi_2$ layer, a transition-metal (TM) atom is coordinated by six Si atoms whereas a Si atom is coordinated by three transition-metal atoms and three Si atoms and it is this atomic arrangement that is the most characteristic feature commonly observed for transition-metal disilicides with $C11_b$, C40 and C54 structures. The generation of the three different structures is accomplished by changing the stacking order of the $TMSi_2$ layers; the $C11_b$, C40 and C54 structures are based respectively on the AB, ABC and ADBC stacking sequences. Thus, {110)<111] slip in the $C11_b$ structure, (0001)<11$\bar{2}$0> slip in the C40 structure and (001)[110] slip in the C54 structure are all equivalent. Dislocations belonging to these slip systems are known to dissociate into two-coupled partials separated by a stacking fault. For example, 1/2<111] dislocations in the $C11_b$ structure dissociate into two identical 1/4<111] partials separated by a stacking faults. The stacking across the fault is ABC and resembles the stacking of (0001) in the C40 structure. Hence, the addition of elements that form a C40 disilicide may cause the energy difference between $C11_b$ and C40 structures to decrease so that the energy of the stacking fault would also be decreased. From this point of view, we may expect that the deformability at low temperatures increases upon alloying

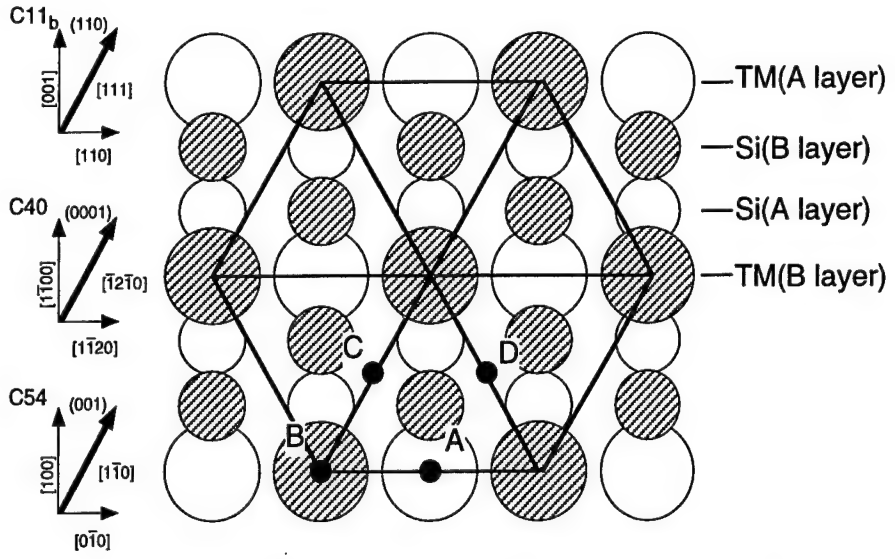

Fig.1 Atomic arrangements in the TMSi2 layers and crystallographic directions are given with respect to C11b, C40 and C54 structures.

$MoSi_2$ with elements that form a C40 disilicide. However, we have found that the solid solubility of these elements in $MoSi_2$ is rather limited (at most, several atomic %). Thus we prepared single crystals with compositions of $(Mo_{0.97}V_{0.03})Si_2$, $(Mo_{0.97}Cr_{0.03})Si_2$ and $(Mo_{0.97}Nb_{0.03})Si_2$. The solid solubility for Al in $MoSi_2$ seems to be much higher than those for V, Cr and Nb, and the composition of $Mo(Si_{0.97}Al_{0.03})_2$ was prepared for the Al addition.

W and Re have been believed to form a complete $C11_b$ solid-solution with $MoSi_2$. In this case, we may expect that the increased high-temperature strength is achieved through a solid-solution hardening mechanism, since we can make a large amount of additions of these elements. For this purpose, we prepared single crystals of $(Mo_{1-X}W_X)Si_2$ with X=0.03, 0.25. 0.5 and 0.75 as well as those of $(Mo_{0.97}Re_{0.03})Si_2$. Although single crystals of $(Mo_{0.97}Re_{0.03})Si_2$ have the $C11_b$ structure, we have recently found that the disilicide formed with Re is an off-stoichiometric (defective) compound formulated to be $ReSi_{1.75}$. The compound $ReSi_{1.75}$ has a monoclinic crystal structure with an ordered Si vacancy arrangement in the parent $C11_b$ lattice at room temperature and exhibits a twinned microstructure. The details of crystal structure assessment for $ReSi_{1.75}$ will also be given in the conference.

3. Effects of alloying elements that form a C40 disilicide

The yield stresses obtained for binary and V-, Cr-, Nb- and Al-bearing $MoSi_2$ single crystals with the [0 15 1] orientation are plotted in Fig. 2 as a function of temperature. As seen in Fig. 2, plastic deformation is possible even at room temperature for binary $MoSi_2$ and all the ternary disilicides. For this orientation, the yield stress decreases with increasing temperature at low and high temperatures, while at intermediate temperatures it increases anomalously with increasing temperature. In the anomalous temperature range, a serrated flow is usually observed to occur in the stress-strain curves and thus, the anomaly has been attributed to the so-called Portevin-Le Chatelier effects in which interaction between dislocations and point defects (impurities and vacancies) plays a role [3]. The extent of the

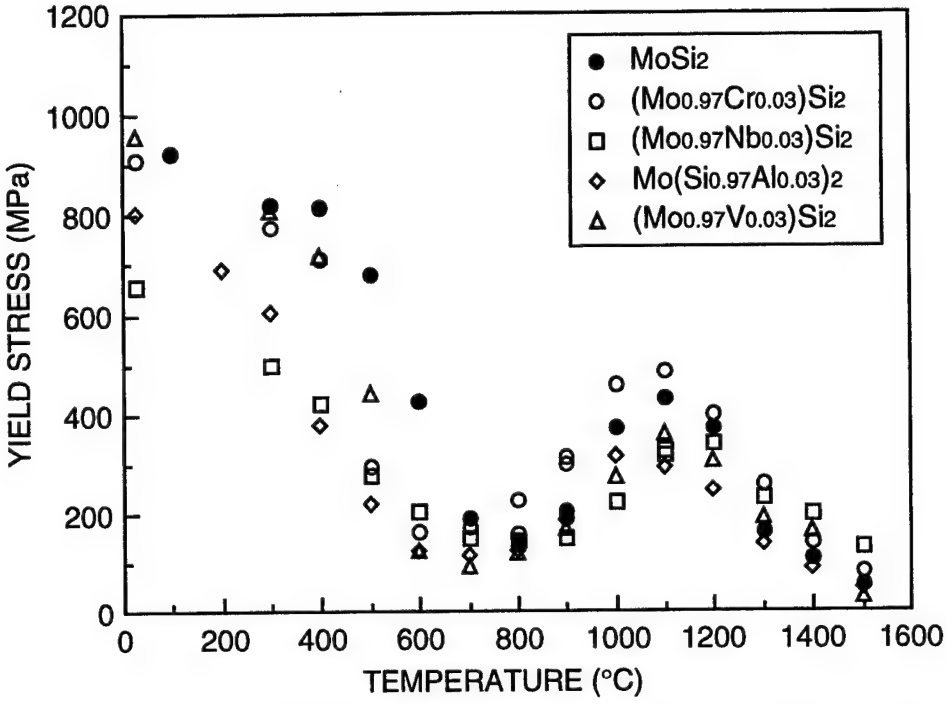

Fig.2 Temperature dependence of yield stress obtained for binary and some ternary $MoSi_2$ single crystals with the [0 15 1] orientation.

anomaly as well as the anomalous temperature range vary with alloying elements. The transition temperatures marking the anomalous yield behavior regimes (i.e. the bottom and peak temperatures) are 800 and 1000°C for $MoSi_2$ and $(Mo_{0.97}Nb_{0.03})Si_2$, 700 and 1100°C for $(Mo_{0.97}Cr_{0.03})Si_2$ and are 700 and 1000°C for $(Mo_{0.97}V_{0.03})Si_2$ and $Mo(Si_{0.97}Al_{0.03})_2$ respectively. When compared to the binary counterpart, the extent of anomaly tends to increase for the Cr-bearing ternary while it tends to decrease for the Nb-bearing ternary.

At low temperatures (blow 800°C), the yield stress for all the ternary disilicides containing a transition metal is lower than that of binary $MoSi_2$. Weak-beam microscopy of 1/2<111] dislocations gliding on {110) has indicated that their dissociation width is larger for the ternaries than for the binary. This is exactly what we expected to occur in $MoSi_2$ containing alloying elements that form a C40 disilicide. As seen in Fig. 2, Nb and Al seem to be the most effective in reducing the yield strength (in increasing the deformability) of $MoSi_2$ at low temperatures.

At high temperatures (above 1300°C), the yield stress for all the ternary disilicides except for the Al-bearing one is higher than that for the binary counterpart. This is contrary to the fact that the dissociation width for 1/2<111] dislocations is larger for the ternaries than for the binary, but transmission electron microscopy has indicated that 1/2<111] dislocations decompose into some unit dislocations involving climb motion. As seen in Fig. 2, the addition of Nb seems to be very effective in increasing the yield stress at high temperatures. The yield strength measured for the [001] orientation is found to be the highest for Nb at 1400 and 1500°C. These indicate that alloying elements that form a C40 disilicide are effective both in decreasing the yield strength at low temperatures and in increasing the yield stress at high

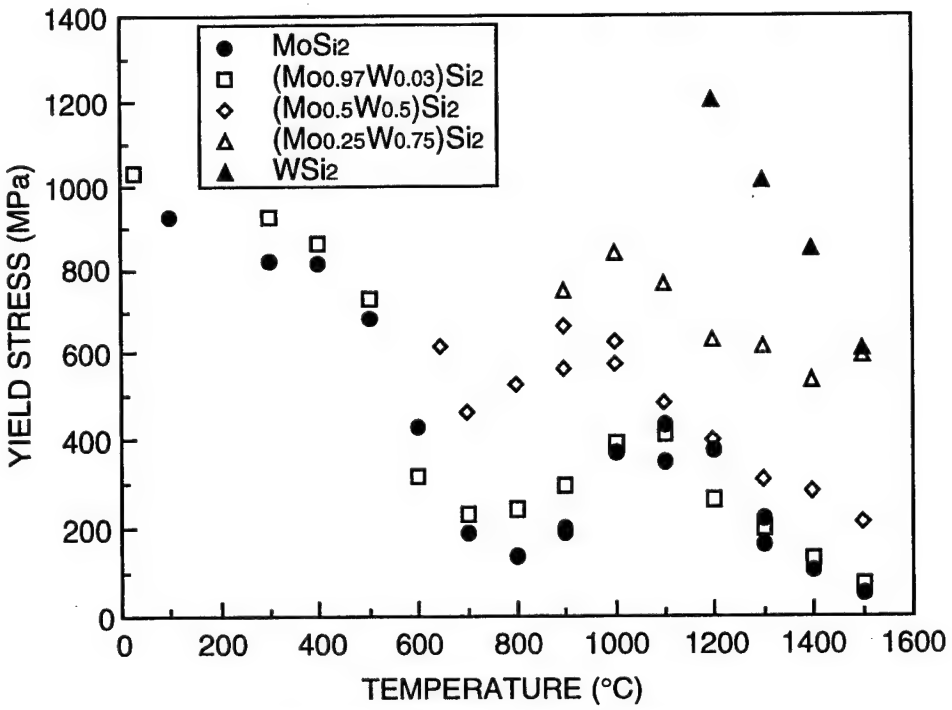

Fig.3 Temperature dependence of yield stress obtained for binary and W-bearing ternary MoSi2 single crystals with the [0 15 1] orientation.

temperatures and this is the most significantly observed for Nb.

4. Effects of alloying elements that form a $C11_b$ disilicide

The yield stresses obtained for $MoSi_2$ single crystals with the [0 15 1] orientation are plotted in Fig. 3 as a function of temperature for $(Mo_{1-X}W_X)Si_2$ with X=0, 0.03, 0.5, 0.75 and 1. As seen in Fig. 3, plastic deformation is possible even at room temperature for $(Mo_{0.97}W_{0.03})Si_2$ but the onset temperature for plastic flow increases with the increase in the amount of W additions. These are 600 and 900°C for $(Mo_{0.5}W_{0.5})Si_2$ and $(Mo_{0.25}W_{0.75})Si_2$, respectively. At all temperatures, the yield strength for $(Mo_{0.97}W_{0.03})Si_2$ is only little higher than that for the binary counterpart and the deformation behavior for the two disilicides is essentially the same. Weak-beam microscopy has indeed indicated no significant difference in the dissociation width of 1/2<111] dislocations between in $MoSi_2$ and in $(Mo_{0.97}W_{0.03})Si_2$. However, the larger amount of W additions is effective in increasing the yield strength of $MoSi_2$, especially at high temperatures; the ratio of the CRSS values for $MoSi_2$, $(Mo_{0.5}W_{0.5})Si_2$ and $(Mo_{0.25}W_{0.75})Si_2$ is increased from 1:1.5:2 at 1000°C to 1:4:10 at 1500°C [4]. The anomalous increase in CRSS observed at the intermediate temperature range (800~1100°C) for $MoSi_2$ is observed also for both $(Mo_{0.50}W_{0.50})Si_2$ and $(Mo_{0.25}W_{0.75})Si_2$ with the extent of the anomalous strengthening decreasing with the increase in W concentration. Accordingly, both the amplitude and frequency in stress-strain curves in the anomalous temperature range becomes less marked with the increase in W concentration.

The addition of Re significantly increases the yield strength of $MoSi_2$. As a result, the Re-bearing disilicide loses the deformability at low temperatures so that the onset temperature

for plastic flow is increased to 400°C for $(Mo_{0.97}Re_{0.03})Si_2$. An anomalous increase in yield stress at intermediate temperatures is eliminated for the Re-bearing disilicide, although a plateau in yield stress is observed at temperatures between 600 and 800°C. The high-temperature strength (above 1300°C) for $(Mo_{0.97}Re_{0.03})Si_2$ is extremely high and is comparable to that attained by $(Mo_{0.50}W_{0.50})Si_2$.

5. Conclusions

(1) Alloying elements (V, Cr and Nb) that form a C40 disilicide are effective both in decreasing the yield strength at low temperatures and in increasing the yield stress at high temperatures. This effect occurs the most significantly for Nb.

(2) A small amount of W additions does not significantly affect the deformation behavior of $MoSi_2$, as observed for $(Mo_{0.97}W_{0.03})Si_2$. In contrast, a large amount of W additions is effective in increasing the yield strength at high temperatures, although the deformability at low temperatures declines.

(3) A small amount of Re additions significantly increases the yield strength of $MoSi_2$.

Acknowledgments

This work was supported by JSPS Grant for "Advanced High Temperature Materials - Development of Practicable High Temperature Intermetallics" (JSPS-RFTF 96R12301) and Grant-in-Aid for Scientific Research (No.07405031) from the Ministry of Education, Science, Sports and Culture, Japan.

References

[1] A.K. Vasudevan and J.J. Petrovic, *Mater. Sci. Eng.*, **A155** (1992) 1.

[2] S.A. Maloy, T.E. Mitchell and A.H. Heuer, *Acta Metall. Mater.*, **43** (1995) 657.

[3] K. Ito, H. Inui, Y. Shirai and M. Yamaguchi, *Phil. Mag. A*, **72** (1995) 1075.

[4] H. Inui, T. Nakamoto, K. Ishikawa and M. Yamaguchi, *Mater. Sci. Eng.*, in press.

Elastic constants and electron distribution in transition metal disilicides

Katsushi TANAKA, Keigo NAWATA, Kazuki YAMAMOTO†,Haruyuki INUI,
Masaharu YAMAGUCHI and Masahiro KOIWA
Department of Materials Science and Engineering, Kyoto University
†Department of Physics, Nara Women's University

Introduction

Elastic constants are fundamental parameters to describe mechanical properties of the materials. Since the values reflect interatomic interaction of the substance, the knowledge of elastic properties is indispensable to understand the material properties. Recent studies on the plastic property of transition metal disilicides have revealed their extreme brittleness at low temperatures [1]-[4]. The brittleness is considered to be closely related to the elastic property of the crystal. For example, the Pugh criteria of B/G where B and G are bulk and shear moduli, respectively, is sometimes used to predict the brittleness. The smaller is the ratio, the more brittle is the crystal. The elastic constants of the transition metal disilicides measured at room temperature have been reported by several authors [5][6], and the temperature dependence of the elastic constants of $MoSi_2$ and $TiSi_2$ from 4K to 1200K have been reported by the present authors [7][8]. We have also attempted to analyze the values of elastic constants by adopting an approach similar to the valence-force-field approach in order to elucidate the directional nature of atomic bonding [9]. The directionality in atomic bonding in $C11_b$ disilicides is stronger than any other disilicides with the C40 and C54 structures.

In this paper, we first review our previous analysis, and then report some preliminary results of the X-ray diffraction study for the precise determination of the position of silicon atoms in materials with the $C11_b$ and C40 structures together with the electron distribution in $MoSi_2$ with the $C11_b$ structure. The detailed information of the crystallographic structure is indispensable for the better analysis and understanding of the elastic property.

Analysis of elastic constants

The simplest model to describe the elastic property of the crystal lattice is the one based on the pair potential approach, in which the elastic energy U is written as

$$U = \Sigma\, W(\mathrm{d}r_{ij}), \tag{1}$$

where $\mathrm{d}r_{ij}$ is the change in the distance between i th and j th atoms. For such crystals formed by purely central forces, the Cauchy relation holds; for cubic crystals, the relation is given by

$$c_{12} - c_{44} = 0. \tag{2}$$

In most real materials, however, the Cauchy relation is not obeyed, which indicates the presence of non-central force. Musgrave and Pople [10] have introduced such non-central force in their valence-force-field approach; the interatomic forces were resolved into bond-stretching and bond-bending forces. We have adopted their approach also in our analysis of the elastic property of disilicides, as described below.

For the analysis of elastic properties in terms of atom-atom interaction, one first defines a cluster of atoms representing the relevant crystal structure. Figure 1 shows the cluster for the $C11_b$ structure, and Figure 2 for the C40 and C54 structures. We consider three types of interactions in the cluster.

(i) The first nearest central interaction: This is the bond stretching term for the first nearest atoms.
(ii) The first nearest neighbor non-central interaction: This is the bond-bending term associated with the change in the bond angles between the two first neighbor bonds originating from the central atom (see Fig. 1)
(iii) The second nearest neighbor non-central interaction: The same as item (ii) in the above, but the two outer atoms are in the second neighbor relation (see Fig. 1).

If we neglect cross terms of these interactions, the total elastic energy, U, can be written with three force constants k, a and b

$$U = k\,\Sigma(\mathrm{d}r_i)^2 + a\,\Sigma(\mathrm{d}\theta^1{}_{ij})^2 + b\,\Sigma(\mathrm{d}\theta^2{}_{ij})^2 \tag{3}$$

where $\mathrm{d}r_i$ is the change in the bond length for the i-th atom and $\mathrm{d}\theta^1{}_{ij}$ and $\mathrm{d}\theta^2{}_{ij}$ are the change in the angle between i-th and j-th atoms in the first- and second-nearest neighbors, respectively. For the C40 and C54 disilicides, the first-nearest-neighbor distance in the $TMSi_2$ layer is

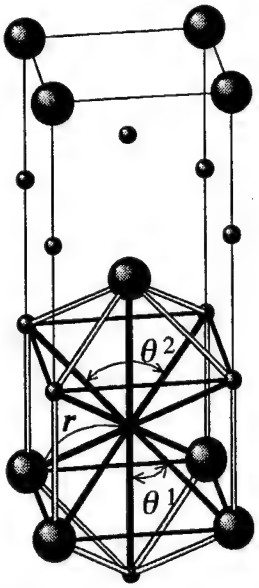

Fig. 1. Model cluster used for analyzing elastic constants of $MoSi_2$. The notations of r, θ^1 and θ^2 indicate first-nearest central, first-nearest non-central and second-nearest non-central interactions, respectively.

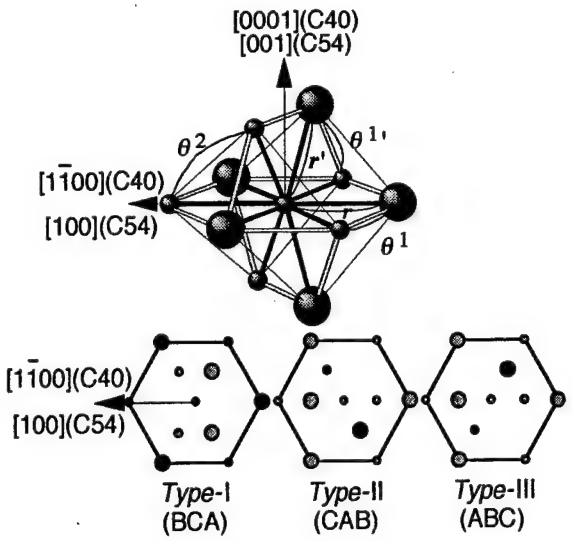

Fig. 2. Model cluster used for analyzing elastic constants of disilicides with the C40 and C54 structures. The (0001) projection of atom positions for three different clusters considered for the C40 structures is also indicated.

different from that out of the layer in real crystals with these two structures. We thus introduce two additional force constants, k' and a', corresponding to the first-nearest central and first-nearest non-central interactions, both of which are interactions out of the $TMSi_2$ layer. Then, the elastic energy U is expressed by the five force constants as:

$$U = k\,\Sigma(\mathrm{d}r_i)^2 + k'\,\Sigma(\mathrm{d}r_i')^2 + a\,\Sigma(\mathrm{d}\theta^1{}_{ij})^2 + a'\,\Sigma(\mathrm{d}\theta^1{}_{ij}')^2 + b\,\Sigma(\mathrm{d}\theta^2{}_{ij})^2. \quad (4)$$

Values of the force constants are determined by minimizing the following quantity S:

$$S = \sum_{i,j}\left(\frac{c_{ij}^{exp} - c_{ij}^{cal}}{c_{ij}^{cal}}\right)^2 \quad (5)$$

where c_{ij}^{exp} is the experimentally determined elastic constants as listed in Table 1 [5]-[7] and c_{ij}^{cal} is those calculated by assuming appropriate values for the three force constants. The values of force constants thus determined are listed in Table 2. The values of elastic constants calculated with the derived force constants are also listed in Table 1. Although the reproducibility of the absolute values of c_{ij} is not very satisfactory, the overall trend of elastic anisotropy is fairly well represented for all the disilicides.

Since the absolute values of the force constants are different for different crystals, some normalization is necessary for the comparison of the directionality of the atomic bonding. This is achieved by normalizing with k (for the $C11_b$ structure) or $(k + k')/2$ (for the C40 and C54 structures); the latter two quantities correspond to the bulk modulus, which does not include any anisotropic nature of atomic bonds. The normalized values are also listed in Table 2. The larger are the values of angular-dependent terms (a, a' and b), the stronger the directionality in atomic bonding is. Since the number of force constants varies with crystal structure, it is difficult to make a direct comparison for a different crystal structures. In order to make comparison, we now introduce a parameter, α, that represents the directionality averaged per atomic bond. The parameter α is expressed as;

$$\alpha = \frac{N_a a + N_a' a' + N_b b}{N_a + N_a' + N_b} \quad (6)$$

where N_a, N_a' and N_b are the numbers of the corresponding atomic bonds in the relevant cluster (see Figs. 1 and 2). The values of α for the two $C11_b$ disilicides are larger than those for C40 and C54 disilicides (Table 2), indicating the strongest directionality in atomic bonding

Table 1. Elastic constants of transition-metal disilicides with the $C11_b$, C40 and C54 structures. Values experimentally determined and those calculated in the present study are listed in the first and second rows for each of disilicides, respectively.

Material	Structure	c_{11} (GPa)	c_{22} (GPa)	c_{33} (GPa)	c_{12} (GPa)	c_{13} (GPa)	c_{23} (GPa)	c_{44} (GPa)	c_{55} (GPa)	c_{66} (GPa)	Ref.
WSi_2	$C11_b$	442.8		552.3	121.7	81.0		211.6		217.5	5
		(372)		(596)	(116)	(81.6)		(211)		(236)	
$MoSi_2$	$C11_b$	403.7		505.3	114.5	88.0		202.7		194.8	7
		(345)		(547)	(109)	(87.7)		(190)		(220)	
$CrSi_2$	C40	372.2		385.2	45.3	82.6		149.1		163.5	5
		(372)		(441)	(45.3)	(68.3)		(146)		(163)	
VSi_2	C40	357.8		422.3	50.6	68.1		135.7		153.6	5
		(356)		(430)	(50.6)	(67.0)		(135)		(154)	
$NbSi_2$	C40	380.2		468.0(	75.9	88.3		145.3		152.2	6
		(380)		508)	(75.9)	(80.4)		(144)		(152)	
$TaSi_2$	C40	375.3		476.7	78.4	90.1		143.7		148.5	6
		(375)		(517)	(78.4)	(82.1)		(142)		(148)	
$TiSi_2$	C54	317.5	320.4	413.2	29.35	38.45	86.0	112.5	75.8	117.5	5
		(276)	(302)	(394)	(29.9)	(33.4)	(93.5)	(119)	(75.5)	(134)	

Table 2. Force constants of transition-metal disilicides calculated from the experimentally determined elastic constants listed in Table 1. Values determined and those normalized are listed in the first and second rows for each of disilicides, respectively (see text).

Material	WSi_2	$MoSi_2$	$CrSi_2$	VSi_2	$NbSi_2$	$TaSi_2$	$TiSi_2$
k (GPa)	189.7	180.5	129.9	127.2	141.7	140.8	98.51
	(1.0)	(1.0)	(0.806)	(0.807)	(0.778)	(0.766)	(0.724)
k' (GPa)			192.4	187.9	222.8	227.0	173.7
			(1.194)	(1.193)	(1.222)	(1.234)	(1.276)
a (GPa)	9.94	7.32	8.82	7.65	4.95	4.44	9.67
	(0.0524)	(0.0386)	(0.0547)	(0.0486)	(0.0272)	(0.0241)	(0.0711)
a' (GPa)			0	0	0	0	0
			(0)	(0)	(0)	(0)	(0)
b (GPa)	13.31	12.28	12.91	11.39	10.56	10.02	5.62
	(0.0702)	(0.0647)	(0.0801)	(0.0723)	(0.0579)	(0.0545)	(0.0413)
α	0.0595	0.0490	0.0485	0.0435	0.0313	0.0290	0.0379

for the $C11_b$ disilicides. $TiSi_2$ with the C54 structure exhibits a value of α intermediate between those for C40 disilicides of the stronger directionality group ($CrSi_2$ and VSi_2) and those for C40 disilicides of the weaker directionality group ($NbSi_2$ and $TaSi_2$).

Position of silicon atoms

The position of silicon atoms is important to discuss the directionality of the atomic bonding. When silicon atom is located at the ideal position, (0, 0, 1/3), (1/6, 1/3, 0) and (1/3, 0, 0) for the $C11_b$, C40 and C54 structure, respectively, the distance from the transition metal atom to the surrounding silicon atoms in the $TMSi_2$ plane is exactly the same as that for the C40 structure or almost the same in the $C11_b$ and C54 structures. Hence it is not a worse assumption that all interatomic bonding are treated as the same one. If the silicon atom is displaced from the ideal position, the distance and the strength of the interatomic bonding are different. This affects the elastic properties of the material via a different response of each bond to the external stress.

Figure 3 shows possible displacements of the silicon atom under the certain space group of the material. The displacement is described by only one parameter Δ; (0, 0, 1/3 + Δ), (1/6 - Δ, 1/3 - 2Δ, 0) and (1/3 + Δ, 0, 0) for the $C11_b$, C40 and C54 structure, respectively. The displacement, Δ, has already been reported for $MoSi_2$, $NbSi_2$ and $TiSi_2$ [11][12]. We have determined the displacement for the materials with the $C11_b$ and C40 structure by X-ray diffraction from single crystal of spherical shape with about 0.3 mm in diameter. Table 3 lists preliminary results: the displacement of silicon atom and some other crystallographic

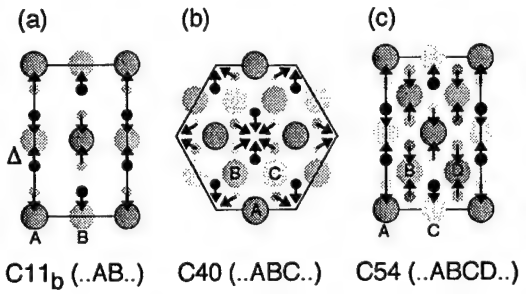

Fig. 3. Possible displacements of silicon atoms under certain space group; $C11_b$: I4/mmm, C40: $P6_422$ or $P6_222$ and C54: Fddd, respectively.

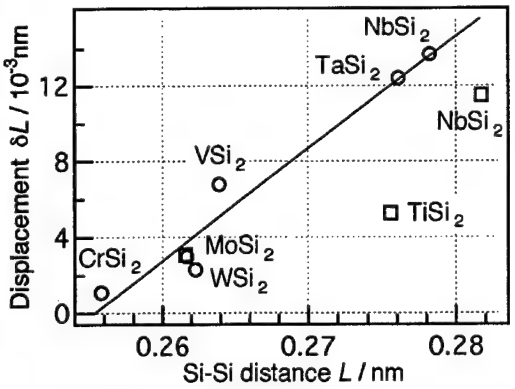

Fig. 4. Relationship between distance of Si-Si bond without the displacement, L, and the change in the length with the displacement, δL, (see Table 3).

parameters. The result for $MoSi_2$ is in good agreement with that reported by Harada *et al.* [11]. The silicon atom is displaced from the ideal position in all the materials.

The magnitude of the displacement, Δ, is not directly related with the extent of directionality. Figure 4 shows the relation of absolute value of the distance of Si-Si bond without the displacement, L, and the change in the length with the displacement, δL. The almost linear relationship suggests that the displacement is governed by the lattice parameters of $TMSi_2$ plane.

Electron distribution

The electron distribution map, constructed from the X-ray diffraction data, can demonstrate most directly the details of interatomic bonding. The maximum entropy method is considered to be very effective in reproducing a high quality electron distribution map. To apply the method, one has to obtain structure factors for a large number of diffractions with low to high indices. Experimentally, it is important to avoid the extinction effect, particularly for low index diffractions. For this purpose, we use a specimen of $MoSi_2$ deformed 2% at 1473K.

Figure 5 (a) shows the {110} cross-section of the electron density map and (b) is the corresponding difference electron density map. The latter is constructed by subtracting the electron density of the neutral atoms located at the determined position, and best demonstrates the redistribution of electrons resulted from the bond formation. The excess electron charge near the midpoints of the bonds indicates the formation of strong covalent bonds.

Note that the bond strengths are not the same for all the Mo-Si bonds; the [001] bonds are weaker than those in the other direction. The Si-Si bonds are stronger along the [001] direction than the others. The anisotropy of the interatomic bonding may be schematically represented by Fig. 6. Under the application of a tensile stress along the [001] direction, the

Table 3. Preliminary results of the determined displacement of silicon atom and other crystallographic parameters (see text). The values in the last three rows are the values previously reported.

Material	displacement	lattice parameters [12]			length of Si-Si bond	
	Δ	a (nm)	b (nm)	c (nm)	L (nm) (Δ=0)	δL (nm)
WSi_2	0.0014	0.3211		0.7868	0.2623	0.0023
$MoSi_2$	0.0019	0.3202		0.7851	0.2617	0.0030
$CrSi_2$	0.00073	0.4431		0.6364	0.2558	0.0011
VSi_2	0.0043	0.4571		0.6372	0.2639	0.0068
$NbSi_2$	0.0082	0.4819		0.6592	0.2782	0.0137
$TaSi_2$	0.0075	0.47821		0.65695	0.2761	0.0124
$MoSi_2$ [11]	0.0020	0.32064		0.78478	0.2616	0.0031
$NbSi_2$ [12]	0.0068	0.4819		0.6592	0.2817	0.0115
$TiSi_2$ [12]	0.0032	0.8267	0.4800	0.8551	0.2756	0.0053

elongation will be realized mostly by the extention of weaker bonds (thin lines), as shown in Fig. 6 (b). In order to confirm such displacements of Si atoms, a detailed X-ray measurement for a single crystal specimen under the applied stress is being carried out.

Conclusion

We have analyzed elastic constants of the transition metal disilicide with the $C11_b$, C40 and C54 structures by a similar method to the valence force field approach. The result indicates that the directionality in atomic bonding in $C11_b$ disilicides is stronger than those with the C40 and C54 structures. The directionality in C40 disilicides is classified into two groups; stronger directionality group, $CrSi_2$ and VSi_2, and weaker directionality group, $NbSi_2$ and $TaSi_2$.

The position of silicon atom was examined by the X-ray diffraction. The silicon atom is displaced from the ideal position in all the compounds. The magnitude of the displacement is governed with the lattice parameter of $TMSi_2$ pseudo hexagonal plane. Corresponding to the displacement, the anisotropic interatomic bond was observed in the charge density map derived by the maximum entropy method.

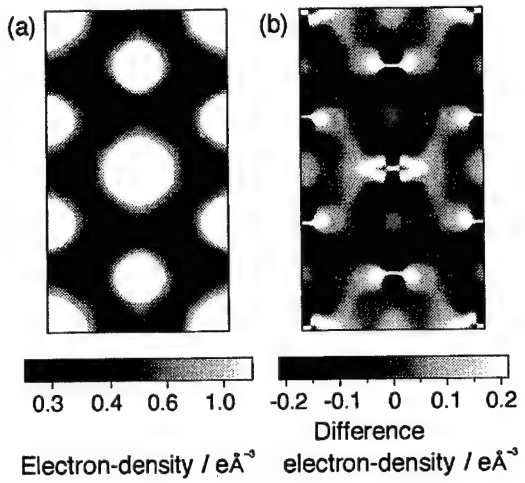

Fig. 5. Cross-section of electron density map of $MoSi_2$ on the {110} plane (a), and difference electron density map (b).

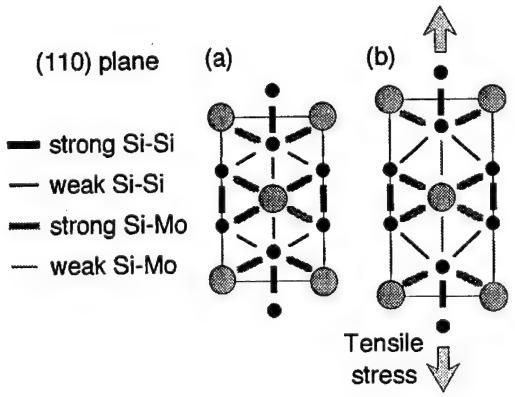

Fig. 6. Schematically illustrated of bonding strength in $MoSi_2$ (a), and supposed atom movement under the application of a tensile stress (b).

References

(1) A. K. Vasudevan and J. J. Petrovic; Mater. Sci. Eng., A155 (1992), 1.
(2) Y. Umakoshi, T. Sakagami, T. Hirano & T. Yamane; Acta Metall. Mater., 38 (1990), 909.
(3) S. A. Maloy, A. H. Heuer, J. J. Lewandowski and T. E. Mitchell; Acta Metall. Mater., 40 (1992), 3159.
(4) K. Ito, H. Inui, Y. Shirai and M. Yamaguchi; Phil. Mag. A, 72 (1995), 1075.
(5) M. Nakamura, S. Matsumoto and T. Hirano; J. Mater. Sci., 25 (1990), 2209.
(6) F. Chu, M. Lei, S.A. Maloy, J. J. Petrovic and T. E. Mitchell; Acta Mater., 44 (1996), 3035.
(7) K. Tanaka, H. Onome, H. Inui, M. Yamaguchi and M. Koiwa; Mater. Sci. Eng., A239-240 (1997), 188.
(8) K. Tanaka, K. Nawata, H. Inui, M. Yamaguchi and M. Koiwa; will be published.
(9) K. Tanaka, H. Inui, M. Yamaguchi and M. Koiwa; Mater. Sci. Eng., in press.
(10) M. J. P. Musgrave and J. A. Pople, Roy. Soc. London A, 268 (1962), 474.
(11) Y. Harada, M. Morinaga, D. Saso, M. Takata and M. Sakata; Intermetallics, 6 (1998), 523.
(12) P. Villars and L. D. Calvert, Pearson's Handbook of Crystallographic Data for Intermetallic Phases, (1985).
(13) L. Pauling, Nature of the Chemical Bond, 3rd. ed., Cornell University, Ithaca, (1960).

Experiments and Recent Computer Simulation Studies on the Deformation Behavior of $MoSi_2$ Single Crystals

K. ITO[1], H. INUI[1], M. YAMAGUCHI[1], V. VITEK[2] and M.I. BASKES[3]

1. Department of Materials Science and Engineering, Kyoto University, Sakyo-ku, Kyoto, 606-8501.
2. Department of Materials Science and Engineering, University of Pennsylvania, Philadelphia, PA 19104-6272.
3. Department 8712 Materials Science 9403, Sandia National Laboratories, Livermore, California 94551-0969.

Introduction

In recent years there has been an increasing interest in mechanical, chemical and physical properties of transition metal (TM) silicides formed from refractory metals. The motivation is that these materials may become the basis for a new generation of high-temperature structural materials that can lead to a qualitative improvement of the thermal efficiency of energy conversion systems and advanced engines. The important assets are their excellent oxidation resistance, high melting point, relatively low density, high thermal conductivity and thermodynamical compatibility with many ceramic reinforcements. Until recently the studies of the deformation properties of TM silicides concentrated on disilicides, in particular on $MoSi_2$ which crystallizes in a relatively simple tetragonal $C11_b$ structure. A number of compression tests have been made for single crystals of $C11_b$ $MoSi_2$ [1-3]. The present understanding of the deformation behavior of $MoSi_2$ single crystals investigated in our group is summarized below.

In this material dislocation core structure is likely to play dominant role. Common signatures of dislocation core effects are unexpected deformation modes and slip geometries, strong and unusual dependence of flow stresses on crystal orientation and temperature, and, very commonly, a break-down of the Schmid law. Such phenomena have been commonly observed in bcc metals and intermetallic compounds. Indeed, all these aspects of the deformation behavior have been observed in studies of $MoSi_2$ single crystals. Recently we demonstrated by atomic computer simulation that the effect of non-Schmid slip behavior in bcc metals is a direct consequence of the non-planar core structure of 1/2<111> screw dislocations and their response to the applied stress tensor [4]. In order to give a new insight into the non-Schmid behavior of $MoSi_2$ single crystals, I summarize the result of the atomic computer simulation made in bcc metals below.

Plastic deformation of $MoSi_2$ single crystals

In single crystals with the orientation of the compressive axis away from the [001]

direction, plastic flow is possible even at room temperature. But, for orientations of compressive axes close to [001] plastic flow has been found only above 900℃ with the yield stress 3 to 10 times larger than the other orientations. Five slip systems have been identified, depending on the crystal orientation: {013}<331>, {110}<111>, {011}<100>, {010}<100> and {023}<100>. The {013}<331> and {011}<100> slip systems were found to operate even at room temperature and the {110}<111> system above about 400℃, as shown in Fig. 1. While the {010}<100> system was only found in temperature range 600-900℃ and {023}<100> system only above 800℃. In all cases the critical resolved shear stress (CRSS) decreases with increasing temperature and a mild anomalous increase of the CRSS with temperature has been observed for all the slip systems but {023}<100>. The anomalous temperature range varies with slip system. For the {110}<111> slip system this phenomenon can be explained by the Portevin-LeChatelier effect, but for the other system no conclusive interpretation is available.

Polycrystalline ductility of $MoSi_2$ is considered on the basis of the temperature dependence of CRSS for the slip systems identified. A number of independent slip system is at most four even for any combination of slip systems except {013}<331>. Thus, {013}<331> slip has to be activated to achieve five independent slip systems. Therefore {013}<331> slip plays a key role in polycrystalline ductility, in particular at low temperatures.

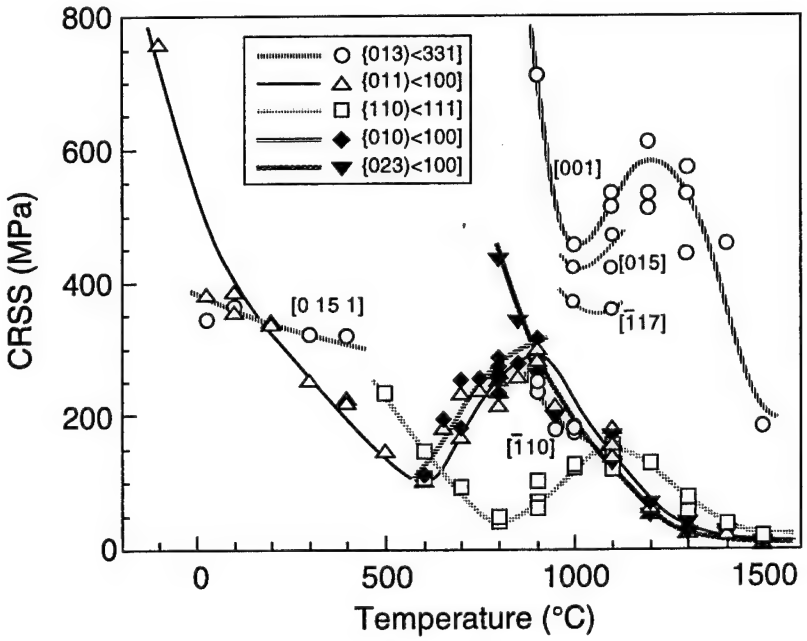

Fig. 1 Temperature dependence of CRSS for slip systems in $MoSi_2$ single crystals.

The Schmid law has been found to be valid for the slip systems {110}<111>, {011}<100> and {023}<100> but not for the {013}<331> system. The CRSS for the latter system is strongly dependent on orientation of the compressive axis and it is the highest for orientations close to [001]. In fact single crystals with orientations close to [001] deform only above 900℃ while the slip on {013}<331> has been observed at room temperature for the orientations close to [010]. Such slip behavior suggest that the dislocation core is controlling the CRSS of the {013}<331> system. This assertion is further corroborated by the observation that 1/2<331> dislocations on {013} planes tend to have <331> screw and mixed orientations and <100> orientation.

When analyzing dislocation cores the first most important phenomenon which needs to be investigated is possible dissociation into partials bounding metastable stacking fault-like defects. Recent weak beam and HRTEM studies of 1/2<331> dislocations suggests that the following two dissociations can occur:

$$1/2\langle 331\rangle = 1/6\langle 331\rangle + 1/3\langle 331\rangle \quad (1)$$

$$1/2\langle 331\rangle = 1/2\langle 111\rangle + \langle 110\rangle \quad (2)$$

The dissociation (1) is planner and involves an APB on the {013} plane. Thus 1/2<331> dislocation dissociated in this way can glide in this plane. In contrast, the dislocation dissociated according (2) is not glissile in the {013} plane since the Burgers vectors of dislocations dissociated do not lie in this plane: for instance, 1/2<111> and <110> lie in the {110} plane when the dislocations are parallel to <331>-screw orientation while 1/2<111> lies in the {011} and <110> in the (001) plane when the dislocations are parallel to <100> orientation. Since both dislocations involved in the splitting (2) are lattice dislocations they could glide independently in their respective slip planes but {110}<110> and (001)<110> system has not been observed.

For [001] orientation of the compressive axis the Schmid factor is zero for such slip systems other than {011}<111> which suggests that the splitting (2) might be responsible for rapid hardening of the {013}<331> system in this case. However, the CRSS for this slip system decreases rapidly with small deviation of the compressive axis away form [001] and this cannot be explained in the framework of this mechanism. Hence, comprehension of the immobilization of 1/2<331> dislocations for [001] compressive axis requires understanding of the details of the core structure of these dislocations and/or partials involved in dissociation (1) and (2). The break down of the Schmid law for the {013}<331> system, indeed, suggests that a subtle core configuration is responsible for this behavior, perhaps via the effect of non-Schmid shear stresses that are not parallel to the Burgers vector. Such phenomena have been commonly observed in bcc metals and intermetallic compounds and may affect profoundly macroscopic plasticity. We demonstrated by atomic computer simulation that effect of non-glide components of the stress tensor on deformation behavior of bcc transition metals and will describe below.

For other dislocations that may be involved in the plastic deformation of $C11_b$ disilicides, the following dissociation can occur for the 1/2<111> dislocation on the {110} plane:

1/2<111>=1/4<111>+1/4<111> (3)

The splitting (3) involved a superlattice intrinsic stacking fault (SISF). The dislocation display features suggesting high Peierls stresses, at least for certain orientations of the dislocation line. For instance, very straight 1/2<111> dislocations parallel to the <110> directions have been observed in the anomalous regime. This is a direction of interaction of several low-index planes (e.g. {110}, (001)) and a non-planer core of the total dislocation or 1/4<111> partials may ensue. Understanding of these phenomena can only be achieved by studying the atomic structures of corresponding dislocations.

Atomistic computer simulation made in bcc metals

The analysis has been carried out in detail for tantalum and molybdenum using the Finnis-Sinclair type central force many-body potentials. The results of computer simulations illustrate that tantalum exhibits two distinct types of non-Schmid behavior. The first is related to the twinning-antitwinning asymmetry of slip on {112} plane. This asymmetry is such that the CRSS is always lower when maximum resolved shear stress plane is closer to a {112} plane sheared in the twinning sense than to a {112} plane sheared in the antitwinning sense. This is an intrinsic effect related to the symmetry of the bcc lattice [5].

The second is an extrinsic effect of non-glide stress components. The calculations demonstrate that the non-Schmid effect arising from the influence of non-glide stress components is controlled by the shear stress in the direction perpendicular to the total Burgers vector on the {110} planes into which the stress-free core spreads. These shear stress components affect the core structure by exerting a force on the edge components of the fractional dislocations forming the core 1/2<111> screw dislocations. While the non-glide stress components cannot move the dislocation, the edge and screw components are linked within the fractional dislocations and shifts in edge components induce shifts in screw component and thus affect the overall core structure and transformations occurring prior to the dislocation motion. These changes of the core structure may lead to either increase or decrease of the CRSS depending on the orientation of the applied stress.

Based on the results of the simulations, the effect of non-glide stress components on {110} planes upon the critical shear stress is such that the critical shear stress decreases rapidly with increasing non-glide stress components. No dislocation motion takes place for large negative non-glide stress components when the mrss plane is a{112} plane sheared in the antitwinning sense, corresponding compression tests with [001] axis. The analysis has been carried out for $MoSi_2$ using the modified embedded-atom potentials constructed by Baskes. The stress-free core of a 1/2<331> screw dislocation in $MoSi_2$ also spreads into

{110} and {013} planes. Immobilization of 1/2<331> screw dislocation in compression test with [001]-oriented $MoSi_2$ single crystals may be expected to be explained by similar frame work.

Acknowledgments

This research was supported by JSPS Grant for 'Advanced High Temperature Materials-Development of Practicable High Temperature Intermetallics' and Grant-in-Aid for Scientific Research (No. 07405031 and No. 08242216) from Ministry of Education, Science, Sports and Culture, Japan, and in part by the NEDO International Research Grant for the Intermetallics Team and the research grant from R & D Institute of Metals and Composites for Future Industries (RIMCOF). The one of authors (KI) greatly appreciates the support from Research Fellowships of the JSPS for Young scientists and the JSPS Postdoctoral Fellowship for Research Abroad. This research was also supported by the Advanced Strategic Computing Initiative of the U.S. Department of Energy through LLNL (VV).

References

1. K. Ito, H. Inui, Y. Shirai and M. Yamaguchi, Phil. Mag. A **72**, 1075 (1995).
2. K. Ito, T. Yano, T. Nakamoto, H. Inui and M. Yamaguchi, Intermetallics **4**, S119 (1996).
3. K. Ito, M. Moriwaki, T. Nakamoto, H. Inui and M. Yamaguchi, Mat. Sci. Eng. A**233**, 33 (1997).
4. K. Ito and V. Vitek, MRS Proc. (1999) in press.
5. M.S. Duesbery and V. Vitek, Acta Mater. **46**, 1481 (1998).

PHASE STABILITY AND MICROSTRUCTURE CONTROL IN HIGH TEMPERATURE Mo-Si-B ALLOYS

J. H. Perepezko, R. Sakidja, S. Kim, J. Myers and H. Sieber*
Department of Materials Science and Engineering
University of Wisconsin
1509 University Avenue
Madison WI 53706
* University of Erlangen-Nürnberg
Department of Materials Science (III) Glass and Ceramics
Mastenssatraße 5, Erlangen, D-91058, Germany

1. Motivation

For high temperature application, materials with a high melting point and oxidation resistance are essential. In terms of structural applications candidate materials must also demonstrate adequate toughness, strength and creep resistance, which are strongly influenced by microstructural design; especially based upon multiphase assemblies [1]. At high temperature (>1300°C) SiO_2 layers are favored for oxidation resistance which in turn highlights the importance of silicides [2]. A notable candidate is $MoSi_2$, but this has been shown to offer limited opportunity for a multiphase microstructure design [3]. A viable alternative has been identified in the Mo-Si-B and Nb-Si-B systems where a ternary $(Mo/Nb)_5SiB_2$ intermetallic is in equilibrium with a refractory solid solution [4]. Based upon this materials selection, the initial objective is to define the phase stability in the ternary systems in order to establish a basis for microstructure control.

2. Research Objectives and Approach

a) Objectives

The main objective of the current research is to evaluate the potential of a two-phase microstructure consisting of an intermetallic phase Mo_5SiB_2 (T2) and a ductile Mo solid solution, Mo(ss), phase as a candidate for high temperature structural applications. In order to accomplish this goal a systematic study of the phase stability and microstructure control is being conducted and includes the following key points :

I. Examination of Phase Stability in the Mo-Si-B System

a) evaluation of the phase equilibria for the Mo-rich section of the Mo-Si-B system at 1600°C and 1200°C.
b) determination of the solidification pathways in the Mo-rich section of the Mo-Si-B system with emphasis on the Mo(ss) + T2 two-phase field region.
c) examination of the high-temperature diffusion characteristics involved in the Mo(ss) + T2 two-phase alloys.
d) examination of possible defect structures in the T2 phase in the Mo-Si-B system.
e) investigation of phase stability in the companion Nb-Si-B system.

II. Investigation of Microstructural Development in Mo(ss) + T2 Alloys

a) evaluation of microstructural modification of the two-phase alloys utilizing the rapid solidification processing (RSP).
b) evaluation of solid-state phase transformations involved in the two-phase field region.
c) analysis of the structure and crystallography of the $(Mo,Nb)_{ss}$/T2 interface via High-Resolution Transmission Electron Microscopy (HRTEM)

b) Approach

Alloy compositions are prepared by non-consumable arc melting of pure Mo, Nb, Si and B in a titanium gettered argon atmosphere. To expedite the approach to equilibrium at relatively low annealing temperature, some of the alloys are rapidly solidified via splat quenching (SQ) and drop-tube processing (DTP). The arc-cast samples and the splats are wrapped in a Ta foil, placed in an Al_2O_3 crucible and heat treated in an Al_2O_3 tube furnace at 1200°C and 1600°C for extended periods. Both splat quenching and drop-tube processing are being employed to evaluate the extent of microstructural tailoring that can be attained via RSP. Annealing treatments at 1600°C for varying times are being conducted to evaluate solid-state reactions that are characterized by using SEM and TEM. The structure and the crystallographic relationships between Mo(ss) and T2 has been elucidated using HRTEM and Fourier-filtered images. In an effort to map out phase reaction sequences, selected diffusion couples have been designated to identify component diffusivities in the T2 phase based upon the analysis of layer thickening and composition measurements by electron probe microanalysis (EPMA).

3. Research Progress and Highlights

The focus of the investigation has been on the phase stability and the microstructural control in the Mo-B-Si system. The stability of the Mo(ss) + T2 two-phase field at high temperature (1200-1600°C) has been examined and confirmed. Similarly, the phase relations between the T2 phase and the neighboring phases have been established at 1600°C as shown in Figure 1a. Similar phase relations have been found in the 1200°C isotherm. From the careful assessment of the solubility limit of the T2 phase and those of relevant phases, the 1600°C isotherm has been revised from an earlier report [5]. In addition, the results from the isothermal study have defined the solubility range of the Mo(ss) + T2 two-phase field. A companion study on the Nb-Si-B system is now in progress. As indicated in Figure 1b in the diagram reported by Nowotny [6], the T2 phase in Nb-Si-B alloys has a significantly larger existence range than that observed in Mo-Si-B alloys. A number of alloy compositions have been identified and are being examined to confirm the solubility range. Preliminary results tend to support a large solubility range for the T2 phase in Nb-base alloys.

The complete mapping on the solidification pathways on the Mo-rich section of the ternary system has been carefully assessed and has been used to guide further materials processing (see Figure 2). The liquidus projection of the Mo-rich section on the Mo-B-Si ternary system has provided a number of valuable points concerning alloy phase stability and processing. First, both Mo(ss) and T2 phase have a high melting point (in excess of 2000°C). This is of primary importance since it confirms the significant potential of the two-phase alloys for ultra-high temperature application. Secondly, the solidification pathway in the Mo-rich portion of the

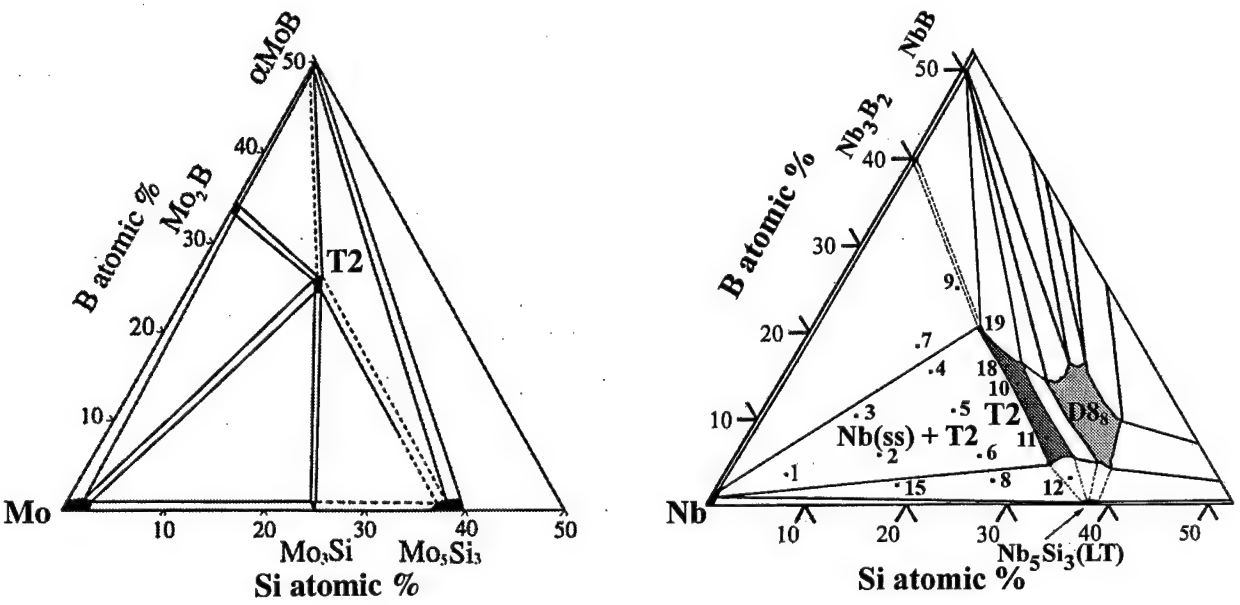

Figure 1 : 1600°C Isothermal section of the metal-rich portion of **a)** Mo-Si-B (from current study [4]) and **b)** Nb-Si-B system (from [5]). Numbered points denote alloy compositions under study.

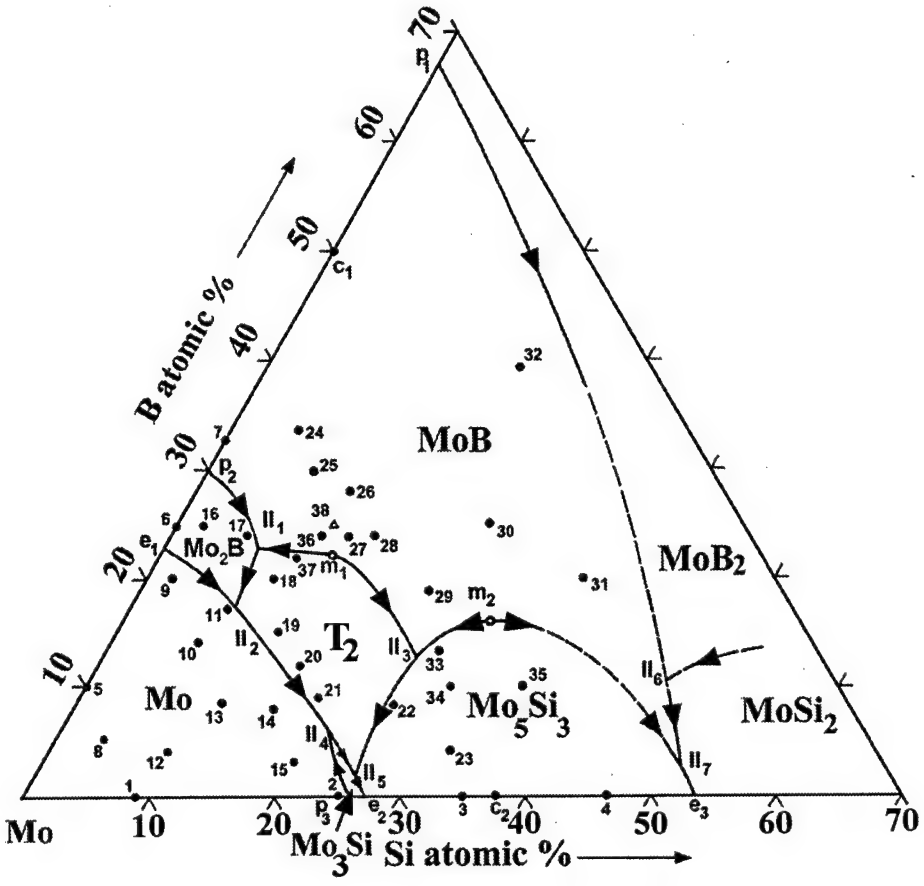

Figure2 : Liquidus projection of Mo-rich portion of Mo-Si-B system.

ternary system reveals the extensive compositional segregation encountered in this system. The segregation is revealed by the form of formation of borides and silicides such as MoB and Mo_5Si_3 which require an extended solid-state annealing at very high temperature (in excess of 1600°C) for homogenization (Figure 3a and 3b). The slow dissolution rate is consistent with the fact that sluggish diffusion of the component species is one of the main attibutes of this high-temperature material. In this regard, Rapid Solidification Processing (RSP) has been found to be effective in expediting the attainment of equilibrated two-phase microstructures due to a much shorter diffusion path involved and the capability to suppress the segregation products such MoB and Mo_5Si_3 during solidification [7]. Furthermore, uniformly dispersed two-phase microstructures can be successfully obtained after subsequent solid-state annealing treatment at a lower temperature such as 1200°C (see Figure 4). Moreover, the microstructural scale appears to resist coarsening during extended annealing.

The solidification study on alloys forming the T2 phase also reveals the fact that unlike most of the refractory silicides, the intermetallic T2 phase can not be regarded as a line compound. The compositional trace on the as-solidified T2 phase exhibits a range of Mo solubility. Thus, Mo supersaturation in the T2 phase is present in the as-solidified alloys. The retention of a Mo(ss) supersaturation in as-cast alloys is another consequence of sluggish solid state diffusion. As a result of the initial supersaturation, subsequent annealing treatment of the as-solidified Mo(ss) + T2 two-phase alloys generates the precipitation of Mo(ss) phase in the T2 phase matrix as shown in Figure 3b. The Mo precipitates appear as plates and show a specific crystallographic orientation relationship with the T2 matrix; Mo(ss) {111} || T2(001) ; Mo(ss) <011> || T2 <110> [8]. Furthermore, the High-Resolution TEM analysis on the structure of Mo(ss) precipitate//T2 matrix broad interface shows the semi-coherent nature of the interface (Figure 5). As a result, the precipitates exhibit a high resistance towards coarsening even at temperatures as high as 1600°C. Preliminary observations further suggest that the presence of the Mo(ss) precipitates in the T2 matrix may provide a significant contribution toward the apparent enhancement of toughness and strength of the two-phase alloys after annealing treatment [9]. Further work to evaluate the toughening potential of in-situ Mo(ss) precipitates is in progress.

A central issue in the operational stability of high temperature materials systems is the diffusion behavior which influences the microstructural evolution, oxidation behavior and creep resistance. In order to develop quantitative information on the diffusion behavior in the T2 phase, diffusion couples between binary end members (i. e. borides and silicides) that produce the T2 phase as a reaction product are being examined systematically. For example, Figure 6 shows the back-scattered (BS) image of the cross section of a diffusion couple between Mo_5Si_3 and Mo_2B after annealing at 1600°C for 400 hours. The reaction between Mo_2B and Mo_5Si_3 produced the T2 phase which exhibits a columnar growth with parabolic diffusion controlled kinetics. It is also interesting to note here that cracks in Mo_5Si_3 are stopped and/or diverted in front of the T2 phase indicating that the toughness of the T2 phase is higher than that of Mo_5Si_3 (T1).

4. Potential Structural Applications and Engineering Issues

The two-phase alloys consisting of the ductile Mo(ss) phase uniformly dispersed in the T2 phase matrix have an attractive potential for structural applications at elevated temperatures. The two-phase microstructure and the two-phase field are very stable at high temperatures. A significant improvement of toughness and strength at both high temperature and low temperature has been shown due to the Mo(ss) precipitates present in the T2 matrix and the operating

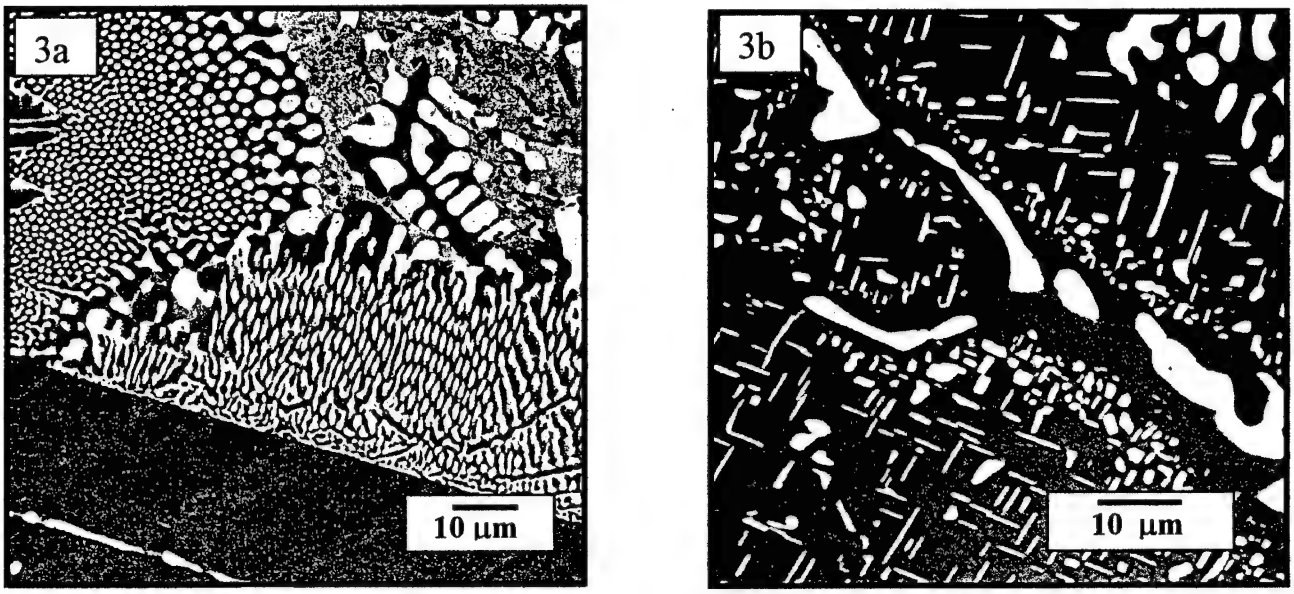

Figure 3: Back-scattered SEM image of **a)** as-cast Mo-20B-10Si (at. %) alloy microstructure consisting of the T2 (dark), Mo (bright) and Mo_3Si (gray) phases **b)** Mo-20B-10Si (at. %) alloy microstructure annealed at 1600°C for 150 hours.

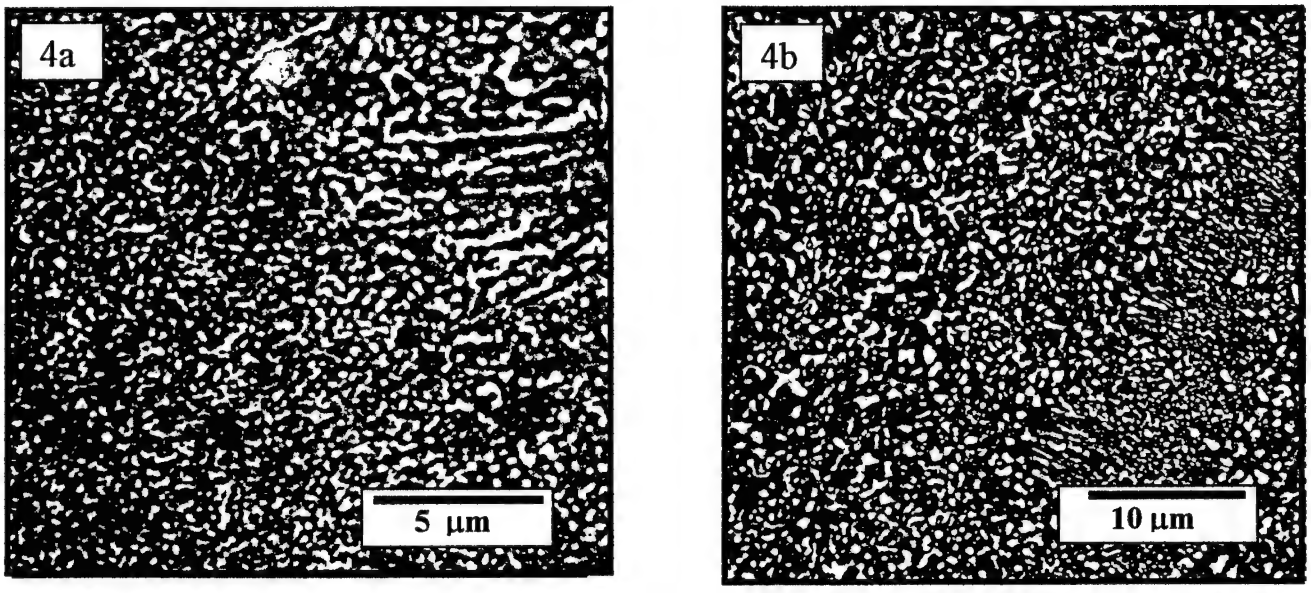

Figure 4: Back-scattered SEM image of **a)** Mo-20B-10Si (at. %) splat-quenched alloy **b)** Mo-20B-10Si (at. %) alloy splat-quenched and annealed at 1200°C for 150 hours showing the two-phase microstructure consisting of Mo (bright) phase dispersed in the T2 (dark) matrix.

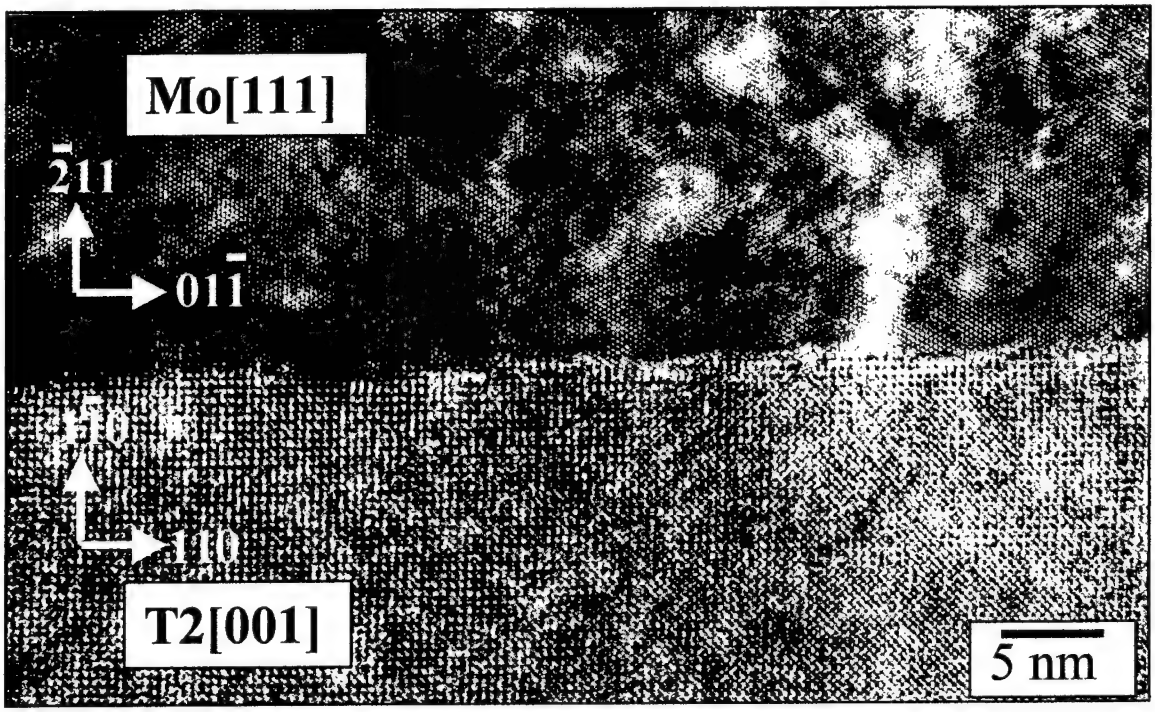

Figure 5: HRTEM image of the broad face of a plate-like Mo precipitate within the T2 matrix following a specific crystallographic orientation [8].

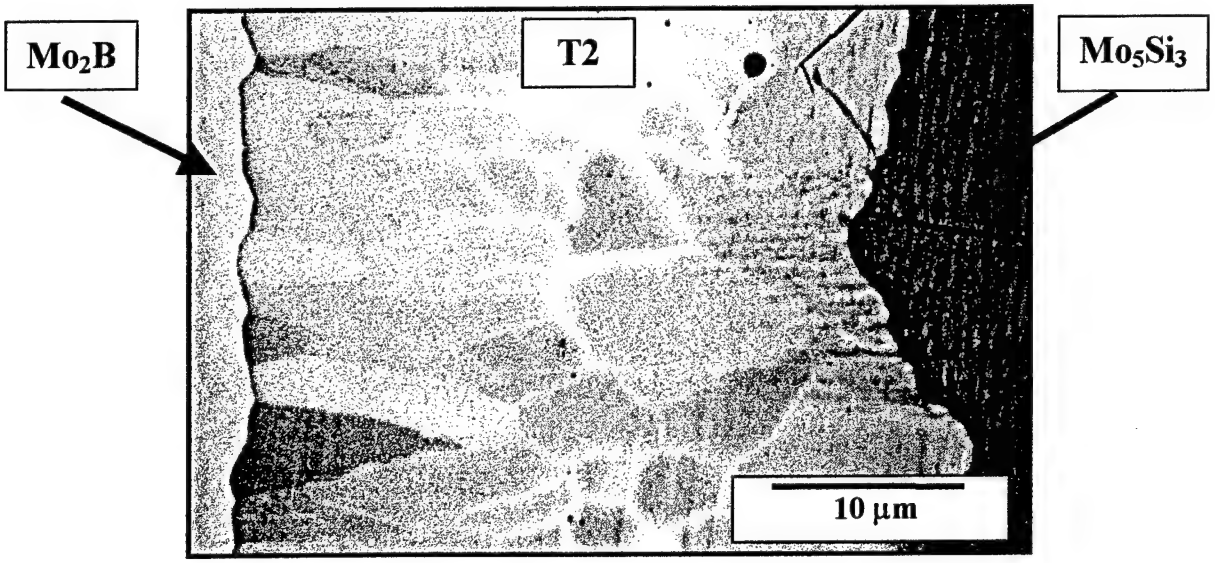

Figure 6: Back-scattered image of the cross section of the diffusion couple Mo_2B/Mo_5Si_3 annealed at 1600°C for 400 hrs.

toughening mechanism such as crack bridging by the Mo(ss) phase. The presence of the oxidation-resistant T2 phase provides for a borosilicate surface layer and low metal recession levels that approach those for $MoSi_2$ [10]. The feasibility of utilizing RSP to facilitate the attainment of equilibrium and provide an effective means for microstructure control of the two-phase alloys has also been shown. This development previews the use of powder processing for large scale component production. The favorable characteristics that can be developed in the Mo(ss) + T2 alloys establish them as a strong material candidate for ultra-high temperature structural application.

5. Critical Scientific Issues and Challenges

The optimal Mo(ss) + T2 two-phase microstructures require a balanced design of microstructural stability, chemical stability and mechanical integrity between the two constituents. In this context, a complete assessment of the diffusion behavior involving the two phases and the surrounding phases is essential since most of the beneficial high-temperature phenomena exhibited by these alloys (the high temperature stability of the two-phase field, the Mo precipitation, the suppression of intermetallic formation by RSP and oxidation behavior) are governed by the diffusion processes involved. In addition, the underlying defect mechanism involved in the T2 phase must also be explored. The knowledge on the defect structure can guide further advances in materials processing and alloying strategies to achieve optimal materials properties. More quantitative oxidation studies coupled with mechanistic modeling of the controlling diffusion transport is essential. Once a more complete analysis of the phase stability and microstructure development is available, the mechanical properties should be examined in a systematic manner. In this regard, careful attention to materials processing will be essential to a meaningful evaluation of mechanical properties.

6. Acknowledgements and References

a) Acknowledgement

The support from the Air Force Office of Scientific Research (AFOSR F49620-96-1-0286) is most gratefully acknowledged.

b) References

1. Perepezko, J. H., Nunes, C. A., Yi, S. H. and Thoma, D. J., in *High-Temperature Ordered Intermetallic Alloys VII*, edited by C.C. Koch, C. T. Liu, N. S. Stoloff and A. Wanner, Mater. Res. Soc. Symp. Proc. **460**, pp 1-14 (1997).
2. Birks, N. and Meier, G. H., "Introduction to High Temperature Oxidation of Metals" (E. Arnold, London) 1983.
3. Boettinger, W. J., Perepezko J. H. and Fankwicz, P. S., Mater. Sci. Eng., **A155**, pp. 33-44, (1992).
4. Nunes, C. A., Sakidja, R. and Perepezko, J. H., in *Structural Intermetallics 1997*, edited by M. V. Nathal, R. Darolia, C. T. Liu, P. L. Martin, D. B. Miracle, R. Wagner and M. Yamaguchi, (TMS, Warrendale, PA), pp.831-839 (1997).
5. Nowotny, H., Benesovsky, F., Rudy, E. and Wittman, A., Monatshefte Für Chemie, **91**, pp.

975-990 (1960).
6. Nowotny, H., Kieffer, F., Benesovsky, F., Planseeberichte Für Pulvermetallurgie, **5**, 86 (1957).
7. Sakidja, R., Sieber, H., Wilde, G., Perepezko, J. H., Symposium of *High-Temperature Ordered Intermetallic Alloys VIII,* Mat. Res. Soc. Symp. Proc. **552** (1999) in press.
8. Sakidja, R., Sieber, H. and Perepezko, J. H., "The Formation of Mo Precipitates in a Supersaturated Mo_5SiB_2 Intermetallic Phase," *Philosophical Magazine Letters* (1999) in press.
9. Sakidja, R., Sieber, H. and Perepezko, J. H., in *Molybdenum and Molybdenum Alloys*, edited by A. Crowson, E. S. Chen, J. A. Shield and P. R. Subramanian (TMS, Warrendale, PA) pp. 99-110 (1998).
10. Thom, A. J., Meyer, M. K., Akinc, M. and Kim, Y., in *Processing and Fabrication of Advanced Materials for High Temperature Applications III*, edited by T. S. Srivitsan and V. A. Ravi, (TMS, Warrendale, PA) p. 413 (1993).

Processing and Mechanical Properties of Ultra-High Temperature Mo-Si-B Intermetallics

Joachim H. Schneibel and C. T. Liu

Metals and Ceramics Division, Oak Ridge National Laboratory, Oak Ridge, TN, U.S.A.

Research Objectives and Approach

Silica formers such as Mo-Si intermetallics can exhibit excellent oxidation resistance as exemplified by $MoSi_2$, which is widely used for resistance heating furnace elements. Molybdenum silicides with lower Si concentrations, such as Mo_5Si_3 and Mo_3Si, exhibit limited oxidation resistance at high temperatures. Based on earlier work by Nowotny et al., recent work at Ames National Laboratory [1,2] has shown that additions of B can significantly improve the oxidation resistance of silicides based on Mo_5Si_3. In view of the high melting temperatures of Mo_3Si (2025°C) and Mo_5Si_3 (2180°C), superior creep resistance is expected. However, little is known about the physical, mechanical, and corrosion properties of these intermetallics. In order to advance these novel intermetallics, basic research [1-5] as well as research focusing on alloy development and optimization are required. The basic research needs to address issues such as the ternary Mo-Si-B phase diagram, melting points in that phase diagram, and the physical and mechanical properties of Mo_3Si, Mo_5Si_3, and Mo_5SiB_2. In systems containing toughening α-Mo, additional issues have to be considered. One of these is the influence of microstructure on strength and fracture toughness. Another issue is the influence of dissolved Si and B on the mechanical properties of toughening α-Mo. To address all these issues, processing techniques suitable for generating the desired microstructures have to be identified. Micro- and macro-alloying additions to improve the oxidation resistance of the α-Mo will have to be investigated as well.

Research Progress and Highlights

Melting temperatures of Mo-Si-B intermetallics were estimated in the following way: approximately 4 g silicide material with the desired composition was placed on a ZrO_2 substrate in a He or Ar environment and heated by a slowly ramped-up induction unit while continuously monitoring the temperature. Thermal arrests, as well as the temperatures at which the specimen became fully liquid, were monitored. The liquidus temperature of the B-containing Mo_5SiB_2 phase (2160 – 2200°C) was found to be similar to that of Mo_5Si_3 (2180°C). Measurements for some compositions, e.g., Mo-11Si-15B (at. %) suggested the possibility of liquids solidifying at relatively low temperatures such as 1950°C.

Two series of Mo-Si-B alloys containing approximately 50 and 20 vol.%, respectively, of α-Mo were cast [6]. The oxidation resistance tended to increase with decreasing α-Mo volume fraction and with increasing B concentration. Whereas castings containing ~ 50

vol.% of α-Mo were usually free of macrocracks, those containing only 20 vol.% α-Mo always contained macrocracks. The room temperature strengths depended not only on the α-Mo volume fraction, but also on the B concentration. The strength could be qualitatively related to the microstructures. Room temperature strengths up to approximately 600 MPa were found. Annealing for 1 day at 1600°C in vacuum usually increased the room temperature strength. Again, these strength changes could be qualitatively related to annealing-induced changes in the microstructures.

Extremely fine microstructures, with phase sizes of a few μm, were observed in compositions near the pseudo-binary Mo-Mo_5SiB_2 eutectic. By tayloring the composition, the formation of large particles of primary α-Mo or Mo_5SiB_2 could be almost completely eliminated. Mechanical property determinations of these alloys are in progress.

Annealing for 1 day at 1600°C increased the room temperature fracture toughness of a Mo-12Si-8.5B (at. %) alloy containing appr. 40 vol.% α-Mo from 7 to about 10 MPa $m^{1/2}$. This increase is attributed to microstructural coarsening and removal of supersaturated Mo and Si from the α-Mo inclusions. Figure 1 shows an SEM micrograph of a fracture surface illustrating the ductile phase toughening due to the α-Mo inclusions. Testing at 500°C increased the strength from 450-500 MPa to 700 MPa, possibly because the ductile-to-brittle transition temperature of the α-Mo was reached. The fracture toughness at 500°C showed also a slight increase, as compared to room temperature.

An alloy with the composition Mo-12Si-8.5B was also prepared by powder metallurgy (PM) starting with pure Mo, Mo_3Si, and Mo_5SiB_2 powders. Since the Mo_3Si and Mo_5SiB_2 powders were relatively large (<150 μm), the microstructure was coarse, and the brittle intermetallic particles were often cracked. Very importantly, in contrast to the cast structure corresponding to this composition, the PM material consisted of intermetallic particles in a continuous α-Mo matrix (and not α-Mo particles in a continuous intermetallic matrix). The coarse microstructural size as well as the particular

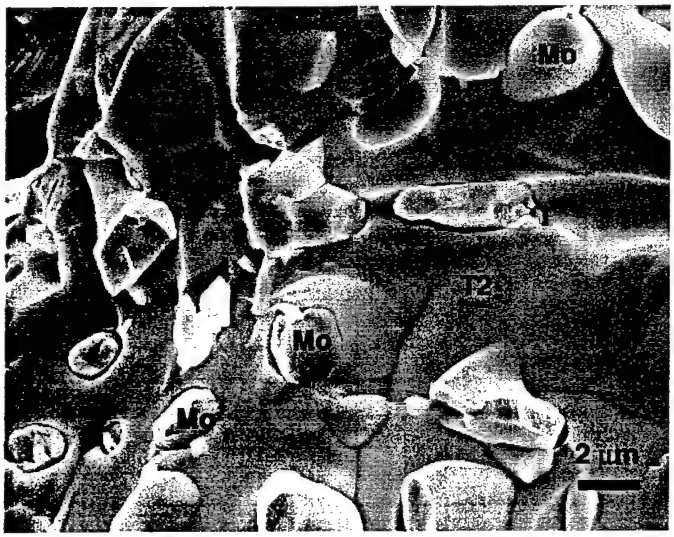

Fig. 1. Room temperature fracture surface of Mo-12Si-8.5B (at. %) illustrating ductile phase toughening due to α-Mo inclusions

microstructure are thought to be the reasons for the high fracture toughness of the PM material (14 - 15 MPa $m^{1/2}$) as compared to 10 MPa $m^{1/2}$ for the cast and annealed material.

Alloy Design Issues

Two design issues are considered important for developing Mo-Si-B intermetallics:

(1) It is likely that alloys of interest must contain some α-Mo. If α-Mo is avoided, one is committed to those phase triangles of the ternary Mo-Si-B phase diagram which contain only brittle phases such as Mo_3Si, Mo_5Si_3, Mo_5SiB_2, and MoB. While it is in principle possible that these phases could be toughened or ductilized, experience with ceramics and intermetallics exhibiting large crystallographic unit cells makes this somewhat unlikely.

(2) Instead of toughening Mo-Si-B intermetallics with ductile α-Mo inclusions, it may be preferable to toughen them with a continuous α-Mo matrix. In a material containing discrete α-Mo inclusions, only a fraction of an advancing crack front will interact with these inclusions. When the α-Mo matrix is continuous, the crack front will have a much higher probability of interacting with toughening α-Mo.

Critical Scientific Issues

Precise knowledge of the physical and mechanical properties of the intermetallic phases Mo_3Si, Mo_5Si_3, and Mo_5SiB_2 is critical for the understanding of materials systems based on Mo-Si-B. In the case of Mo_5Si_3, a lot of this information has already been gathered [4,5]. Determinations of solidus and liquidus temperature are also important since they form the scientific basis for processing. The respective roles of the microstructure (α-Mo inclusions in a brittle matrix vs. brittle silicides in ductile α-Mo matrix) and the microstructural scale need to be understood as well. Previous work on FeAl-carbide composites suggests that α-Mo may exhibit a brittle-to-ductile transition as it decreases in size or thickness. This effect needs to be verified for the Mo-Si-B system. The effects of micro- and macro-alloying additions on the fracture toughness and ductility of α-Mo need to be investigated as well. Both size and compositional parameters are important for controlling the oxidation resistance of the α-Mo.

References

[1] M. Meyer, M. Kramer, and M. Akinc, "Boron-Doped Molybdenum Silicides," Adv. Mater. 8 (1996) 85-88.

[2] M. K. Meyer, M. J. Kramer, and M. Akinca [sic], "Compressive Creep Behavior of Mo_5Si_3 with the Addition of Boron," Intermetallics 4 (1996) 273-81.

[3] C. A. Nunes, R. Sakidja, and J. H. Perepezko. "Phase Stability in High Temperature Mo-rich Mo-B-Si Alloys," Structural Intermetallics 1997, M. V. Nathal et al., eds., Seven Spring Mountain Resort, Champion, PA, TMS, 1997, pp. 831-839.

[4] F. Chu, D. J. Thoma, K. McClellan, P. Peralta, and Y. He, "Synthesis and Properties of Mo_5Si_3 Single Crystals," in press, Intermetallics.

[5] C. L. Fu, Xindong Wang, Y. Y. Ye, and K. M. Ho, "Phase Stability, Bonding Mechanism, and elastic constants of Mo_5Si_3 by first-principles calculation," in press, Intermetallics.

[6] J. H. Schneibel, C. T. Liu, D. S. Easton, and C. A. Carmichael, "Microstructure and mechanical properties of Mo-Mo_3Si-Mo_5SiB_2 silicides," Mater. Sci. Eng., in press (1998).

Acknowledgments

Funding of this work by the Division of Materials Sciences, the Fossil Energy Advanced Research and Technology Development Program, and the Synthesis and Processing Center Project on "Design and Synthesis of Ultra-High Temperature Intermetallics," U.S. Department of Energy, is gratefully acknowledged.

Alloy design of multi-phase alloys based on $MoSi_2$ in various ternary Mo-Si-X Alloys

Yoshinao Mishima

Department of Materials Science and Engineering,
Interdisciplinary Graduate School of Science and Technology,
Tokyo Institute of Technology,
Nagatsuta, Midori-ku, Yokohama 226-8502, Japan

1. Research Objectives and Approach

The objectives of the present work is to impart some room temperature ductility to the molybdenum disilicides which has a very high melting temperature and thus has been expected to be developed for ultra-high temperature structural applications.

The approach is to design multi-phase alloys based on $MoSi_2$ and to control the microstructure in ternary Mo-Si-X alloys. The eutectic microstructure consisting of $MoSi_2$ and Mo_5Si_3 in the binary system is taken as a base. Investigations on the microstructure of the two phase alloys and also of the three-phase with other intermetallic compound are systematically carried out with X being Nb, V, Al, C, Hf, and Zr. Hardness tests are done mainly for the purpose to judge room temperature ductility of the alloys by observing the occurrence of crack formation around the indentation. Fabrication of the alloys besides the button arc-melting is attempted by plasma-arc melting and floating zone melting in some alloys in order to obtain useful information on the effect of processing to the soundness of the microstructure and ductility.

2. Research Progress and Highlights

Lamellar microstructure consisting of $MoSi_2$ and Mo_5Si_3 is found to be finer in the binary Mo-Si alloy and in the alloys with ternary additions of Nb and Hf. The structure becomes obviously coarser for the additions of V and Al. For the additions of ternary elements which forms XSi_2 with C40 ordered structure, the microstructure could be of three phase consisting of C11b MSi_2, C40 MSi_2, and M_5Si_3. In the alloys with a larger Hf and Zr contents the alloys become multi-phase involving their silicides.

Regardless of the finess in microstructure it was unsuccessful to evaluate the strength and ductility of all the alloys at room temperature even by compression tests. By hardness tests, however, some indication for room temperature ductility is found in alloys with Nb, Hf and Zr.

The brittleness of the ingots was basically not improved even by employing

other processing than button arc-melting such as plasma-arc and floating zone melting. It seems that the only powder metallurgy involving mechanical alloying would be the only fabrication method to obtain a sound ingot.

3. Acknowledgement

The present work is a part of a joint effort made by Tokyo institute of Technology and Japan Ultra-high Temperature Materials Laboratory under the sponsorship by NEDO of Ministry of Trade and Industry of the Japanese Government.

MECHANICAL PROPERTIES OF SPARK PLASMA SINTERED Nb-Al-N AND Nb-Si-B COMPACTS

T. Murakami[a], A. Kitahara[b], M. Kawahara[c], Y. Takahashi[d], H. Inui[e] and M. Yamaguchi[e]

a) Mechanical Engineering Laboratory, Tsukuba 305-8564, Japan, b) Kyushu Nat. Ind. Res. Inst., Tosu, Saga 841-0052, Japan, c) Sumitomo Coal Mining Co., Ltd., Kawasaki 213, Japan

d) Oita Ind. Res. Inst., Oita 870, Japan, e) Kyoto Univ., Kyoto 606-8501, Japan

RESEARCH OBJECTIVES

Evaporation of aluminum is one of the most serious problems with melting Nb-Al alloys. Spark plasma sintering (SPS) is very attractive with respect to this problem since sintering of blended or mechanically alloyed constituent powders is usually completed within five minutes and thus aluminum loss is almost negligible. Hot pressing and subsequent HIPing is a powder metallurgy process comparable to SPS. However, it is much more time consuming and costly than SPS. The purpose of this study is firstly to report the microstructure, mechanical properties and oxidation resistance of SPS compacts of Nb-Al-N and Nb-Si-B systems, and secondly to examine the performance and adequacy of SPS to prepare compacts composed of refractory metals such as Nb and elements such as Al with a much lower melting point than Nb or such as B which forms high-temperature borides of refractory metals and may cause difficulty in sintering.

SPARK PLASMA SINTERING

Compositions of Nb-Al-N compacts investigated are plotted on the 1773K isotherm of the Nb-Al-N ternary phase diagram [1] (Fig.1). Compacts were prepared via the following three different routes: (i)

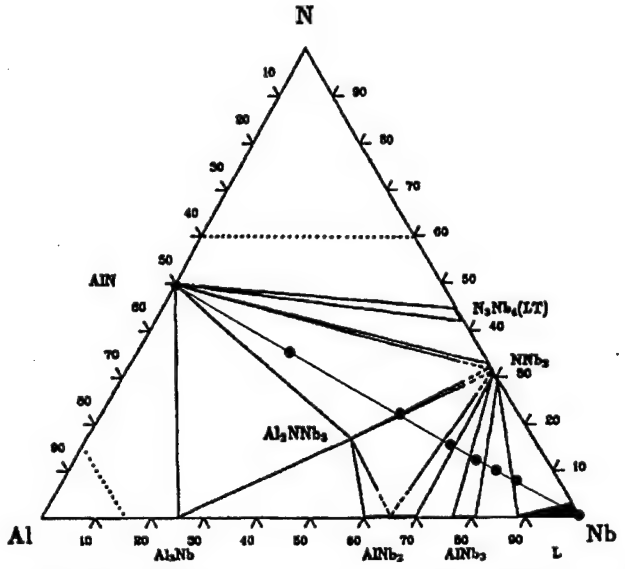

Fig. 1 Compositions of Nb-Al-N compacts (open circles) plotted on the 1773 isotherm of the Nb-Al-N phase diagram [1].

Nb (99.99% pure, -325 mesh) and AlN (99.8% pure, -300 mesh) powders were blended in a hexane-filled rotational ball mill for 0.5 hours and then consolidated in a SPS furnace at a temperature between 1623 – 1973K for 5 minutes under a consolidation pressure of 49 MPa in a vacuum of 6 Pa, (ii) two constituent powders were mechanically alloyed in an argon-filled planetary ball mill for 6 hours and consolidated similarly to (i), and (iii) pulverizing compacts prepared via route (i) and consolidated once again similarly to (i). We call compacts prepared via these three different routes (i) blended (BL) powder compacts, (ii) mechanically alloyed (MA) powder compacts and (iii) pre-sintered and milled (PSM) powder compacts, respectively.

Compositions of Nb-Si-B compacts investigated are given in Fig.2 [2]. BL, MA and PSM powder compacts with these compositions and dimensions 20 mm diameter and 5 mm thickness were prepared using Nb, Si (99.9% pure, -300 mesh) and B (99% pure, -300 mesh) powders. Blending and mechanical alloying of elemental powders was performed for 1 hour and 10 hours, respectively. After sintering, the microstructure and mechanical properties of compacts were examined.

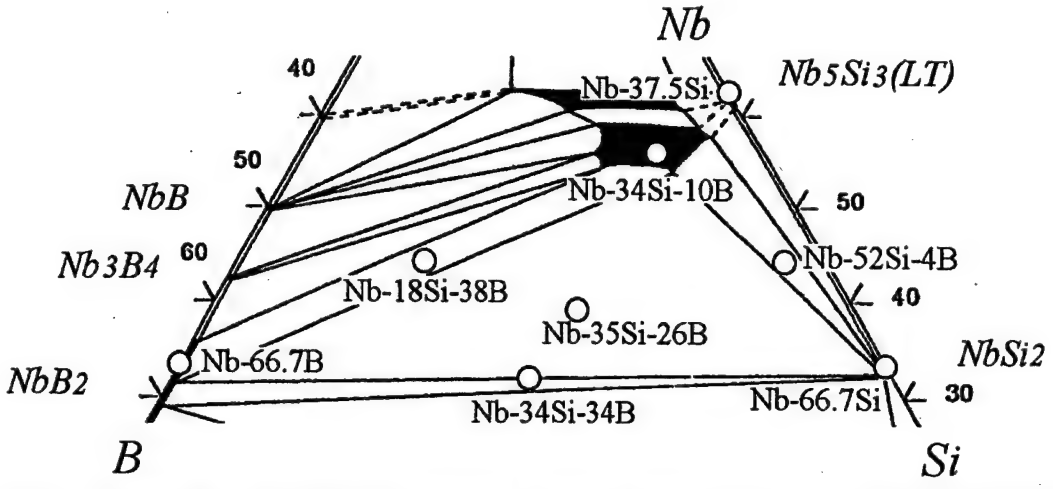

Fig. 2 Compositions of Nb-Si-B compacts (open circles) plotted on the 1873 isotherm of tl Nb-Si-B phase diagram [2].

RESEARCH PROGRESS AND RECENT RESULTS

Adding nitrogen was easily done by blending or mechanically alloying Nb and AlN powders and then sintering them. The addition of nitrogen caused the formation of Nb_2N in all the Nb-Al-N compacts and Nb_2N and Nb_3Al_2N in compacts with high aluminum and nitrogen contents. The highest room-temperature hardness and the highest yield stress at 1473K were observed for compacts consisting Nb_2N and Nb_3Al_2N and those consisting of Nb_2N and Nb_2Al, respectively.

Compacts of the Nb-Si-B system were found to consist of two or three of NbB_2, Nb_5Si_3, $Nb_5Si_3B_2$ and $NbSi_2$ phases depending on composition unless a large amount of silicon is consumed by forming SiO_2. A large amount of SiO_2 was observed in the MA powder compacts. The formation of such a large amount of SiO_2 leads to consumption of silicon. BL and PSM powder compacts are much less contaminated by oxygen than MA powder compacts. However, BL powder compacts exhibit an

inhomogeneous microstructure and often contain a large amount of pores. In comparison to BL powder compacts, PSM powder compacts show a homogeneous microstructure. PSM powder compacts generally show higher density than MA and BL powder compacts. Lower density of MA powder compacts may be interpreted in terms of a large amount of SiO_2 contained in MA compacts.

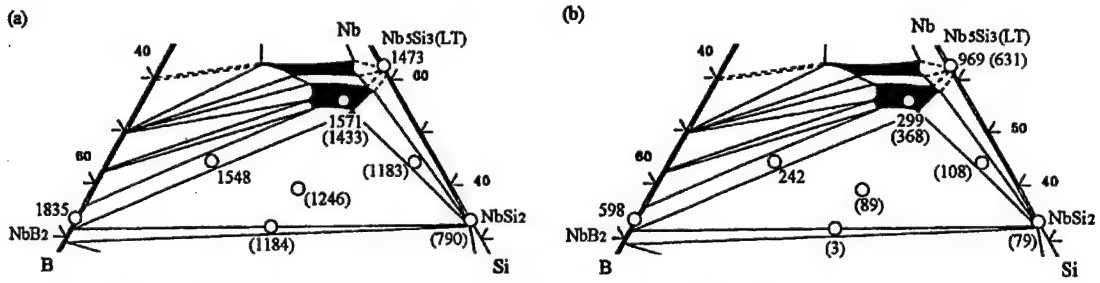

Fig. 3 (a) Microvickers hardness at room temperature and (b) yield stress in compression at 1673K for PSM powder compacts consolidated at 1973K and 1873K. Hardness and yield stress values for compacts consolidated at 1873K are shown in parentheses.

Contributions of NbB_2, Nb_5Si_3 and $Nb_5Si_3B_2$ phases to room-temperature hardness and yield stress at high temperatures were found to be much larger than those of $NbSi_2$ (Fig.3). BL and PSM powder compacts show a higher hardness than MA powder compacts. This may also be due to the presence of a large amount of SiO_2 in MA powder compacts. In view of the results described above, PSM compacts are superior to BL and MA powder compacts with respect to the extent of oxygen contamination, the amount of voids and the homogeneity of microstructure.

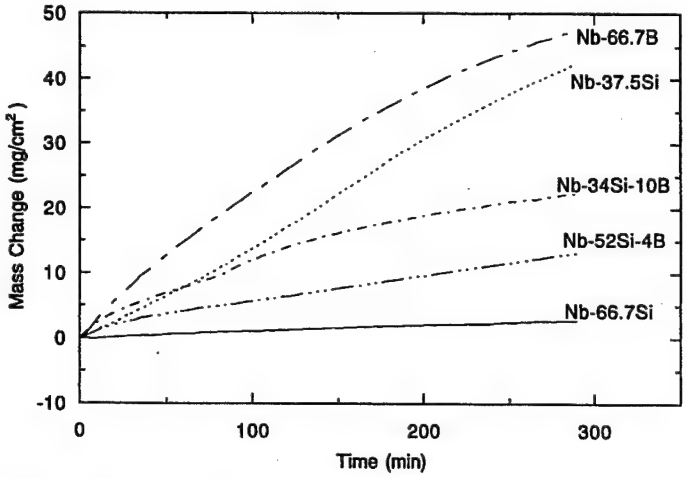

Fig.4 Oxidation-induced mass change of PSM powder compacts with five different compositions in the Nb-Si-B system at 1523 in air as a function of time.

Figure 4 shows oxidation-induced mass change of PSM powder compacts with five different compositions at 1523K in air as a function of time. Matrix phases of Nb-66.7B, Nb-37.5Si , Nb-34Si-10B and Nb-66.7Si compacts are NbB_2, $Nb5Si_3$, $Nb_5Si_3b_2$ and $NbSi_2$. Thus, the result of Fig.4 clearly shows that oxidation resistance of these phases increases in the sequence NbB_2, Nb_5Si_3, $Nb_5Si_3B_2$ and

$NbSi_2$. The oxidation resistance of $Nb_5Si_3B_2$ is found to be better than that of Nb_5Si_3, but it is not improved to a level near that of $NbSi_2$ by the boron addition responsible for the formation of $Nb_5Si_3B_2$. When a small amount of boron is added to Mo_5Si_3, a non-porous, protective scale forms [3,4]. The difference in oxidation resistance between boron-doped Mo_5Si_3 and $Nb_5Si_3B_2$ may be interpreted in terms of that Nb_2O_5 does not volatilize and thus a thin protective borosilicate layer does not form on $Nb_5Si_3B_2$. The oxidized layer on the Nb-34Si-10B ($Nb_5Si_3B_2$) compact did not spall, while that on the Nb-37.5Si (Nb_5Si_3) compact was easily spalled. This results in a large difference in oxidation resistance between Nb-37.5Si (Nb_5Si_3) and Nb-34Si-10B ($Nb_5Si_3B_2$) compacts. Thus, adding boron to Nb_5Si_3 is effective to prevent the spalling of oxidized layer formed on the silicide, although reasons for this have yet to be clarified.

CONCLUSIONS

(1) Dense compacts of Nb-Al-N and Nb-Si-B systems can be produced by SPS.

(2) Pre-sintered and milled (PSM) powder compacts is superior to blended (BL) powder and mechanically alloyed (MA) powder compacts in achieving microstructural homogeneity and reducing oxygen contamination.

(3) Compacts of the Nb-Al-N system consisted of phases expected from the Nb-Al-N system. Compacts of the Nb-Si-B system also consisted of phases expected from the Nb-Si-B system unless a large amount of silicon is consumed by forming SiO_2.

(4) $Nb_5Si_3B_2$ shows better oxidation resistance than Nb_5Si_3. However, the oxidation resistance of $Nb_5Si_3B_2$ is not as good as that of $NbSi_2$.

ACKNOWLEDGEMENTS

This was supported by JSPS Grant (JSPS-RFTF 96R12301) and MESSC Grant (No.1045026).

REFERENCES

[1] Schuster, J. C. and Nowotny, H., Z. Metallkd., 76 (1985) 728.

[2] Handbook of Ternary Alloy Phase Diagrams, edited by Villars, P., Prince, A. and Okamoto, H., Vol. 5, ASM International, Metals Park, Ohio, 1995, p. 5815.

[3] Meyer, M., Kramer, M. and Akinc, M., Adv. Mater., 8 (1996) 85.

[4] Meyer, M. K. and Akinc, M., J. Am. Ceram. Soc., 79 (1996) 938.

Synthesis and Mechanical Properties of Nb Matrix In-situ Composites

S. Hanada

Institute for Materials Research, Tohoku University, Sendai 980-8577, Japan

1. Research Objectives and Approach

The main objective of this study is to develop structural materials which can be used at elevated temperature exceeding the limiting temperature of conventional Ni base superalloys. Candidates to meet this demand are "in-situ composites" consisting of refractory intermetallics or ceramics in which a ductile phase is incorporated, because the composites are thermodynamically stable and exhibit no interfacial reactions between the constituent phases during holding at elevated temperature. In this study Nb_3Al/Nb_{ss} (Nb solid solution) and $TiC/Nb(Mo)_{ss}$ are selected as typical examples of ductile phase-toughened refractory intermetallics and ceramics by considering density and melting temperature. Since both the constituent intermetallic and ceramic are intrinsically very brittle at ambient temperatures, the incorporation of a ductile phase is essential to increase fracture toughness. Nb_3Al/Nb_{ss} and $TiC/Nb(Mo)_{ss}$ in-situ composites were synthesized by arc-melting, and their microstructures were controlled by heat-treatment or thermo-mechanical processing. Mechanical properties were investigated at temperatures between ambient temperature and 1500℃.

2. Research Progress and Highlights

2.1 Nb_3Al/Nb_{ss} in-situ composites

Preliminary experimental results on binary Nb-Al alloys indicate that although monolithic Nb_3Al has high strength at 1100-1300 ℃, the incorporation of Nb_{ss} particles in Nb_3Al leads to a remarkable decrease in strength at high temperatures [1]. Accordingly, solid solution strengthening due to ternary additions was investigated for each of the constituent phases in order to increase high temperature strength of Nb_3Al/Nb_{ss} in-situ composites [2]. High temperature strength of Nb_3Al/Nb_{ss} in-situ composites alloyed with ternary elements, which were prepared by isothermal forging, was examined in the microstructure of equiaxed grains with a similar size as a function of volume fraction of Nb_{ss}. It is found that Mo alloying of 30-60 mol% is very effective to increase high temperature strength of the in-situ composites. Creep strength was evaluated using Mo-containing Nb_3Al/Nb_{ss} in-situ composites with two typical microstructures (Fig.1); equiaxed (Nb_3Al+Nb_{ss}) grains (microstructure A) and unidirectionally arranged Nb_{ss} filaments in coarse Nb_3Al grains (microstructure B). Nb-18Al-31Mo alloy containing the filament-like Nb_{ss} phase possesses excellent creep strength at 1300℃, as compared with other refractory intermetallics (Fig.2)[3].

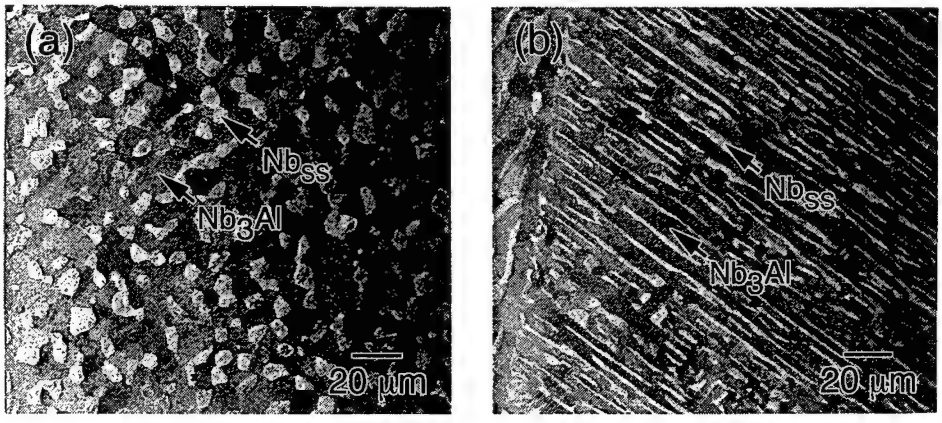

Fig.1 Scanning electron micrographs of Nb-18Al-31Mo annealed at 1500℃ for 100 h after isothermal forging (a) and solution treated at 1900℃ for 3 h and annealed at 1500℃ for 100 h after isothermal forging (b).

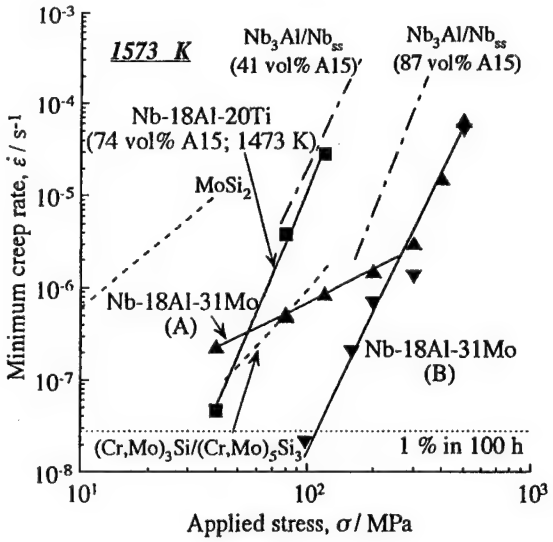

Fig.2 Stress dependence of minimum creep rate at 1300℃ for Nb-18Al-31Mo in comparison to refractory intermetallic base alloys.

2.2 TiC/Nb(Mo)$_{ss}$ in-situ composites

Microstructures and mechanical properties were investigated using TiC/Nb(Mo)$_{ss}$ in-situ composites with nominal compositions of Nb-40%TiC, Nb-20%Mo-40%TiC, Nb-40%Mo-40%TiC and Mo-40%TiC (mol%). For as-arc melted samples no precipitate can be seen in primarily solidified TiC except for Nb-40%TiC. After annealing at 1600℃ for 24 h, fine bcc-precipitates appear in the primary TiC for all samples. The precipitate size increases with increasing Nb content. In as-arc melted samples, cracks introduced by an indenter propagate straight to a long distance, while in annealed samples, introduced cracks exhibit 'bridging' by bcc-precipitates. As a result the length of cracks is shortened in the latter samples, indicating that the composites are ductile phase-toughened by the bcc phase. Above 1200℃ compressive yield strength of Nb-40%Mo-40%TiC and Mo-40%TiC is found to be higher than that of single phase TiC [4].

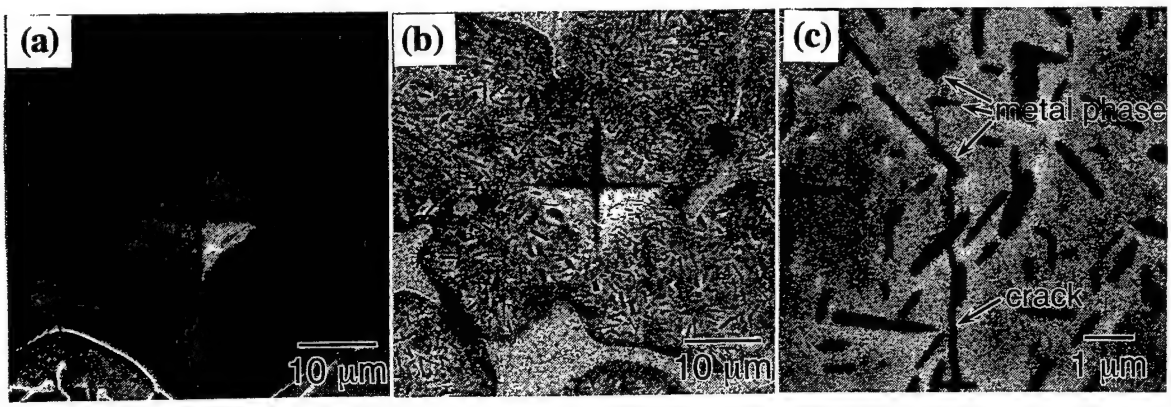

Fig.3 Microstructures of Nb-20Mo-40TiC after indentation test for (a) as-cast and (b) annealed composite. (c) crack tip in (b).

3. Critical Scientific Issues and Challenges

Fracture toughness values over 15 MPa$\sqrt{m}$ have not been obtained for Nb$_3$Al/Nb$_{ss}$ and TiC/Nb(Mo)$_{ss}$ in-situ composites, although the composites alloyed with ternary elements possess excellent high temperature strength. It is known that the fracture toughness of ductile phase-toughened composites is sensitive to size, volume fraction and distribution of the ductile phase. Therefore, fracture

toughness will be further improved, if microstructure is highly controlled. Otherwise, the low fracture toughness of the in-situ composites may be due to low ductility of Nb_{ss} as well as insufficient microstructure control. Experimental data on solid solution strengthening of Nb by substitutional and interstitial elements in relation to ductility or toughness seem to be still lacking.

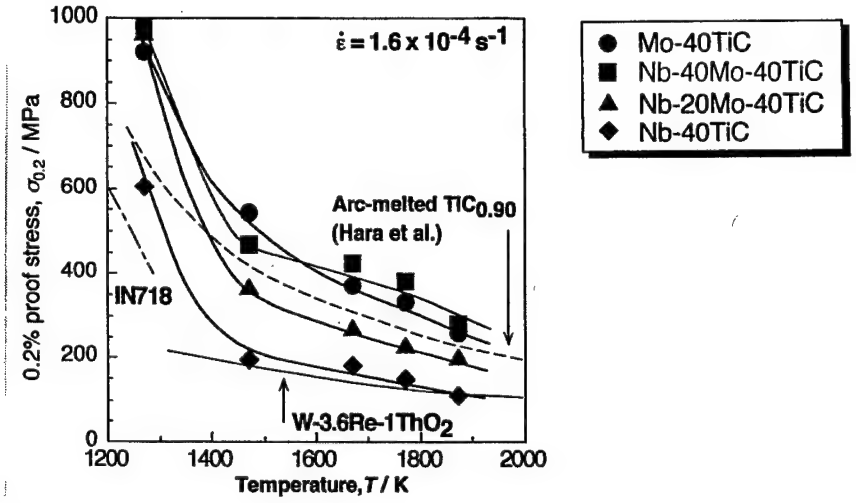

Fig.4 Temperature dependence of 0.2% proof stress of Nb-Mo-TiC composite.

Another critical issue is low oxidation resistance of Nb_{ss}. Although the oxidation resistance of Nb_{ss} has been considerably improved by alloying and surface coating, there are still serious problems above 1200℃. Surface coating technology based on a new concept should be developed [5, 6].

Publications

[1] Y. Murayama, T. Kumagai and S. Hanada: High-Temperature Ordered Intermetallic Alloys V, Ed. by I. Baker et al., MRS, 1993, p.95.
[2] S. Hanada et al. : Thermomechanical Processing of Steels & Other Materials, Ed. by T. Chandra et al., TMS, 1997, p. 1583.
[3] T. Tabaru and S. Hanada: Intermetallics, 6(1998) 735.
[4] N. Nomura, K. Yoshimi, T. Konno and S. Hanada: Advanced Materials and Processing (PRICM 3), Ed. by M. A. Imam et al., TMS, 1998, p.543.
[5] M. Matsubara and S. Hanada: J. Japan Inst. Metals, to be published.
[6] H. Hosoda, S. Watanabe and S. Hanada: High-Temperature Ordered Intermetallic Alloys VIII, MRS, to be published.

Alloy Design of Laves Phases Systems: Focus on Nb-Cr-Ti

Dan J. Thoma, Fuming Chu, Katherince C. Chen, Paul G. Kotula, John M. Wills, and Robert D. Field - *Los Alamos National Laboratory*
C.T. Liu, J. Zhu, M. Yoo, and C.L. Fu – *Oak Ridge National Laboratory*

Research Objectives and Approach

With intermetallic research focusing primarily upon the simple ordered structures, the more complicated topologically close-packed (TCP) structures have been largely ignored for high temperature structural applications. Among the TCP phases are Laves phases, which are the most abundant class of intermetallics with over 360 binary phases. Furthermore, Laves phases are capable of dissolving considerable amounts of ternary alloying additions, and over 900 combined binary and ternary Laves phases have been documented. Laves phases form at or near the AB_2 composition, and the abundance of Laves structures among intermetallic compounds has been attributed to geometric principles for the arrangement of atoms on ordered lattice sites [Laves]. For example, metallic compounds have a tendency to form with close packing of atoms, homogeneous bonding, and high atomic symmetry, and Laves phases satisfy the geometric conditions (similar to metallic materials) more efficiently than other metallic compound structure types.

Even though the geometrically structured Laves phases are the most abundant amongst the various intermetallics, they are the least utilized. Historically, Laves phases have been perceived as a "pest" to the steel and superalloy industries due to grain boundary embrittlement problems associated with Laves phase precipitates [Livingston]. Stoichiometric binary Laves phases display low toughness (<5 $MPa/m^{1/2}$) at low temperatures, contributing to the grain boundary embrittlement. For this reason, Laves phases were typically avoided, until it was discovered that Laves phase precipitates ($TaFe_2$) distributed in the matrix of ferritic steels (as opposed to grain boundaries) yielded remarkable wear resistant properties (as well as good elevated temperature strengths) without sacrificing the low temperature ductility [Bhandarkar et al.]. As a result, it has been realized that Laves phases have unique properties which make them attractive for high temperature structural applications. For example, they retain their high strength (>0.85 of ambient yield strength) at half of the homologous melting temperature, which is the highest of all intermetallics [Fleischer]. Many of these phases also have high melting temperatures, excellent creep properties, reasonably low densities, and good oxidation resistance for alloys containing Cr, Al, Si or Be. However, low temperature deformability needs to be addressed.

Recent results suggest that Laves phases have intrinsic features that might favor deformability at ambient temperatures. For example, monolithic Laves such as HfV_2 [Chu et al] and $NbCr_2$ [Chu and Thoma et al] have high Poisson's ratios (0.39 and 0.34, respectively) and low shear modulus values (30 GPa and 80 GPa, respectively). The high Poisson ratios are an indication of a lack of strong directional bonding as compared to other intermetallics with Poisson ratios near 0.2 ($MoSi_2$, NiAl, TiAl). The low shear modulus values suggest a *potential* for resistance to brittle failure. For example, the Rice-Thomson criteria suggests that when $G\mathbf{b}/\gamma < 10$, there is a tendency for resistance to brittle failure. With calculated surface energies (γ) and by assuming

that **b** = 1/6<112> synchro-Shockley partial dislocations are mobile, both materials have a Rice-Thomson value near 5.0 (HfV_2 ~ 3.7 and $NbCr_2$ ~ 6.0).

Although experience indicates that monolithic Laves phases are brittle, dual-phase alloys of a bcc phase and C15 phase demonstrate encouraging deformability. Multilayers of HfV_2 + Nb have been cold-rolled up to 30% without fracture [Inoue and Tachikawa]. In addition, dual phase $NbCr_2$/Cr structures display 5-10% ductility with yield strengths that are twice that of commercial superalloys [Takeyama and Liu]. Dual phase alloys based upon $HfCr_2$/Cr(Hf) indicate promising ambient fracture toughness, with values ranging from 7 MPa/$m^{1/2}$ to 15 MPa/$m^{1/2}$ [Kumar and Miracle].

Applications that utilize Laves phases for high-temperature structural applications stem from optimizing the deformability of the materials. Three approaches have been documented to achieve this goal: 1) alloying of the monolithic intermetallic, 2) incorporating ductile phases, and 3) tailoring of microstructures through processing pathways. Significant advances have been characterized through the applications of these three defined approaches in the Nb-Cr-Ti system.

Research Progress and Highlights

Alloying of the monolithic Laves phase to impart deformability requires understanding of the deformation mechanism. Synchroshear apparently controls dislocation formation as well as twinning. Therefore, three possible factors that influence synchroshear have been investigated: 1) stacking fault energy, 2) anisotropic softening (owing to phase instabilities), and 3) size arguments. Of these factors, size arguments provide the most consistent explanation of results. In the deformable $\alpha c\beta$ stacking sequence in the Laves phases, substitution of a smaller A-site atom in the AB_2 phase most always results in lower moduli and increased toughness values (provided that that the packing efficiency in the deformable stacking sequence is reduced). For a base $NbCr_2$ system, titanium additions fit this criterion, and in fact, increases the toughness by 50%.

Despite modest increases to the toughness of monolithic Laves phases, toughness values over 5 MPa $m^{½}$ are experimentally rare. Therefore, a second, more ductile phase, is required to realize the potential of the alloys. Most binary Laves phase systems in equilibrium with a disordered phase are limited to bcc phases. In the Nb-Cr-Ti system, the Laves phase is in equilibrium with both a Cr-rich solid solution and a (Nb,Ti) solid solution. Based upon the thermodynamics and Laves phase monolithic deformability, a two-phase alloy in equilibrium with maximum deviations from the Laves phase stoichiometry was chosen. The alloy, Nb-36Cr-27Ti (at.%), also has been explored by Davidson to demonstrate high K_{Ic} values (15-25 MPa $m^{1/2}$) [Davidson]. In addition, Nb-based intermetallic systems offer potentially attractive refractory properties owing to the high melting temperature and low density of Nb.

Plasma arc melting was used to cast 3 kg ingots. In the as-cast condition, the alloys displayed a high room temperature compressive yield strength (1.6 GPa), compressive ductility (16%), and reasonable fracture toughness (> 15 MPa $m^{1/2}$). The alloys still have high strength (1 GPa) at

1000°C. In tension, alloys typically failed at 500 MPa. Failure occurred at the continuous Laves phase network at grain boundaries.

In an effort to potentially optimize the tensile properties, rapid solidification processes have been used supersaturate the bcc phase and control the Laves phase precipitation during heat-treatment. Melt-spun and hot-isostatically pressed alloys have outstanding compressive strengths (UTS of 2.35 GPa at ambient temperatures), and tensile investigations are currently underway.

Potential Structural Applications and Engineering Issues for Systems of Interest

The development of high temperature materials typically results in a direct comparison to the mature property base of Ni-base superalloys. However, for increased operating efficiencies in a variety of applications, temperature greater than 1000°C are sought. Although a compromise of properties are most likely required, particularly with ambient temperature deformability, goals for new high-temperature structural materials must include high-temperature strength and stability to at least 1200°C as well as some level of inherent oxidation resistance. Many Laves phase/bcc phase systems demonstrate the potential properties required to fit these needs. However, experience dictates that bcc materials are not best for creep behavior, even though the Laves phases have documented potential. Recently, Liu has investigated a Cr-rich Laves phase system, and at 1000°C and 140 MPa (in air), creep lives are currently at 1500 hours. Conventional polycrystalline superalloys under these conditions have rupture times of 100 hours.

Critical Scientific Issues and Challenges for the System of Interest

To fully develop the potential of Laves phases, three main issues need to be addressed: (1) alloy design, (2) structure stability, and (3) property evaluations. First, alloy design is required to fully recognize the enormous base of alloying potential in Laves phases. As examples, the role of defects and vacancies, stacking fault energies, and bond strengths need to be better understood to provide founded alloying schemes, particularly in light of size arguments on deformability. Second, structure stability is governed by the electronic structure in Laves phases, and a structural instability may give rise to a tendency for twinning at ambient temperatures. This phenomenon has been illustrated for (Hf, Nb)V_2 and warrants further evaluations. Finally, the properties (both physical and mechanical) need to be fully characterized in Laves phases. Properties can vary drastically in the literature, presumably because of sample quality in the brittle materials. Moreover, the deformation modes and mechanisms require better definition to couple with the mechanical behavior of the material. With respect to the deformability of Laves phases in bcc/Laves dual phase alloys, deformability of Laves phases have been observed, and the role of the bcc phase on the Laves phase deformation needs more attention.

References

Bhandarkar, M.D., M.S. Bhat, E.R. Parker, and V.F. Zackay, *Metall. Trans.* **7A** 753 (1976).
Chu F., D.J. Thoma, Y. He, T.E. Mitchell, S.P. Chen, and J.H. Perepezko, *MRS. Symp. Proc.*, **364** 1085-1090 (1995)
Chu, F., Ming Lei, A. Migliori, S.P. Chen, and T.E. Mitchell, *Phil. Mag. B* **70** 867 (1994).
Davidson, D.L. and K.S. Chan, AFOSR Report F49620-95-C-0043, (1998).
Fleischer, R.L., *MRS Symp. Proc.* **133** 305 (1989).
Inoue, K., and K. Tachikawa, *IEEE Trans. Magn.* **MAG-15** 635 (1979).
Kumar, K. S. and D. B. Miracle, *Intermetallics* **2** 257 (1994).
Laves, F., in *"Theory of Alloy Phases"*, (ASM, Cleveland, OH) 123 (1956).
Livingston, J.D., *Phys. Stat. Sol. (a)* **131** 415 (1992).
Takeyama, M. and C.T. Liu, *Mater. Sci. & Eng. A* **132** 61 (1991).

Acknowledgements

This work was funded by the U.S. Department of Energy, Office of Basic Energy Sciences, Division of Materials Science.

INVESTIGATION OF THE FRACTURE CHARACTERISTICS OF LAMELLAR NANOCOMPOSITES AND *IN SITU* FORMED COMPOSITES DESIGNED FOR HIGH TEMPERATURE SERVICE

D.L. Davidson and K.S. Chan
Southwest Research Institute
San Antonio, TX 78228

Summary of Research on *in situ* Composites

Research funded by Air Force office of Scientific Research,
Contract F49620-95-C-0043

If new, high temperature materials are to replace the Ni-based superalloys in the hot sections of gas turbines, then they must achieve adequate resistance to creep, oxidation, and fracture. Creep and oxidation resistance are requirements at high temperature. Fracture resistance is both a high and low temperature characteristic. Adequate fracture resistance consists of three parts: fatigue crack initiation, fatigue crack growth, and fracture toughness. This program has focused on understanding the materials science of composites formed *in situ* containing the intermetallic Cr_2Nb that is known to exhibit high temperature oxidation and creep resistance, but to have very low fracture toughness at ambient temperature. If materials with good fracture toughness at ambient temperature can be found or designed, then fracture toughness at high temperature should be adequate.

The principal objective of this part of the program was to increase the ambient temperature fracture toughness of composites containing ≈ 40 v/o Cr_2Nb. This lev el of intermetallic should be sufficient to impart oxidation and creep resistance at high temperature. An alternative goal would be to explain why it is not possible to obtain the level of fracture toughness desired. Achieving a rule-of-mixtures derived fracture toughness level of 30 - 50 MPa$\sqrt{m}$ was the goal. This magnitude of fracture toughness would fully use the high fracture toughness of the matrix (≈ 80 MPa$\sqrt{m}$). A rule-of-mixture level of fracture toughness has been achieved by the Co/WC composites, so this is a reasonable goal for materials development.

The approach used to examine the fracture toughness of the Nb-Cr-Ti *in situ* composites included a combination of experiment and modeling. The following tasks describe the research scope: (1) perform detailed analyses of growing crack tips experimentally, (2) measure and compute the constraining effect of particles on matrix deformation, (3) model the fracture process to search for a microstructure that would optimize fracture toughness, and (4) try to fabricate the microstructure to examine the concepts derived.

Research Progress: The low fracture toughness of cast *in situ* composites was found to be caused by (1) failure of the matrix by cleavage, (2) fracture of the large Cr_2Nb particles in antishielding locations, and (3) constraint of deformation in the matrix by the particles. It became clear that the size of the Cr_2Nb should be reduced to avoid particle fracture, but that particle size reduction would increase constraint and promote cleavage fracture in the matrix.

The microstructure of the *in situ* composites was modified by rapid solidification and mechanical alloying to reduce particle size. Both of these fabrication methods resulted in reduction of the size of the Cr_2Nb particles, but the magnitude of the fracture toughness was not increased. Constraint was measured and found to be high in these materials and the matrices failed by cleavage. An extensive effort was made to determine why these manufacturing methods for increasing toughness were ineffective.

Several models using different assumptions about how to compute fracture toughness were formulated that included all of the relevant factors related to the fracture of these composites: (1) failure mode of the matrix by cleavage, (2) volume fraction, size, and fracture toughness of the particles, (3) the effect of particle constraint on fracture strain at the crack tip, and (4) the stress level within the process zone. Two of the models approximately fit the existing fracture data for the Nb-based *in situ* composites, and the best of these models was used to predict the highest fracture toughness that could be expected from an optimum microstructure containing $\approx$ 40 vol. % Cr_2Nb particles. The model predicted that a fracture toughness of $\approx$ 25 MPa$\sqrt{m}$ was the maximum that could be attained, and that the optimum size of the particles would be 2 μm diameter. To attain the rule-of-mixtures fracture toughness with $\approx$ 40 vol. % Cr_2Nb, the fracture toughness of the 2 μm diameter particles would have to be doubled to at least 3 MPa$\sqrt{m}$.

Meanwhile, mechanically alloyed composites were being made in the U.K. so that materials supersaturated in Cr could subsequently be heat treated to form Cr_2Nb particles by precipitation. Thus, control of particle size with good dispersion could be attained by carefully controlled heat treatment schedules. Powders of the material compositions that were mechanically alloyed formed either no Cr_2Nb or only small amounts, as determined by x-ray diffraction. However during the powder consolidation process at 1300°C, two of the compositions precipitated large numbers of Cr_2Nb particles with high contiguity. The third material was found to have little to no Cr_2Nb, but upon heat treatment, up to 30 v/o intermetallic could be precipitated. Size of the precipitated intermetallic particles was in the 1-2 μm range, as determined by optical microscopy. Fracture toughness measurements from these materials indicated little influence of composition or heat treatment. The best fracture toughness attained was $\approx$ 12 MPa$\sqrt{m}$.

A detailed examination was made of the material from which Cr_2Nb could be precipitated by heat treatment. Interstitials to be at a low enough level in these materials that the fracture toughness should

not have been affected. Auger electron spectrometry revealed that the treatment altered the composition of the matrix; Ti was found segregated into small regions, thereby depleting the matrix of Ti. Measurements by x-ray diffraction showed that with increasing volume fraction of Cr_2Nb, the lattice parameters of the matrix increased and that of the intermetallic decreased. This was another indication that the matrix was depleted of Ti and that the intermetallic was being enriched with Ti. A lattice strain of about 7% would have been required to maintain coherency between Cr_2Nb and the matrix. Examination by TEM of one of the heat treatments showed that the dislocation structure of the matrix was quite different from that of the high toughness matrix alloy, being closer to that of deformed pure Nb instead.

Many questions remain unanswered concerning the precipitation of Cr_2Nb from the mechanically alloyed materials. Precipitation appears to be a much more complex process than anticipated from the phase diagram. Until the mechanical alloying process and effect of subsequent heat treatment on intermetallic and matrix compositions are understood, together with the effect of segregation during heat treatment, this processing route is unlikely to provide microstructures with maximum fracture resistance.

Fatigue crack growth resistance of all the materials examined were similar. At very low growth rates, the slopes of the crack growth rate - stress intensity factor curves were very high (≈ 30), and similar to pure Nb, while above a growth rate of 10^{-9} m/cycle, the slope of the curve was dependent on the fracture toughness. For the high toughness matrix alloy with no Cr_2Nb particles, the slope was about 4. Threshold stress intensity factors (ΔK_{th}) were in the range 6 ± 1 MPa$\sqrt{m}$, with materials containing Al on the low side and materials containing Cr_2Nb on the high side. This difference can be attributed to a modulus effect, but the basis of the intrinsic ΔK_{th} is not known. Because none of these experiments were conducted in vacuum, there results may include some effects of environment.

Conclusion: When all these results are considered together, it appears that it will be very difficult to elevate the ambient temperature fracture toughness of Cr_2Nb containing *in situ* composites to near rule-of-mixture levels. If a manufacturing technology can be found that will allow the dispersion of particles that are small enough to preclude their fracture, then they provide so much constraint that plasticity in the matrix is limited to values that preclude the achievement of high fracture toughness.

If the particles could be made coherent with the matrix, then it might be possible to relieve constraint by the shearing of particles by dislocations. It does not appear possible to alter the lattice parameters of matrix and intermetallic by alloying to achieve coherency because Nb has the largest size of any of the possible alloying elements; thus, the lattice parameter of the matrix can only be decreased by alloying; whereas it needs to be increased to match the lattice parameter of Cr_2Nb.

Future direction: To obtain a high fracture toughness *in situ* composite, it appears to be necessary to

find a system where coherency can be maintained between the matrix and intermetallic. This would allow the constraint of deformation in the matrix to be relieved by shearing of the particles. The second best alternative will be to find or make by alloying an intermetallic that has a fracture toughness of at least 6 MPa$\sqrt{m}$. This would allow much more of the high toughness of the matrix to be utilized in imparting fracture resistance to the composite.

A fracture micromechanics study of one form of *in situ* composite containing Nb_5Si_3 indicated that particles of this intermetallic could deform some before breaking in the elevated stress field of a crack tip. Therefore, composites based on this intermetallic may be preferable to those based on Cr_2Nb. However, a much more detailed study of the fracture processes of *in situ* composites based on this intermetallic would be required to examine this hypothesis.

Effects of Alloying Addition on Fatigue and Fracture of Nb-Based Alloys and *In-Situ* Composites

Kwai S. Chan and David L. Davidson
Southwest Research Institute
San Antonio, TX78238

Research Objective and Approach

The objective of this research is to develop a fundamental understanding of the effects of alloying additions on the fatigue and fracture resistance of Nb-based alloys and *in-situ* composites intended for high temperature service. In particular, alloying additions of Ti, Cr, and Al in Nb-Cr-Ti-Al alloys have been studied systematically to evaluate their individual effects on fatigue and fracture resistance for the purpose of developing a tough solid solution alloy matrix for Nb-based *in-situ* composites.

An integrated experimental/computational science approach has been used to discover the role of Ti, Cr, and Al alloying additions in cleavage fracture of Nb-Cr-Ti-Al solid solution alloys. *In-situ* fatigue and fracture experiments were performed in a scanning electron microscope to directly characterize the crack-tip deformation and fracture process. Theoretical modeling of dislocation nucleation at the crack tip and the mobility of dislocations moving away form the crack tip was performed. These effort included theoretical calculations of (1) the unstable stacking energy using a cluster atom approach and Rice's approximation, and (2) the Peierls-Nabarro barrier energy and stress, both as a function of alloying addition. The experimental and theoretical results were compared to elucidate the effects of alloying addition on cleavage fracture by considering the competition of dislocation emission at the crack tip, the mobility of dislocations moving away from the crack tip, and the nucleation and propagation of cleavage cracks.

Research Progress and Highlights

A basic understanding of individual effects of alloying additions of Ti, Cr, and Al in Nb-Cr-Ti-Al alloys has been developed in this program. Cr addition increases the unstable stacking energy (USE), which is a measure of the ease of dislocation nucleation at the crack tip, and the Peierls-Nabarro (P-N) barrier energy , which is a measure of the dislocation mobility moving away from the crack tip. As a result, Cr addition reduces crack-tip dislocation emission, promotes cleavage fracture, and lowers the fracture resistance.

In contrast, Ti addition promotes slip emission from the crack tip by increasing the dislocation mobility through a lowering of the P-N barrier energy. Figure 1 shows slip emission from a crack tip at K = 50 MPa$\sqrt{m}$ in Nb-13Cr-37Ti at ambient temperature and the corresponding crack-tip strain distribution. Extensive slip emission from the crack tip in this alloy suppresses cleavage crack propagation, Figure 2, and leads to a drastic increase in the fracture resistance. Theoretical

calculations show that Ti addition reduces the P-N barrier energy, U_{P-N}, such that the ratio of the surface energy, γ_s, to U_{P-N} exceeds the critical value of 6.3 for the onset of ductile fracture, Figure 3. The consequence is that the fracture toughness increases with Ti addition or decreasing U_{P-N}, as shown in Figure 4.

Al addition increases the USE that has the effect of promoting cleavage fracture by making dislocation nucleation at the crack tip difficult. A summary of the current understanding of the brittle-ductile fracture transition in Nb-Cr-Ti-Al alloys is presented in Figure 5, which shows the brittle fracture boundary in a plot of Ti/Nb atomic ratio and Al + Cr contents. Cleavage fracture with low fracture toughness occurs in the region where the crack-tip slip emission is controlled by dislocation emission at the crack tip (USE), while the fracture toughness in the ductile region is controlled by dislocation mobility away from the crack tip (P-N energy).

Potential Structural Applications and Engineering Issues

The methodology developed in this program can be used to design innovative alloy compositions that provide both oxidation and fracture resistance. Good oxidation resistance in metallic systems often requires the addition of Cr, Al, and Si, which can lead to undesirable reductions in fracture resistance. The basic understanding developed in this work provides a scientific approach for optimizing oxidation and fracture resistance by alloying with the most desirable elements (Ti, Cr, and Al) in the proper amounts.

Outstanding engineering issues are: (1) How to apply the current methodology to develop innovative refractory metal in-situ composites for very high temperature applications where both oxidation resistance and fracture toughness are required? (2) What are the effects of Si addition on fracture resistance and the best way to include Si alloying addition in refractory alloys? (3) How to improve the deformability and fracture resistance of the intermetallic phases (silicides or laves phases) in the in-situ composites?

Critical Scientific Issues and Challenges

The challenge lies in the ability to develop material systems that have both adequate oxidation resistance at very high temperatures and fracture resistance at ambient temperatures. There is a need to balance alloy compositions (Ti, Cr, Al, Si, Hf, etc) in Nb or Mo systems to maximize oxidation resistance without causing reduction in fracture resistance. This requires control of (1) alloy compositions of the matrix and intermetallic phases, and (2) microstructures of the in-situ composites. Good oxidation requires large amounts of alloying additions of elements in the matrix phase and the presence of hard intermetallc particles in the microstructures, both are likely to cause embrittlement and reduction in fatigue and fracture resistance.

To make further advances in the field, there is a need for a breakthrough in understanding the effects of alloying addition on the brittle-to-ductile fracture transition, preferably at the atomic bonding level. The alloying of Al and Si to transition metals such as Nb, Mo, Ti, and Cr requires forming atomic bonds involving electrons in the p, s and d shells. Work in the current programs identifies how the s and d electrons affect the dislocation emission process and their influence of

fracture resistance. Further advance requires developing a understanding of the interactions of the p electrons in Al and Si with the s and d electrons in transition metals such as Ti, Cr, Nb, and Mo, and their consequences on dislocation nucleation, dislocation mobility, cleavage fracture, and fracture resistance. New methods for computing the USE and P-N barrier energy for complex, noncubic crystal structures also required.

Publications

1. K.S. Chan and D.L. Davidson: "Effects of Ti Addition on Cleavage Fracture in Nb-Cr-Ti Solid Solution Alloys," *Met. and Mat. Transactions A, 1999,* (in press).
2. K.S. Chan and D.L. Davidson: "Evidence of Void Nucleation and Growth on Planar Slip bands ," *Met. and Mat. Transactions A, 1999* (in press).
3. D. L. Davidson and K. S. Chan: "The Fatigue and Fracture Resistance of a Nb-Cr-Ti-Al alloy," *Met. and Mat. Transactions A, 1999* (in review).
4. D.L. Davidson: "transition Metal Alloys: Elastic Properties and Peierls-Nabarro Stresses and Barrier Energies," *Materials Science and Engineering, 1998* (in review).
5. D. L. Davidson and R.E.Beissner: "Cluster Model for calculation of Unstable Stacking Energy to Assist in Alloying of Transition Metals," 1998 (in preparation).

Acknowledgements

This research was sponsored by the U.S. Air Force Office of Scientific Research under Contract No. F49620-95-0043, Program Monitor, Dr. Spencer Wu. Supply of Nb-Cr-Ti-Al alloys by Dr. Dan J. Thoma at Los Alamos National Laboratory, Los Alamos, New Mexico, is acknowledged.

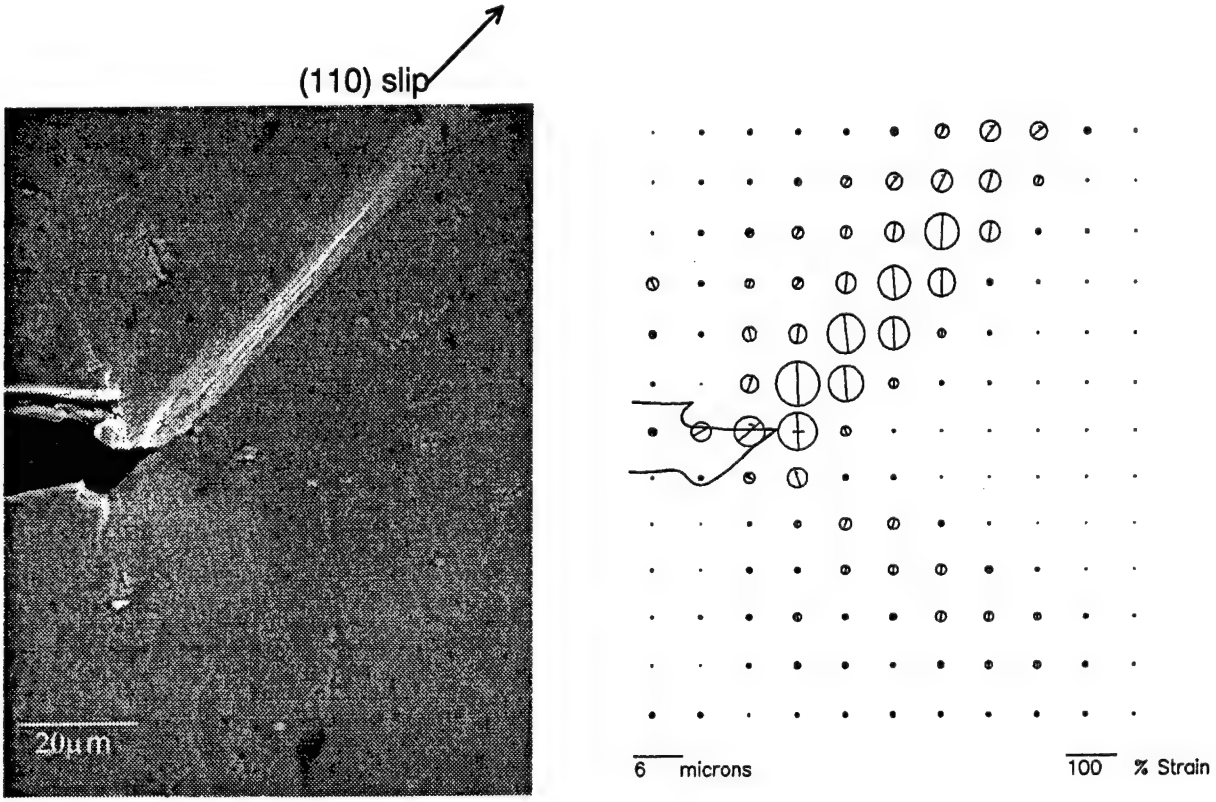

(a) (b)

Figure 1. Near-tip slip behavior in Nb-13Cr-37Ti at 25°C: (a) slip emission from the crack tip at K = 50 MPa√m, and (b) near-tip strain distribution presented in terms of Mohr's circle of strain shows strain concentration along the slip band.

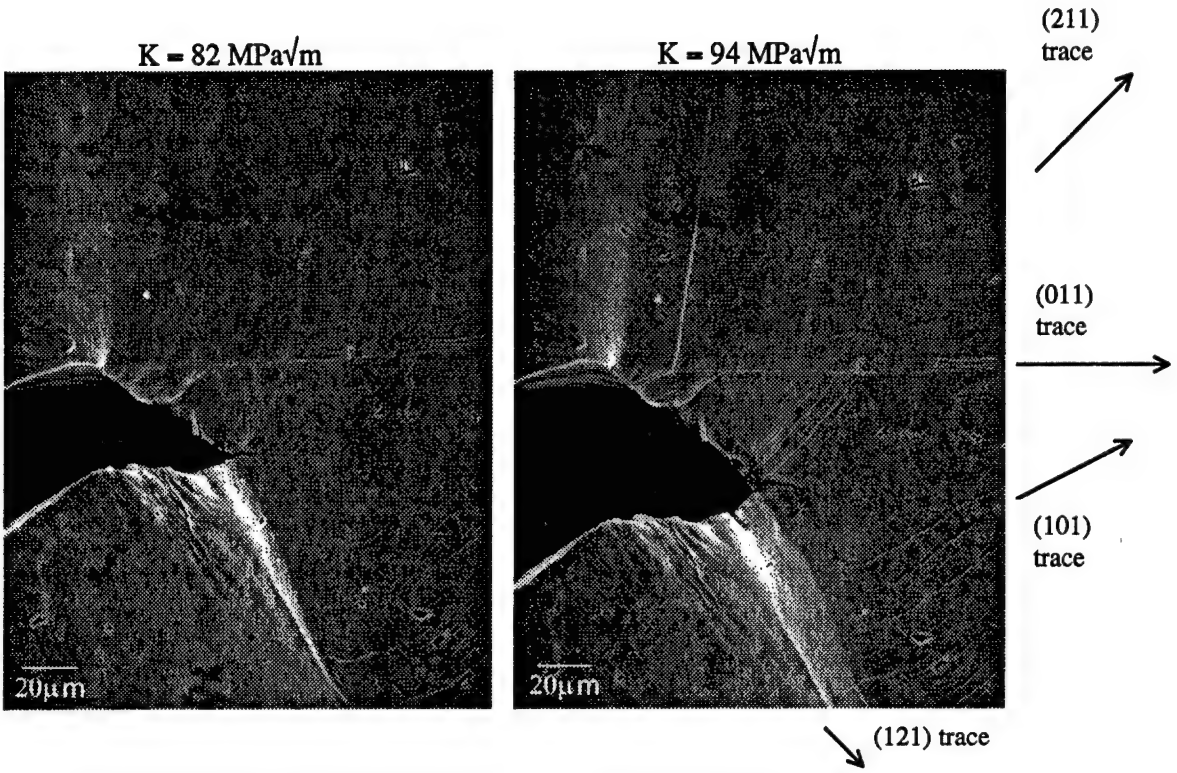

Figure 2. Observations of near-tip slip and fracture process in the Nb-Cr-Ti alloy at 25°C: (a) small extension of the main crack on a plane in the (011) zone at K = 82 MPa√m, and (b) emission of slip on three planes in the (101), (211), and (121) zones suppressed further propagation of the main crack at K = 94 MPa√m.

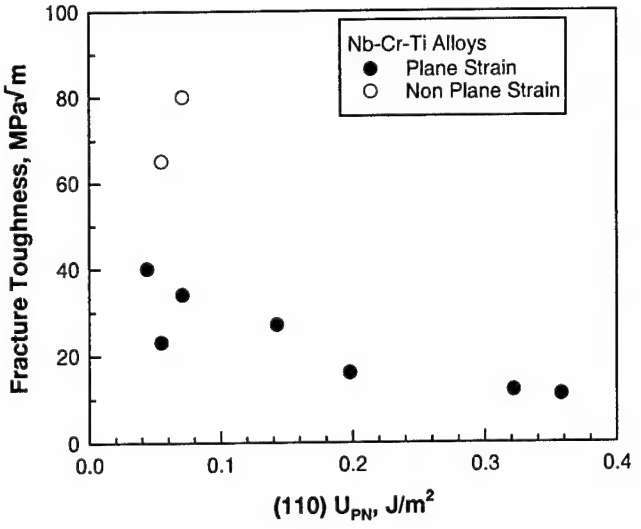

(a)

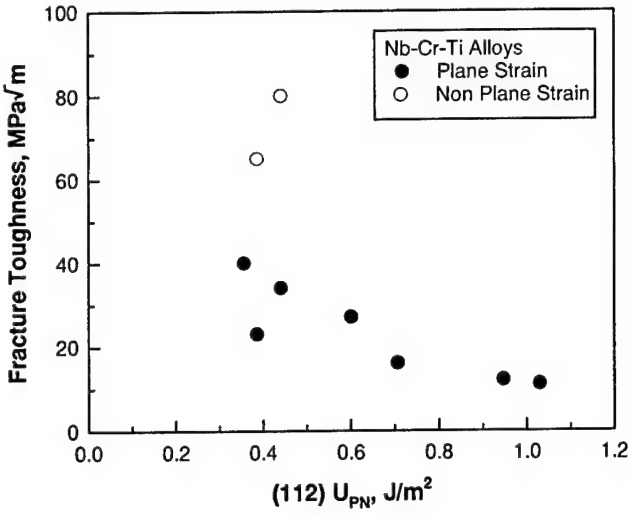

(b)

Figure 3. Correlation of fracture toughness against the P-N energy values: (a) P-N energy for (110) slip, and (b) P-N energy for (112) slip. In both cases, the trend is increasing fracture toughness with decreasing values of the Peierl-Nabarro energy barrier, $U_{P\text{-}N}$.

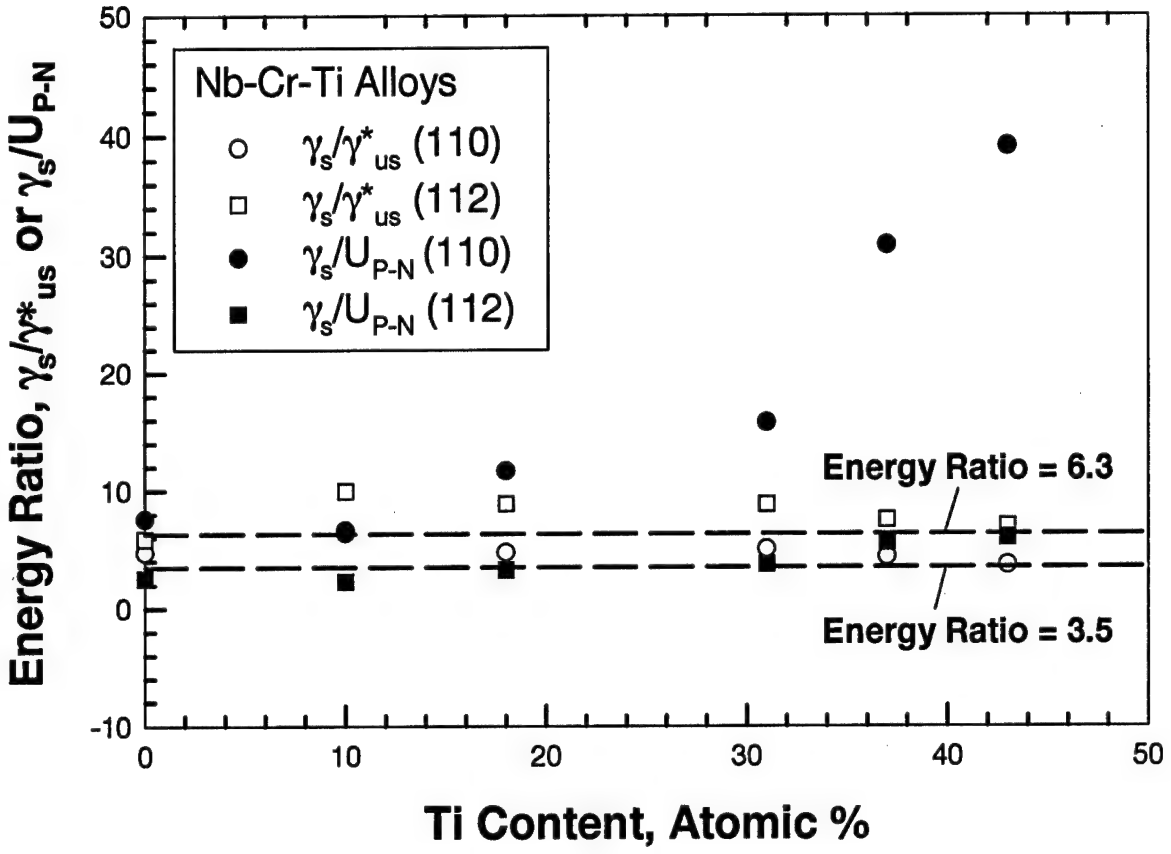

Figure 4. Calculated values of the ratio of surface energy, γ_s, to the unstable stacking energy, γ^*_{us}, based on the atomic cluster model or the Peierls-Nabarro (P-N) barrier energy for (110) and (112) slip. The lowering of the P-N barrier energy increase the γ_s/U_{P-N} ratio for (110) slip to exceed the critical values (> 6.3) required for ductile behavior, while the energy ratios based on the USE are near or below the critical value. The results imply that the brittle-to-ductile fracture transition is controlled by the mobility of, rather than by the nucleation of, dislocations at the crack tip.

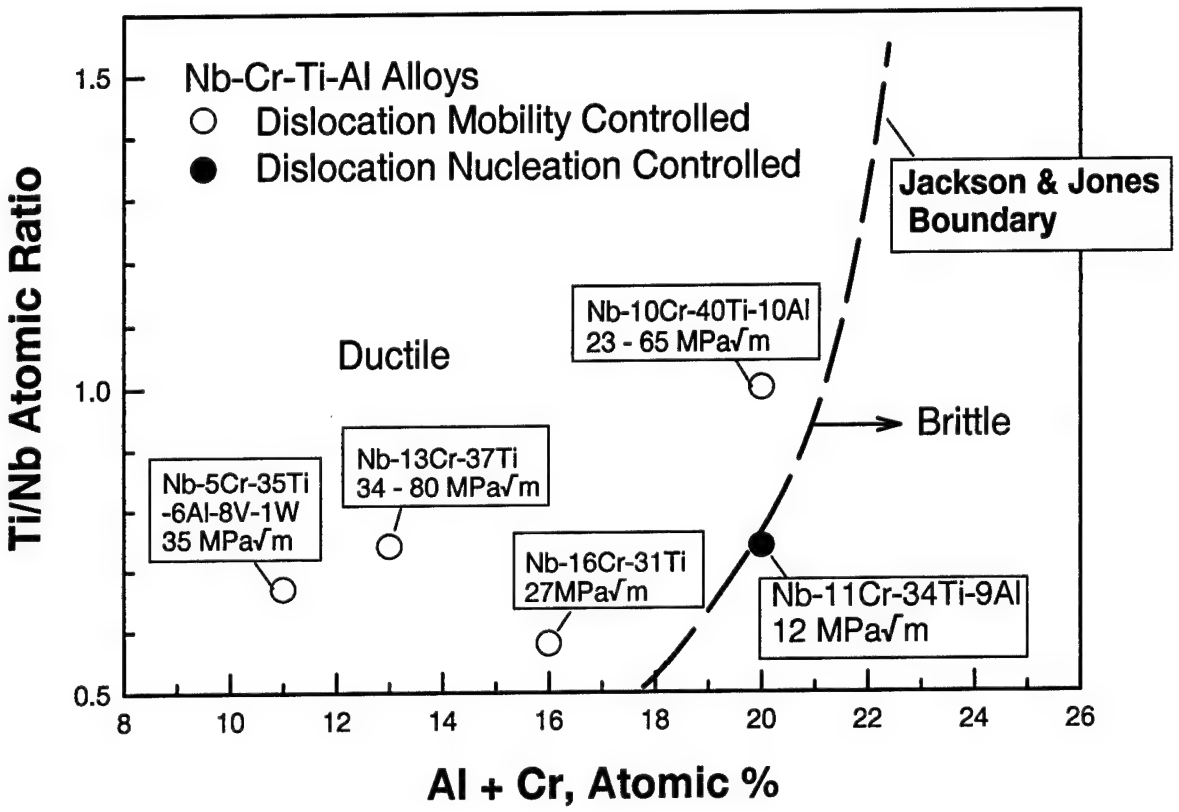

Figure 5. A summary of the brittle and ductile regions in a plot of Ti/Nb versus Al + Cr contents for several Nb-Cr-Ti-Al alloys. The brittle region appears to be controlled by dislocation nucleation at the crack tip, while the ductile region is controlled by dislocation mobility moving away from the crack tip.

Design of Refractory Superalloys Based on Ir and Rh

Y. Yamabe-Mitarai and H. Harada
National Research Institute for Metals
Advanced High Temperature Materials Research Group
1-2-1, Sengen, Tsukuba, Ibaraki, 305-0047, Japan

1. Research Objectives and Approach

We have proposed a new class of superalloys: "refractory superalloys". This new concept is defined as alloys with an Fcc and $L1_2$ two-phase coherent structure similar to Ni-based superalloys, and yet with considerably higher melting temperatures. Ir and Rh were selected as base materials because the melting temperatures of Ir and Rh (2447 and 1963°C, respectively) are higher than that of Ni (1455°C) and they have superior oxidation resistance. The Fcc structure equilibrates with the $L1_2$ structure in some of the Ir and Rh binary systems. We started investigation of compressive mechanical properties of Ir-based and Rh-based binary alloys. However high density (20 g/cm^3 for Ir-based alloys and 12 g/cm^3 for Rh-based alloys) and high price are disadvantage of these alloys. Ir-based alloys are failed by intergranular fracture, although Rh-based alloys have good ductility. To solve these problems, we have suggested adding Ni for Ir-based or Rh-based alloys because Ni is all-proportion miscible for Ir and Rh and density (8.5 g/cm^3) and price of Ni are low. For other possibility, we have suggested the quaternary alloys designed by mixing and melting of Ir-based (or Rh-based) and Ni-based binary alloys. If both alloys have the Fcc and $L1_2$ two-phase structure, it is expected that quaternary alloys have also the Fcc and $L1_2$ two-phase structure. The quaternary alloys will have advantages from both alloys, that is, high strength at high temperature of Ir-based or Rh-based alloys and high ductility and low density of Ni-based alloys.

2. Research Progress and Highlights

The Ir-V, Ir-Ti, Ir-Nb, Ir-Ta, Ir-Hf, Ir-Zr, Rh-Ti, Rh-Nb, and Rh-Ta binary alloys have been investigated [1-5]. The Fcc and $L1_2$ two-phase coherent structure is formed in these binary alloys after heat treatment at 1200°C for 1 week. Precipitates shape depends on lattice misfit between the Fcc matrix and the $L1_2$ precipitates. For example, plate-like precipitates form in the Ir-Zr alloys with large lattice misfit. Cuboidal precipitates form in the Ir-Nb alloys with small lattice

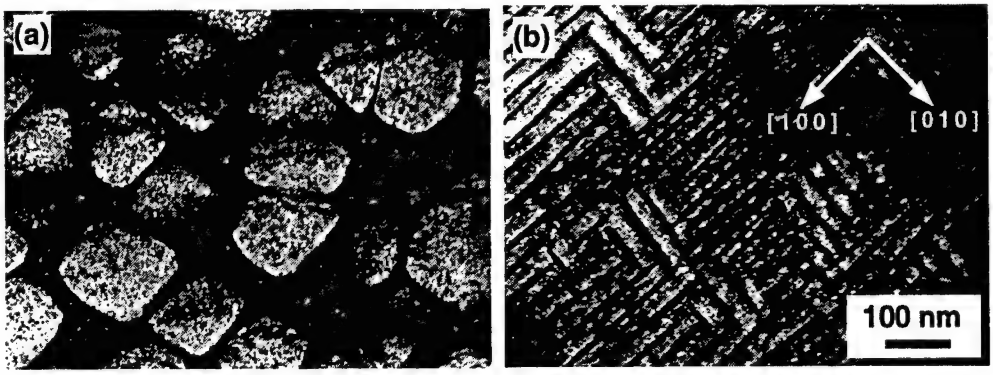

Fig. 1 Dark field images of the (a)Ir-15at% Nb and (b)Ir-15at% Zr alloys which were taken with superlattice reflections (g=110) from the L12 structure in the beam direction of [001]. Lattice misfit of Ir-15at% Nb and Ir-15at% Zr alloys are 0.3 and 2.0%, respectively.

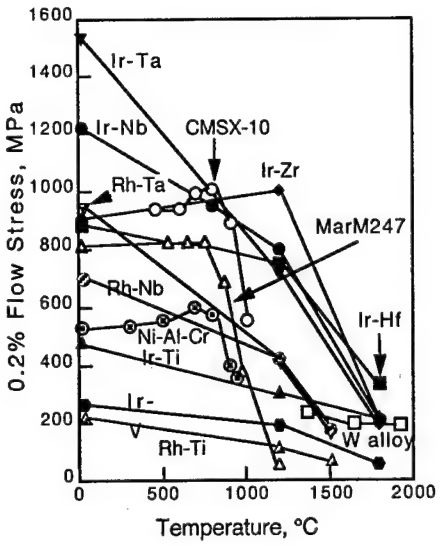

Fig. 2 Temperature dependence of 0.2% flow stress determined by compression tests in as-cast Ir-based and Rh-based with 15at% second elements, Ni-based and W-based alloys.

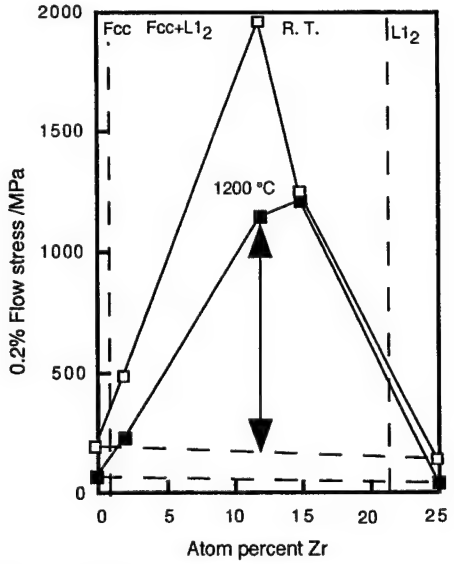

Fig. 3 Zr concentration dependence of 0.2% flow stress in compression at room temperature and 1200 °C for Ir-Zr alloys.

misfit (Fig. 1). The strengths of Ir-based and Rh-based alloys are equivalent to or higher than those of Ni-based superalloys are below 800°C and higher than those of Ni-based superalloys are above 1000°C (Fig. 2). The strengths of them are about 200MPa at 1500°C and 1800°C, which are equivalent to the strengths of the W-based HfC dispersion-hardening alloy believed to be the strongest metallic material available at this temperature. The strength increases with increasing lattice misfit among Ir-based alloys. In the one Ir binary system, the strengths of two-phase Ir-based alloys are higher than those of Fcc or $L1_2$ single-phase Ir-based alloys are (Fig. 3). This shows that main factor contributing to the strength of the Ir-based alloys is precipitation hardening. Precipitation hardening is effective when precipitate shape is plate [6,7].

For the challenge to replace as much as possible in Ir-Nb while still retaining its desirable properties, Ir-Ni-Nb alloys have been investigated [9]. The isothermal section of Ir-Nb-Ni ternary system at 1300°C was determined (Fig. 4). $Ir_{85-X}Nb_{15}Ni_X$ with $X \leq 20$ at% retains the Fcc and $L1_2$ two-phase structure. However a third phase, orthorhombic phase, like δ $(Ir, Ni)_{11}Nb_9$ or γ'' $(Ni, Ir)_3Nb$ form in the alloy including more than 30at% Ni. The compressive properties are shown in Fig. 5. The ductility at room temperature improves up to 20at%Ni because the fracture mode changes from intergranular fracture in the binary Ir-15Nb alloy to transgranular in Ir-15Nb-10Ni alloy and a mixture of intergranular and transgranular fracture in the other tested alloys. Not only ductility but also strength of Ir-15Nb-10Ni at room temperature improves by addition of Ni. Strength of Ir-15Nb-10Ni at 1200°C is equivalent to that of Ir-15Nb. Strength decreases with increasing Ni above 10at%, because coherency of interface lose in Ir-15Nb-20Ni and orthorhombic phases formed in the alloy with Ni above 30at%. The optimum amount of Ni in Ir-15Nb-XNi is approximately 10% to get high strength at both of room temperature and 1200°C and good ductility at room temperature.

Strengths and microstructures of two kinds of quaternary alloys, Ir-Nb-Ni-Al and Ir-Ta-Ni-Al, have been investigated. These alloys were prepared by mixing and melting of the Ir-20at% Nb or Ir-15at%Ta and Ni-16.8at% Al alloys with the Fcc and $L1_2$ two phase structure (Fig. 6). The three-phase equilibrium, that is two kinds of $L1_2$ structures (Ir_3Nb or Ir_3Ta type and Ni_3Al type) and the Fcc structure, exists in the two alloys including 25% and 75% Ir-based alloys at

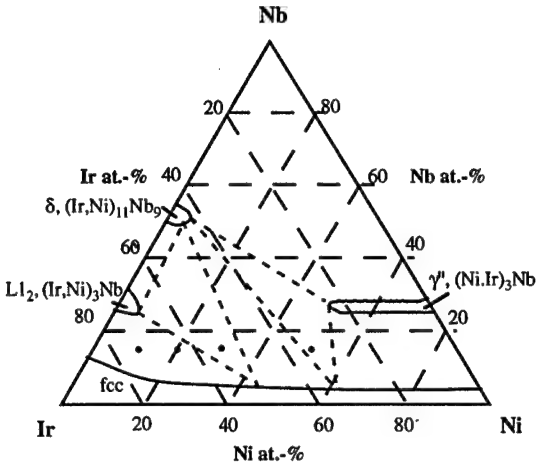

Fig. 4 Isothermal section of the Ir-Nb-Ni ternary system at 1300°C.

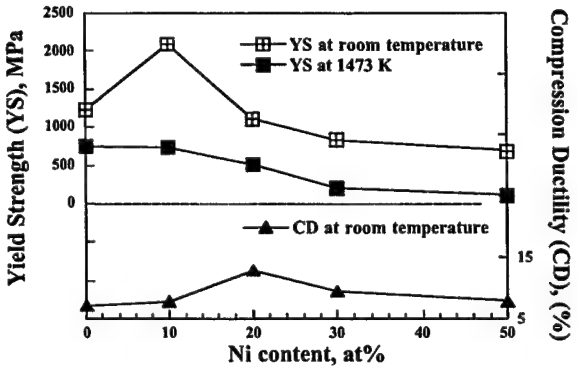

Fig. 5 The compression properties of Ir-15at% Nb alloy with various amount of Ni at room temperature and 1200°C.

1300°C. The four-phase equilibrium, two kinds of $L1_2$, Fcc and B2 (IrAl) structures, exists in the alloy including 50% Ir-based alloy at 1300°C. Although we did not observe the Fcc and $L1_2$ two-phase region, fine cuboidal $L1_2$ precipitates form with coherent interface in the Fcc matrix. The strengths of the quaternary alloys are higher than that of conventional Ni-based superalloys, MarM247, although their strengths are lower than those of the Ir-based binary alloys are (Fig. 7). The quaternary alloys improve the ductility compared with Ir-based alloys (below 10%). The lowest ductility, about 18% is shown in Ir-Ta-Ni-Al with 75% Ir-based alloy. Other alloys were not broken during the compression test after strain reached to 90%. These quaternary alloys are also promising as ultra high temperature materials. It is expected that the Fcc and $L1_2$ two-phase region between Ir-based alloy side and Ni-based alloy side exist if alloy composition is changed.

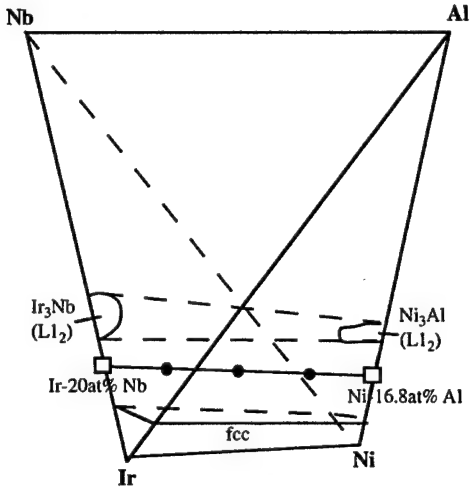

Fig. 6 Schematic quaternary diagram of Ir-Nb-Ni-Al.

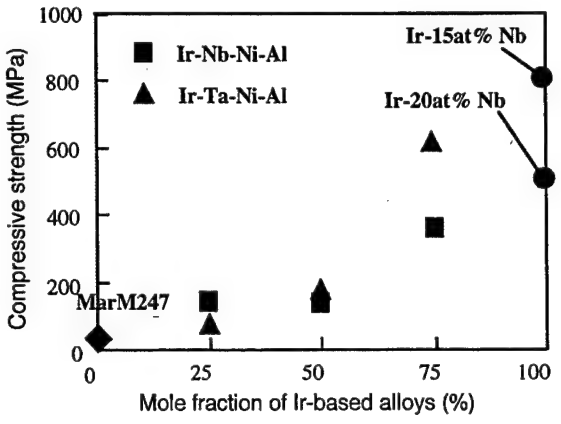

Fig. 7 Compressive strength at 1200°C of Ir-Nb-Ni-Al and Ir-Ta-Ni-Al heated at 1400°C for 1week.

3. Potential Structural Applications and Engineering Issues

In the Ir-based alloys, precipitate shape can be changed drastically by selection of alloy system unlike Ni-based superalloys because of variety of lattice misfit of the Ir-based alloys. If we can control the lattice misfit by addition of other elements, precipitate shape may change in the same alloy. We can chose plate-like precipitates or cuboidal precipitates for demand of temperature capability and strength. By addition of Ni or Ni-based alloys to Ir-based alloys, ductility of the Ir-based alloys can be improved, and density or price of them can be also decreased. Strengthening, while still retaining enough ductility is also expected by controlling of lattice misfit and microstructure.

The advantage of the Rh-based alloys is low density (12 g/cm^3), good ductility above 10% at room temperature (some alloys show 30-40%), and superior oxidation resistance compared with Ir-based alloys. However the melting temperature is slightly lower than that of Ir and price is more expensive than that of Ir is. The strengths of Rh-based alloys are half of those of Ir-based alloys. However the specific strengths of the Ir-based and Rh-based alloys are equivalent to each other because of low density of the Rh-based alloys. The density and price can be decreased more by addition of Ni or Ni-based alloys as well as Ir-based alloys. We will also change precipitate shape by selection of alloy system with different lattice misfit.

For application use, we made thruster of Solar Thermal Propulsion (STP) by pure Ir [8]. The STP is heated by concentrated solar radiation at a high temperature and exhausted propellant gas through a nozzle to produce thrust. Temperature capability and strength to bear for gas pressure are necessary for the thruster. The temperature of propellant gas within the thruster reached higher than 1800°C and Isp was about 750 sec for hydrogen propellant in the thruster mad of Ir. The problem of thruster made of Ir is intergranular fracture. We will try other Ir-based alloys strengthened grain boundary in next step.

4. Critical Scientific Issues and Challenges

We are interested in strengthening mechanism (compressive strength and creep) depended on precipitate shape of Ir-based and Rh-based alloys because precipitates shape is different by variety of lattice misfit in these alloys. Strength behaviour of $L1_2$ single-phase alloy is also interesting issues. We observed that the Ir-based $L1_2$ single-phase alloys show not only anomalous strength behaviour but also high strength at low temperature.

5. Acknowledgements

We thank to D. Yuefeng Gu and Dr. Xihong Yu in our group for research concerning to Ir-based or Rh-based alloys. We are grateful to Mr. S. Nishikawa and T. Maruko of Furuya Metal Co. Ltd., for preparing alloy ingots and Mr. Sasaki and Mr. Y. Matsumoto of the Japan Ultra-high Temperature Materials Research Center for carrying out the compression testing at 1500 and 1800°C.

6. Publications

1. Y. Yamabe, Y. Koizumi, H. Murakami, Y. Ro, T. Maruko, and H. Harada, Scripta Mat., 35, 2, 1996, 211-215.

2. Y. Yamabe-Mitarai, Y. Koizumi, H. Murakami, Y. Ro, T. Maruko, and H. Harada, Mat. Res. Soc. Symp. Proc, 460, 1997, 701-706.

3. Y. Yamabe-Mitarai, Y. Koizumi, H. Murakami, Y. Ro, T. Maruko, and H. Harada, Scripta Mat., 36, 4, 1997, 393-398.
4. Y. Yamabe-Mitarai, Y. Ro, T. Maruko, T. Yokokawa, and H. Harada," Structural Intermetallics 1997", eds. M. V. Nathal, R. Darolia, C. T. Liu, P. L. Martin, D. B. miracle, R. Wagner, and M. Yamaguchi, Seven Springs, PA, TMS, 1997, 805-814.
5. Y. Yamabe-Mitarai, Y. Ro, T. Maruko, and H. Harada, Met. Trans., 29A, 1998, 537-549.
6. Y. Yamabe-Mitarai, Y. Ro, T. Maruko, and H. Harada, Intermetallics, in print.
7. Y. Yamabe-Mitarai, Y. Ro, T. Yokokawa, Yuefeng Gu, T. Maruko, H. Harada, "Materials for Advanced Power Engineering", Proc. of the 6th Liege conference, eds. J. Lecomte-Beckers, F. Schubert, and P. J. Ennis, Liege, EC, 5, part II, 1147-1154.
8. H. Sato, K. Itoh, M. Shimizu, Y. Yamabe-Mitarai, H. Harada, and T. Maruko, 21st International Symposium on Space Technology and Science, 1998.
9. Yuefeng Gu, Y. Yamabe-Mitarai, Y. Ro, T. Yokokawa, and H. Harada, Scripta Mat., 39, 6, 1998, 723-728.

Modeling Solid-Solution Effects in High Temperature Structural Materials

C. Woodward*, S.A. Kajihara*, S.I. Rao*
and D.M. Dimiduk

Materials and Manufacturing Directorate,
Air Force Research Laboratory,
Wright Patterson AFB, OH

*UES Inc, Dayton OH 45432

1 Objectives and Approach

Structural materials are complex alloy systems, which are typically composed of several phases and incorporate many components. For example, the near commercial TiAl alloy Ti-46.5Al-2Cr-3Nb-0.2W-0.2B-0.2C-0.2Si has five phases and six components.[1] Describing the effects of microstructure on materials properties is currently beyond the scope of first principles and atomistic methods. However, significant progress has been made in using such techniques to model poly-component single crystals. We have recently used first principles calculations to predict: the site selection of solid-solutions in ordered intermetallic alloys, the density of constitutional and thermal point defects as a function of composition and temperature, and the strength of solute-dislocation interactions. These methods were used to model solid-solutions (Si, Cr, Nb, Mo, Ta and W) in γ-TiAl.[2,3] Currently the same techniques are being applied to high temperature refractory intermetallics such as Nb/Nb_5Si_3. In this paper we review the results of the solid-solution studies in γ-TiAl and outline similar ongoing research in the refractory intermetallics.

2 Research Progress and Highlights

2.1 Site Selection of Substitutional Solutes in γ-TiAl Alloys

Several research groups recently proposed models for predicting the density of constitutional and thermal point defects in binary intermetallic alloys using calculated defect energies in a canonical ensemble formalism for the free energy.[2,4,5,6] We have extended this model to treat ternary and higher component systems. For example, defect energies of five solid solutions (Si, Nb, Mo, Ta and W) in γ-TiAl were recently studied using a first principles method in local-density-functional theory framework.[2] Relaxed structures and energies of vacancies, antisites and substitutional defects were calculated using a plane-wave pseudopotential method. Results of these total energy calculations were incorporated into a canonical ensemble formalism in order to determine the chemical potentials, formation energies and density of point defect as a function of temperature and stoichiometry. Defect densities are found as a function of alloy chemistry and temperature for binary TiAl and ternary additions (Si, Nb, Mo, Ta and W). The predicted site selection of the solutes are in excellent agreement with recent X-ray emission experiments using

a quantitative statistical method for atom location by channeling enhanced microanalysis (ALCHEMI).[2,7]

2.2 Solid-Solution Strengthening in γ-TiAl Alloys

Once the constitutional point defects are determined for a given composition and temperature the same first principles methods can be used to determine critical solute-dislocation interaction parameters needed to describe solid-solution strengthening. Classic models of solid-solution strengthening are based upon continuum elasticity estimates of the interaction between solutes and dislocations.[8] The interaction parameters, the so-called 'size' and 'modulus' misfit, are derived from the host lattice response to the introduction of the solute atom. Within Fleischer's classical scheme, the interaction parameters are derived from bulk or average changes in lattice parameter and shear moduli with chemistry. The same quantities can be derived using first principles methods by calculating the change in cell volume and the change in the elastic moduli when the solute is introduced into the host lattice. We have calculated the size and modulus misfit parameters for Si, Nb, Mo, Ta and W in γ-TiAl using a first principles, density functional method.[3] Given these results the solute-dislocation interaction can be evaluated using either atomistic or continuum methods.[9,10] Within the continuum model the solute-dislocation interaction energy can be written as an expansion in terms of the strain field of the dislocation, ε_{ij}^{D}:

$$\mathbf{E_{int}(r)} = \left[\mathbf{P_{ij}^{0}} + \alpha_{ijkl}\varepsilon_{kl}^{D}(r)\right]\varepsilon_{ij}^{D}(r). \qquad (1)$$

The first and second order term in the expansion, sometimes referred to as the zeroth order dipole tensor and the diaelastic polarizabilty, can be related to the size and modulus misfits respectively (see reference 3).

The interaction force between the solute and dislocation is evaluated by superimposing the strain field of the solute and the dislocation and evaluating the interaction energy or force using Stroh's theorem.[9] As observed by Fleischer,[11] the energy of interaction between a screw dislocation and a solute is generally found to be proportional to $\Delta\varepsilon = \varepsilon_1 - \varepsilon_3$. Strong solute-dislocation interactions are possible in general as a result of the tetragonal distortion, or 'asymmetrical lattice distortion', produced by some substitutional solute atoms in the $L1_0$ structure. The solute-dislocation interaction is evaluated as a function of the distance of the solute from the dislocation glide plane and the relative distance in the glide plane yielding a two dimensional interaction profile. We have considered both a <101> screw superdislocation and an ordinary screw dislocation dissociated into Shockley partials according to estimates for the respective planar fault energies (γ_{sisf} = 120 mJ/m^2, γ_{111APB} = 550 mJ/m^2, and γ_{CSF} = 450 mJ/m^2).

The flow behavior in TiAl is consistent with dislocation-kink dominated deformation, therefore, trends in solid-solution strengthening are assessed using a model introduced by Petukhov.[12] Renormalizing the interaction strength in terms of the activation energy for kink nucleation, the interaction strengths are sorted into three classes of interactions; weak, strong and very strong. The first produces softening at all temperatures, the second softening at low temperatures and hardening at high temperatures and the last hardening at all temperatures. We have calculated the

renormalized interaction strengths between an ordinary (1/2<110]) screw dislocation and the predicted for the solid-solutions. For these solutes softening is expected for all but Al_{Ti}, Mo_{Al} and W_{Al}. Similar results are found for the <101] screw superdislocation. Calculations for the site preferences of Mo and W in TiAl indicate that the large concentration of the solutes, Mo_{Al} and W_{Al}, are only expected in stoichiometric or Ti rich TiAl.[2] Therefore, solid-solution strengthening by these 'strong' defect centers is not expected for Al rich alloys.

Some results for the binary alloy are available in the γ phase region. Sriram and co-workers found that relative to the stoichiometric alloy Al rich TiAl softened below room temperature and hardened above room temperature.[13] Al rich binary alloy will have a high concentration of Al_{Ti} and the predicted strong interaction with ordinary and <101] screw dislocations is consistent with these experimental observations.

2.3 Intrinsic Point Defect Densities and High Temperature Creep Properties

Recent publications reviewed the influence of grain size, class of microstructure and volume fraction of γ and α_2 phases on creep behavior TiAl.[14,15] Creep rates are often minimized by the introduction of uniformly distributed precipitates which act as strong barriers to dislocation motion. Solid solutions can produce strengthening but represent weak barriers to dislocation motion compared to precipitates. Viscous glide produced by the drag of a solute atmosphere can also enhance creep properties at low strain rates. Variations in alloy chemistry can modify the equilibrium density of point defects, which are limiting diffusional creep processes. In TiAl as well as simple metals the relevant point defects are thermal vacancies.[16,17] Creep rates linked to diffusion creep and dislocation climb mechanisms can be reduced if the density of vacancies is substantially reduced. This may provide a means of improving the intrinsic creep rates of a given alloy in addition to the addition of small precipitates. The density of thermal point defects can be predicted as a function of alloy chemistry and temperature using the same methods described in the previous section. This may provide a computational scheme for screening potential alloy chemistries for their relative intrinsic creep properties.

We have found the predicted density of vacancies in TiAl to be sensitive to the stoichiometry of the γ phase. The calculations show an order-of-magnitude drop in V_{Ti} concentration by changing from Al-rich to Ti-rich materials.[2,3] The effects of all other ternary elements studied are smaller, producing a shift in the onset of change in vacancy density as a function of Al content. Solid solutions with a high solubility can shift the vacancy poor region as to higher or lower Al content by occupying the Ti or Al sublattices respectively. The shift is produced by changes in the underlying constitutional defects and the resulting chemical potentials with the addition of the various solid solutions.[2] Experimental observations of the V_{Ti} concentration as a function of stoichiometry have led to speculation that the V_{Ti} are the rate limiting species for diffusion in TiAl.[18] This would be consistent with the creep experiments of Ishikawa et al. showing lower creep rates with increasing Ti concentration for Al rich materials.[19]

3 Critical Scientific Issues and Challenges for the Systems of Interest: The Advanced Intermetallic Nb/$(Nb\text{-}Ti)_5Si_3$

3.1 Influence of Solid-Solutions on Deformation in the β-Phase

In the refractory metal intermetallics there are a number of alloy design issues that may be addressed by the methods described in the previous section. In the simple metal beta phase solid-solutions will be used to improve strength and creep resistance. Therefore we are investigating the point defect properties of Al, Ti, Cr, and Re as substitutional solid-solutions and C, N and B as interstitials. Size and modulus misfits are being calculated in order to determine which solutes will produce the desired strengthening properties. The misfit interaction parameters can then be used in Petukhov's model of solid-solution strengthening by calculating the interaction strength using anisotropic elasticity or atomistic simulations.

Deformation associated with creep occurs mainly in the β-phase, with the β-phase shedding stress to the stronger intermetallic grains. Creep in the simple metals in usually associated with vacancy assisted diffusion. Using the calculated point defect energies of vacancies and solid-solutions in the β-phase we can use the canonical ensemble formalism to solve for the free energy of this alloy system as a function of composition and temperature. These data can then be used to find which composition, if any, significantly reduces the number of thermal vacancies.

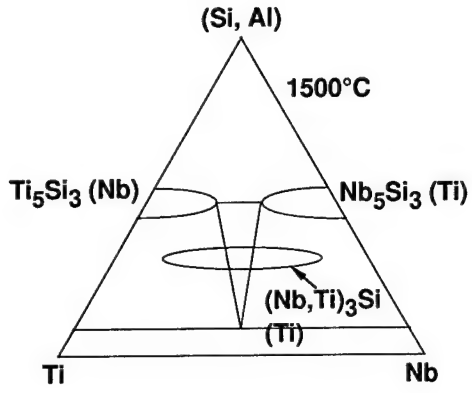

Figure 1. Pseudo-ternary phase diagram for Ti, Nb and (Si, Al).

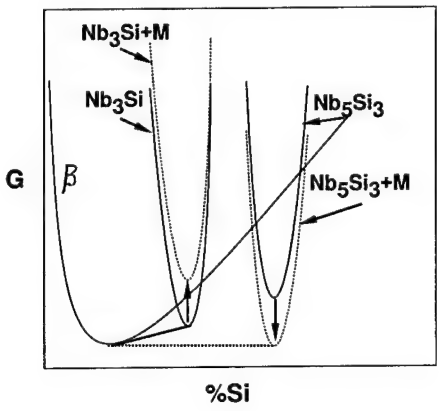

Figure 2. Schematic diagram of the free energy as a function of Nb content.

3.2 Predicting Trends in the Multi-Component Phase Diagram for $Nb/(Nb\text{-}Ti)_5Si_3$

A pseudo-ternary phase diagram for the $Nb/(Nb\text{-}Ti)_5Si_3/(Nb\text{-}Ti)_3Si$ system is shown in Figure 1. Alloy designers are trying to optimize the microstructure for the three phases (Nb, Ti_5Si_3, and Nb_5Si_3) in equilibrium. This is represented by the triangle connecting the three phases in the central portion of the phase diagram. Optimizing this microstructure is complicated by the presence of a third meta-stable phase, $(Nb\text{-}Ti)_3Si$, which forms large brittle grains. The current

alloy design effort is focussed on ways of pinching off this phase by increasing Ti content and by other alloy additions.

One way of influencing the phase diagram is by changing the relative free energy of the $(Ti\text{-}Nb)_5Si_3$ and $(Nb\text{-}Ti)_3Si$ phases. Figure 2 shows a schematic of the free energy of the three phases as a function of Nb content. Adding different ternary elements can shift the relative free energy of the two phases. By finding the correct components or combination of components that simultaneously raising the free energy of $(Nb\text{-}Ti)_3Si$ while lowering the free energy of $(Ti\text{-}Nb)_5Si_3$ we can pinch off the unwanted $(Nb\text{-}Ti)_3Si$ phase.

The canonical ensemble formalism for the point defects of ternary alloys appears to produce a reasonable formation energy for the various point defects considered in this study.[2] However, the current model uses a very simple form for the configurational entropy and ignores vibrational entropy. While vibrational entropy is not needed to determine the slope of an Arhennius plot of the point defect densities (e.g. the formation energy) it is needed to determine the Free energy as a function of composition as shown in Figure 2. The canonical ensemble model can easily be extended to two phase systems. The relative free energy can be calculated from the canonical ensemble formalism as a function of composition provided we have a complete set of point defect energies for all the relevant phases. However, in order to use such a model to address the problem described in the last paragraph information regarding configurational and vibrational entropy will be needed. Several research groups have studied these problems in detail[20,21] and we are currently working to incorporate the point defect formation energies into these models. By adding the formation energy of the point defects to empirical models of phase equilibrium trends in binary and ternary phase diagrams may be more apparent. These point defect energies are now being calculated for the $Nb/(Nb\text{-}Ti)_5Si_3/(Nb\text{-}Ti)_3Si$ system.

4 Acknowledgements

The authors gratefully acknowledge extensive conversations and the dedicated efforts of the members of the Advanced Metals group, Metals Development and Materials Processing Branch, Materials and Manufacturing Directorate, AFRL: Drs. P.M. Hazzledine, T.A. Parthasarathy, J.P. Simmons, S. Kajihara, Y-W Kim, P.R. Subramanian, M.G. Mendiratta, and M.A. Stucke. This work was supported by the Air Force Office of Scientific Research and was performed at the Materials and Manufacturing Directorate, Air Force Research Laboratory, Wright Patterson Air Force Base under contracts No. F33615-96-5258. This work was supported by a grant of HPC time form the DoD HPC centers: CEWES CRAY-YMP, ASC CRAY C90 and NAVO CRAY-T90.

5 REFERENCES

[1] Y.-W. Kim and D.M. Dimiduk, in *Structural Intermetallics1997*, ed. M.V. Nathal *et al.*, (TMS, Warrendale, USA, 1997) p. 531.
[2] C. Woodward, S. Kajihara, and L.H. Yang, *Phys. Rev. B* **57**, 13459 (1998).
[3] C. Woodward, S.I. Rao and D.M. Dimiduk, JOM, Vol. **50**, No. 7, 37 (1998).
[4] J. Mayer, C. Elsasser, and M. Fahnle, *Phys. Stat. Sol.*, **191** (1995) 283.
[5] Y. Mishin and D. Farkas, *Phil. Mag.* A, **75** (1997) 169.
[6] M. Hagen and M. Finnis, *Phil. Mag. A*, **77** (1998) 447.

[7] C.J. Rossouw, C.T. Forwood, M.A. Gibson, and A.R Miller, *Phil. Mag. A*, **74** (1996) 77.
[8] R.L. Fleischer, *Acta Met.*, **9** (1961) 996.
[9] A.N. Stroh, *Phil. Mag.*, **3** (1958) 625.
[10] D.M. Dimiduk, S.I. Rao, T.A. Partharasarthy and C. Woodward, in *Ordered Intermetallics-Physical Metallurgy and Mechanical Behavior*, ed. C.T. Liu *et al.*, (1992 Kluwer Academic Publishers, the Netherlands) 237.
[11] R.L. Fleischer, in *Strengthening of Metals*, ed. D. Peckner, (Reinhold, London 1964) 93.
[12] B.V. Petukhov, *Phys. Met. Metall.*, **56** (1983) 123.
[13] S. Sriram, V.K.Vasudevan, and D.M. Dimiduk, in *High Temperature Ordered Intermetallic Alloys VI*, ed. J.A. Horton *et al.*, MRS Symp. Proc. **364** (1995) 647.
[14] T.A. Partharasarthy, M.G. Mendiratta and D.M. Dimiduk, *Scripta Mater.*, **37** (1997) 315.
[15] J. Beddoes, W. Wallace, and L. Zhao, *International Mat. Rev.*, **40** (1995) 197.
[16] U. Brossmann, R. Wurschum, K. Badura, and H.-E. Schaefer, *Phys. Rev. B*, **49** (1994) 6457.
[17] G. Sattonnay, C. Dimitrov, O. Dimitrov, in *Structural Intermetallics 1997*, ed. M.V. Nathal *et al.*, (TMS, Warrendale, USA, 1997) 205.
[18] G. Sattonnay, C. Dimitrov, O. Dimitrov, in *Structural Intermetallics 1997*, ed. M.V. Nathal *et al.*, (TMS, Warrendale, USA, 1997) 205.
[19] Y. Ishikawa, K. Maruyama, and H. Oikawa, *Mater. Trans., JIM*, **33** (1992) 1182.
[20] M. Asta, M. von Schilfgaard and D. de Fontaine, in *High Temperature Ordered Intermetallic Alloys V*, ed. C.T. Liu *et al.*, MRS Symp. Proc. **288** (1993) 153.
[21] F. Zhang, S.L. Chen, Y.A. Chang and U.R. Kattner, *Intermetallics*, **5** (1997) 471.

Plasticity of RuAl and Related B2 Aluminides

Tresa M. Pollock and Ding-Chung Lu
Carnegie Mellon University
Department of Materials Science and Engineering
Pittsburgh, PA 15213

1. Research Objectives and Approach

Ruthenium aluminides are unusual compounds compared to other B2 intermetallics, since they have a high melting temperature (≈2060°C) and good oxidation resistance along with an apparently high toughness [1 - 3]. However, little is known about deformation mechanisms in this compound. Thus the goal of our research has been to investigate mechanisms of deformation at relatively low temperatures (room temperature and below, where intermetallics tend to be most brittle) in order to assess whether this compound exhibits characteristics of "intrinsic deformability". Two issues of particular interest have been dislocation mobility and substructure and whether deformation occurs on five independent slip systems. The experimental approach has been to couple macroscopic measurements of deformation kinetics with electron microscopy studies in order to identify rate limiting features of deformation and distinguish between extrinsic and intrinsic barriers to deformation. A variety of binary and ternary RuAl alloys have been studied. Additionally, parallel comparative experiments have been conducted on NiAl and Fe-40Al, since they represent two extremes of behavior for B2 aluminides, from brittle to relatively ductile, respectively.

2. Research Progress and Highlights

Several stoichiometric and Ru-rich binary alloys have been studied, including alloys with nominal compositions of RuAl, $Ru_{51.5}Al_{48.5}$, $Ru_{52}Al_{48}$ and $Ru_{54.5}Al_{45.5}$ (atomic %). A number of ternary alloys were also investigated: RuAl+0.5%B, $Ru_{53}Al_{47}$+0.5%B, $Ru_{51}Al_{48}Y_1$, $Ru_{50.5}Al_{44.5}Cr_5$ and $Ru_{52}Al_{43}Sc_5$. The majority of these alloys were arc-melted and thus contained a small amount of porosity and a distribution of grain sizes, with an average grain size of about 100μm. The $Ru_{52}Al_{48}$ material was synthesized by a reactive HIP'ing process which utilizes fine-scale elemental powders of Ru and Al [4], and results in a more uniform grain structure with an average grain size of 15μm. Additionally, [001] single crystals of Fe-40Al-0.2%Zr and polycrystalline as well as single crystals of stoichiometric NiAl were studied for comparison to the RuAl alloys.

Macroscopic deformation kinetics were characterized via strain rate jump experiments over a range of temperature on a large number of samples from each of the three classes of compounds. These strain-rate jump experiments utilized compression specimens and typically consisted of an abrupt increase strain rate imposed by two orders of magnitude,

from approximately $10^{-4}s^{-1}$ to $10^{-2}s^{-1}$ after ≈2% plastic deformation in a screw-driven Instron machine. The typical response of each of the three types of B2 aluminides to a strain rate change at room temperature is shown in Figure 1.

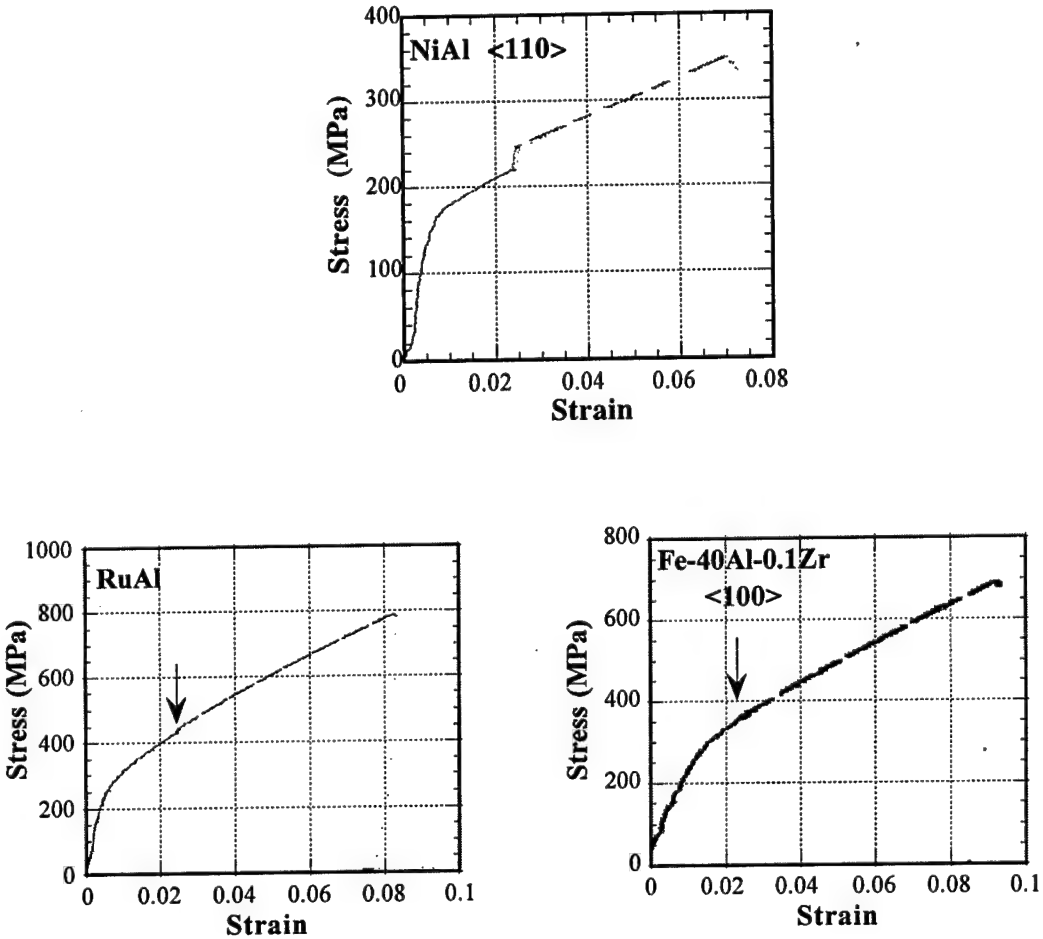

Figure 1 - Results of room temperature strain rate change experiments. Arrows mark the point at which the strain rate change is imposed.

The response of the NiAl material is clearly more rate sensitive than either the Fe-40Al-0.2Zr material or the RuAl. The high rate sensitivity (and the corresponding low tensile ductility at low temperatures) in NiAl is associated with easy double cross slip and the formation of jogged screw dislocations which subsequently introduce a high density of dipole loops and vacancies into the material during deformation [7, 8]. The low rate sensitivity of RuAl, similar to that of the more deformable FeAl, is unexpected since RuAl has a much higher melting point than FeAl. The rate sensitivity of the RuAl alloys at liquid nitrogen temperatures is similar to that observed at room temperature, Table I. It is also interesting that the temperature sensitivity of the flow stress of RuAl alloys is relatively low between

room temperature and -196°C. This is again in contrast to NiAl, which has a very high temperature sensitivity of the flow stress for both "hard" [001] and "soft" [110] type single crystals. Furthermore, the rate sensitivities of all the ternary RuAl-based alloys were similar to those of the binaries, suggesting that dislocation mobility is not strongly affected by alloying additions [5]. These low rate sensitivities are indicative of higher activation volumes for deformation, with corresponding longer-range barriers to dislocation glide, rather than short range barriers such as a high Peierls stress.

Table I - Results of Strain Rate Change Experiments on Selected Materials

Material	Temperature (°C)	Flow Stress at ε=2% (MPa)	Rate Sensitivity, m'
RuAl	25	400	0.0061
"	-196	470	--
RuAl+0.5%B	-196	510	0.0067
$Ru_{51.5}Al_{48.5}$	25	565	0.0072
$Ru_{52}Al_{43}Sc_5$	-196	500	0.0066
"	25	480	0.0059
$Ru_{52}Al_{48}$ (RHIP)	25	510	0.0040
"	-196	605	0.0058
NiAl <110>	-196	1083	0.0219
"	25	231	0.0248
"	25	219	0.0231
NiAl <100>	25	1363	0.0189
	25	1420	0.0153
Fe-40Al-0.2Zr <100>	25	358	0.0023

The substructural features following low temperature deformation of RuAl and RuAl+0.5%B at room temperature and 77K have studied in detail after approximately 2% strain in compression. Conventional tilting experiments were used to characterize Burgers vectors with seven to ten kinds of diffraction vectors ($\vec{g}$) chosen for each analysis. Image simulations were also performed for a variety of imaging conditions by using the program of Head and Humble, utilizing calculated elastic constants [6]. The results of a number of simulations showed that the use of conventional $g \cdot b$ criterion is sufficient for identification of Burgers vectors. Figure 2 shows a typical region after deformation of RuAl+0.5%B at -196°C. The majority of the dislocations have Burgers vectors of either <100> or <110>. Dislocations of the <111> type were only occasionally observed. Dislocations were generally curved and mixed in character, with no obvious preferred line directions. The proportion of <110> and

<100> dislocations varied from grain to grain, but were both typically present. Interestingly, the room temperature substructure was not significantly different from that observed in the liquid nitrogen compressed material (after 2% deformation in both cases), consistent with the small change in flow stress as a function of temperature. Analyses of a number of individual dislocations show that all types lie on {110} planes at both temperatures. These observations are significant, since if both <100> and <110> dislocations glide independently on {110} planes, then RuAl possesses five independent slip systems required for uniform, compatible deformation of polycrystalline material.

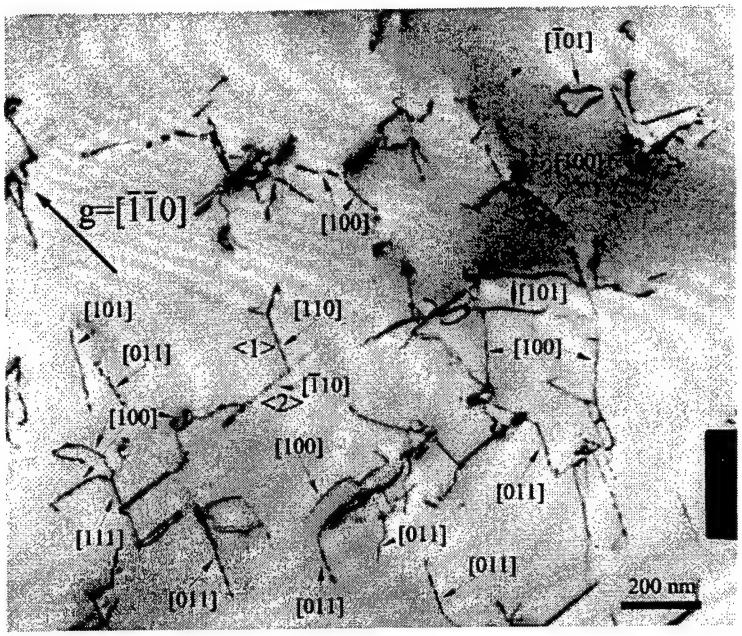

Figure 2 - Substructure of RuAl+0.5%B following 2% compressive deformation at liquid nitrogen temperature. Burgers vectors of individual dislocations are indicated.

To summarize, RuAl alloys display a number of deformation characteristics which are indicative of intrinsic deformability: a low temperature sensitivity of the flow stress, low rate sensitivities for deformation and dislocation substructures that suggest five independent slip systems may operate. Furthermore, the deformation of this compound is quite different from other B2 aluminides, which tend to deform either by glide of <100> type dislocations (i.e., NiAl) or <111> dislocations (i.e. Fe-40Al) at low temperature. Deformation kinetics are also not strongly influenced by ternary additions. Thus, compounds based on this system are not only interesting from the point of view of understanding fundamentals of deformation in B2 compounds, but also may serve as an interesting starting point for the development of multicomponent systems with a desirable combination of properties.

3. Potential Structural Applications and Engineering Issues

With the high melting point of 2060°C, alloys based on RuAl could be of interest for hot section turbine applications such as blades and vanes. Additionally, considering that B2 nickel aluminides and platinum aluminides currently serve as coating systems for nickel-based

superalloys, this compound could be useful as a component of a coating system or multilayered structure. An obvious engineering barrier is the cost and availability of ruthenium. Clearly, multicomponent systems where other elements substitute for Ru or multiphase alloys with only a small volume fraction of RuAl would be more practical. As with any high temperature compound, a significant challenge exists in the development of processing techniques that produce homogeneous microstructures relatively free of "extrinsic" defects. Further development of processing routes for this compound would permit critical properties such as tensile ductility and fracture toughness to be measured.

4. Critical Scientific Issues and Challenges for the System(s) of Interest

RuAl alloys clearly display a deformation behavior that is different than other B2 compounds, with <100> and <110> dislocations present after deformation, even at liquid nitrogen temperatures. Deformation and microscopy studies of single crystals would clearly be useful for measurement of critical resolved shear stresses and unambiguous determination of active slip systems. Further analysis of substructure development at low strains would also be of interest, to determine what, if any, role <111> dislocations play in the process. The <111> dislocations undergo a decomposition at high temperatures in NiAl, but it is not clear that such processes occur in RuAl. Atomistic studies would be useful with regard to understanding what properties of RuAl (such as elastic anisotropy, fault energies, dislocation core structures) result in this markedly different deformation behavior; such understanding could provide guidance for development of other B2 compounds. While RuAl alloys display interesting low temperature deformation characteristics, no studies of high temperature deformation have yet been conducted. Finally, exploration of multicomponent Ru-Al-X systems, both experimentally and from the point of view of thermodynamic modeling, is needed for a better understanding of the behavior of this class of compounds.

5. References

1. R.L. Fleischer and D.W. McKee, Metall. Trans. 24A, 759, (1993).
2. R.L. Fleischer and R. Zabala, Metall. Trans. 21A, 2709, (1990).
3. R.D. Fleischer, R.D. Field and C.L. Briant, Metall. Trans. 22A, 403, (1991).
4. I.M. Wolff, Metall. Mater. Trans. 27A, 3688, (1996).
5. K. Eow, D. Lu and T.M. Pollock, Script Mater. 37, 1065, (1998).
6. M.J. Mehl, B.M. Klein and D.A. Papaconstantopoulos, Intermetallic Compounds, Vol 1, J.H. Westbrook and R.L. Fleischer, eds., Wiley, 195, (1994).
7. K. Kitano and T.M. Pollock , Structural Intermetallics, R. Darolia et. al., eds., TMS, Warrendale, PA, 591, (1993).
8. X. Shi., S. Mahajan, T.M. Pollock and V.S. Arunachalam, Phil. Mag. A, in press.

6. Acknowledgments

The authors gratefully acknowledge Drs. R.L. Fleischer, I.M. Wolff, R.D. Field and G.T. Gray III for contributing experimental materials and for useful discussions. This work was supported by Department of Energy Grant # DE-FG02-95ER45548, under the direction of Dr. H. Kerch.

Constitutional and/or Thermal Vacancies in some B2 Intermetallic Compounds Studied by Positron Lifetime Spectrometry

Yasuharu Shirai

Department of Materials Science and Technology, Osaka University, Suita Osaka 565, Japan

1. INTRODUCTION

The positron is the antiparticle to the electron. The positron has the same rest mass (m_0) as the electron but the opposite charge; that is, one positive elementary charge. In condensed matter, each positron annihilates with an electron into gamma-rays in a very short time (10^{-10}-10^{-9}s). By measuring the angular correlation or the Doppler broadening of the emitted gamma-quanta, or by measuring the positron lifetime, we can deduce the information about electron momentum distribution or electron density at the positron annihilation sites.

Positron applications to the study of crystal lattice defects started around 1970, when it was recognized correctly that positrons are sensitively trapped by vacancy-type defects and annihilate with characteristics of each type of defects.

Here, positron applications to study defects in high temperature intermetallics are shortly reviewed. Special emphasis is put on B2 refractory intermetallic compounds. After an introduction to positron annihilation methods which has been successfully applied to the studies of atomic-scale defects in solids, in-situ measurements of thermal equilibrium defects in some intermetallics are shown. Studies of constitutional defects in B2 intermetallic compounds are also presented.

2. POSITRON ANNIHILATION

In conventional positron annihilation experiments, positrons, which can be readily obtained from such radioactive isotopes as ^{22}Na, ^{58}Co, ^{64}Co and ^{68}Ge, are directly injected into a specimen. The implantation depth of positrons is in the range of 100-1000μm, depending on the positron energy and the density of the sample. Hence, positrons deduce information in the bulk of a specimen in conventional source experiments.

In condensed matter, nearly all (about 99.7%) positrons annihilate each with an electron into two gamma-quanta. Since the total energy and the total momentum are conserved before and after the annihilation of a positron-electron pair, the two gamma-quanta have a total energy of $2m_0c^2$ = 2 x 0.511 MeV (c is the velocity of light) and are emitted from the annihilation site in almost opposite directions. The annihilation rate (λ) is proportional to the electron density at the annihilation site. Positron lifetimes τ ($=\lambda^{-1}$) in well-annealed metallic materials are characteristic of each material and in the range of 1-2 x 10^{-10}sec.

In a perfect crystal, thermalized positron is delocalized (in a Bloch function state). The density has maxima in the interstices, since a positron is strongly repelled by ion cores due to the Coulomb repulsion. When there exist vacancies or vacancy clusters or other defects which have lower densities of ion cores than the surroundings, positrons are trapped in the defects and annihilate there. In such defects, positron lifetime is longer, because electron density (both conduction and core electrons) is lower. The positron lifetime is unique for each kind of defects, and thus make us possible to identify each kind of defects.

The positron sensitivity to such defects is quite high: In the case of vacancies, the concentration of 10^{-6} in atomic fraction is enough to be detected; 10^{-4} vacancies make observed characteristics to be saturated with that of vacancies. The sensitivity for vacancy clusters or secondary defects is even higher. This fact is especially noteworthy, since the relative intensity of the signal of defects is equal to the defect concentration in most experimental methods other than positron annihilation. It can be said that positrons are capable to amplify the signal of defects by the order of 10^4.

For positrons annihilating in a perfect lattice, the decay is simple exponential; the positron lifetime spectrum has the form

$$T(t) = \exp(-t/\tau_1)$$

where the τ_1 is the positron lifetime in the perfect lattice. When positron-trapping centers such as vacancies exist in the lattice, some positrons are trapped and annihilate in them. According to the so-called trapping model [1-3], the positron lifetime spectrum well approximates to two discrete components:

$$T(t) = I_0/\tau_0 \exp(-t/\tau_0) + I_d/\tau_d \exp(-t/\tau_d).$$

where the τ_d is the positron lifetime in the defect which is characteristic of each kind of defects. The relative intensity of the defect

$$I_d = \kappa/(\tau_1^{-1}+\kappa-\tau_d^{-1}),$$

where the κ is the positron trapping rate and is proportional to the concentration of the trapping centers. The specific trapping rate ν, that is the trapping rate per unit concentration of the defect, is dependent on the defect. Values of ν for monovacancies in most metals are 10^{14}-10^{15} per second. The decay constant τ_0 of the other exponential term is given by $(\tau_1^{-1}+\kappa)^{-1}$ which is shorter than τ_1. The mean lifetime is given by

$$\tau_M = I_0\tau_0 + I_d\tau_d.$$

The above treatment is readily extended to the cases in which more than three kinds of defects are included [4,5]. Thus, by measuring and analyzing positron lifetime spectra, information on the concentration and nature of defects can be obtained; the defect nature via τ_d and the concentration via I_d.

3. THERMAL DEFECTS

Positron annihilation methods have been applied to investigate thermal equilibrium defects in intermetallic compounds and ordered alloys. Temperature dependencies of the average positron lifetime for some intermetallics and ordered alloys are shown in Figure 1 [6].

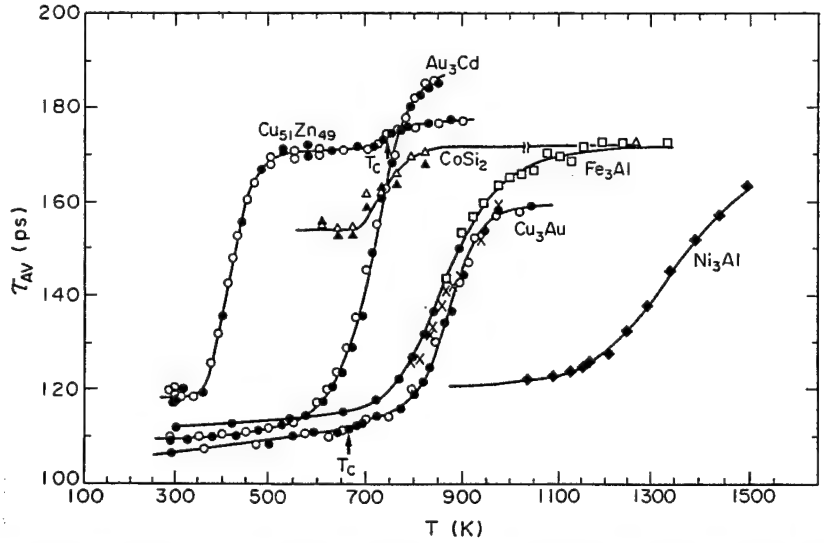

Fig.1: Measurements of thermal equilibrium vacancies with positron lifetime spectroscopy. The average positron lifetime sharply increases due to positron trapping by thermal vacancies. Open and closed circles for $Cu_{51}Zn_{49}$, Cu_3Au and Au_3Cd: heating and cooling runs, respectively; *Tc*: the order-disorder transition temperature. Different symbols for Fe_3Al: different measuring runs. Open and closed triangles for $CoSi_2$: water quenched and air cooled specimens, respectively.

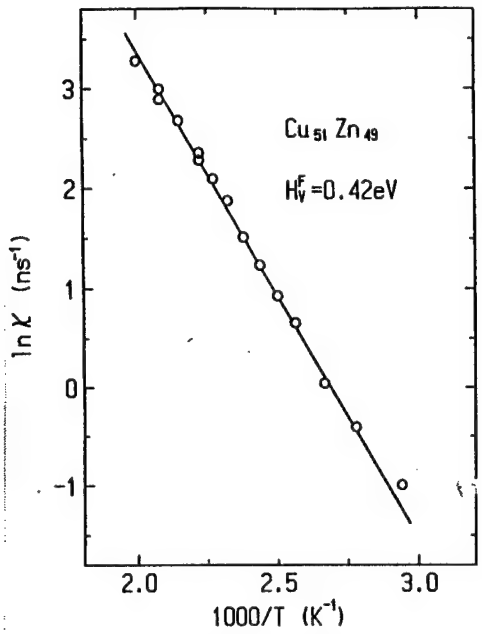

Fig.2: The Arrhenius plot of the positron trapping rate κ (=ν*C*, ν is the specific trapping rate and *C* is the concentration of vacancies) in $Cu_{51}Zn_{49}$. The effective vacancy formation enthalpy in ordered $Cu_{51}Zn_{49}$ has been determined as 0.42 eV by this analysis.

A nearly linear temperature dependence at lower temperatures is due to the thermal expansion of the crystal lattices. At higher temperatures, each plot shows an increased slope demonstrating positron trapping in thermal equilibrium vacancies. Saturation, beginning below the melting point, gives us the *S*-shaped curves as a whole. The well-developed *S* -shaped curves are clearly observed for these ordered materials.

The $Cu_{51}Zn_{49}$ case serves as a good example to illustrate thermal defect in ordered materials. The crystal structure of this alloy is B_2 below the order-disorder transition temperature *T*c (=741K). The steep increase of the positron lifetime due to thermal vacancies starts at the temperature as low as 370K. This is a threshold temperature which measures the onset of thermal-vacancy trapping. The ratio of this threshold temperature to the melting point is only 0.32, which is surprisingly lower than the ratio (around 0.6) for normal metals and disordered alloys. Around 500K and above, average positron lifetime shows saturation behavior, where almost all positrons are trapped in monovacancies and annihilate there with the characteristic lifetime (171psec). The effective vacancy formation enthalpy in ordered $Cu_{51}Zn_{49}$ has been determined as 0.42 eV from the Arrhenius plot of the measured trapping rate κ (see Fig.2) [7].

The effective vacancy formation enthalpies determined in the other intermetallics are 1.42±0.09 eV in disordered Cu_3Au [8], 1.07±0.04 eV in disordered Au_3Cd [9], 0.85±0.02 eV in ordered Au_3Cd [9], 1.18±0.04 eV in Fe_3Al [10], 1.60±0.06 eV in Ni_3Al [11] and 1.41±0.06eV in TiAl [12]. The last three compounds are important as high temperature materials.

4. CONSTITUTIONAL DEFECTS

If a intermetallic compound has an extended phase field, its nonstoichiometry may give rise to the existence of constitutional defects such as atoms occupying atomic sites of a sublattice other than its own sublattice (antisite atoms) or vacancies of deficient atomic species (constitutional vacancies). Which of these defects dominates the defect structure of the nonstoichiometric compound depends on the crystal structure, constituent elements, and bonding nature or the compound as well as on which of the constituent elements is deficient and the amount by which the compound is non stoichiometric [6].

From experimental point of view, defect structures have been studied only in a limited number of intermetallic compounds. Among them, the existence of constitutional vacancies has been found in NiAl, CoAl, CoGa, and FeAl [13] by measuring the lattice parameter and macroscopic length or density.

Application of the positron annihilation technique to study constitutional defects in intermetallic compounds started around 15 years ago. Shimotomai et al. [14] measured the Doppler-broadening line shape parameter for positron annihilation in NiAl as a function of Al composition,

and they confirmed the existence of a large amount of constitutional vacancies on Ni-sublattice in the compound when Ni is deficient.

It is easy to distinguish which kind of constitutional defects exist in a given compound by using positron lifetime measurements. Positron lifetime values in intermetallic compounds directly reflect their defect structures. For example, all intermetallic compounds or ordered alloys shown in Fig. 1 have no constitutional vacancies. In other words, their nonstoichiometry are compensated with anti-site atoms. Because, if constitutional vacancies exist, all positrons are trapped in such constitutional vacancies at any temperatures (concentration of constitutional vacancies is generally much higher than that of thermal vacancies) and no such changes as shown in Fig. 1 should be observed. In the same manner, defect structures can be easily judged by comparing positron lifetime before and after quenching or electron-irradiation, as will be shown in the next section.

Until now, NiAl [14,15] seems to be an almost unique example in which the existence of vacancies compensating nonstoichiometry has been proved by using a positron annihilation method. FeAl [16] shows somehow intermediate nature of vacancies ; although there are no constitutional vacancies, the concentration of thermal vacancies is quite high and they are easily quenched-in and hardly annealed out. Similar behavior of vacancies has been also found in CoSi2 [17], Co2Si [18] and in some other intermetallic compounds.

5. CONCLUDING REMARKS

Distinctive characters of positron annihilation methods are

(1) Defects' signal is highly amplified
(2) Defects with free volume are selectively detected
(3) Species and sizes of atomic or nanometric scale defects are differentiated
(4) The concentration of each defect is independently deduced

These unique characteristics have already been applied in some high temperature materials. Hereafter, defects and their properties at high temperatures will be clarified in many important or potential refractory materials. Such information will be quite useful to develop high temperature materials and processing.

REFERENCES

1. W. Brandt, in *Positron Annihilation*, ed. by A.T. Stewart and L.O. Roeling, Academic Press, New York, 155 (1967).
2. B. Bergersen and M.J. Stott, *Solid State Commun.*, **7**, 1203 (1969).
3. D.C. Connors and R.N. West, *Phys. Lett.* **A30**, 24 (1969).
4. M. Doyama, *J. Phys. Soc. Japan*, **33**, 1495 (1972).
5. A. Seeger, *Appl. Phys.*, **4**, 183 (1974).
6. M. Yamaguchi and Y. Shirai, in *Physical Metallurgy and Processing of Intermetallic Compounds* ed. by N.S. Stoloff and V.K. Sikka, Chapmann and Hall, New York, 3 (1995).
7. Y.Shirai, *Bulletin of the Japan Institute of Metals*, **27**, 869 (1988). (in Japanese)
8. Y. Shirai, F. Nakamura, M. Takeuchi. K. Watanabe and M. Yamaguchi, in Ref. 4, p.488.
9. Y. Shirai, M. Takeuchi and M. Yamaguchi, unpublished.
10. H.E. Schaefer, R. Buerschum, M. Sov, T. Zak, W.Z. Yu, W. Eckert and F. Banhart: *Phys. Rev.*, **41**, 11869 (1990).
11. H.E. Schaefer, R. Buerschum and J. Bub, *Materials Science Forum*, **105-110**, 439 (1992).
12. U. Brossmann, R. Buerschum, K. Badura, and H. E. Schaefer, *Phys. Rev.*, **49**, 6457 (1994).
13. Y.A. Chang and J.P. Neumann, *Prog. Solid St. Chem.*,**14**, 221 (1982).
14. M. Shimotomai, T.M. Wang, T. Iwata and M. Doyama, in *Positron Annihilation*, ed. by P.C. Jain, R. M. Singru and K.P. Gopinathan, World Scientific, Singapore, 140 (1985).
15. Y. Shirai, A. Okamoto and M. Yamaguchi, to be published.
16. Y. Shirai, I. Shishido and M. Yamaguchi, unpublished.
17. Y. Ito, Y. Shirai, Y. Yamada and M. Yamaguchi, *MRS Symp. Proc.*, Pittsburgh, **288**, 275 (1993): Y. Shirai, Y. Ito and M. Yamaguchi, *Materials Science Forum*, **175-178**, 529 (1995).
18. A.G. Balogh, L. Bottyan, G. Brauer, I. Dezsi and B. Molnar, *J. Phys. F: Met. Phys.*, **16**, 1725 (1986).

ON THE DEVELOPMENT OF FATIGUE-CRACK GROWTH RESISTANCE IN INTERMETALLIC ALLOYS

Robert O. Ritchie
Department of Materials Science and Mineral Engineering,
University of California, Berkeley, CA 94720-1760, U.S.A.

RESEARCH OBJECTIVES AND APPROACH

Cyclic fatigue involves the microstructural damage and failure of materials under cyclically varying loads. Structural materials, however, are rarely designed with compositions and microstructures optimized for fatigue resistance. Metallic alloys are generally designed for strength, intermetallics for ductility, and ceramics for toughness; yet, if any of these materials see engineering service, their structural integrity is often limited by their mechanical performance under cyclic loads.

To address this problem, a large volume of literature exists dealing with the mechanics and mechanisms of mechanical fatigue failure; however, the vast majority of this research pertains solely to metallic materials. Despite this preponderance of information on metals, there has been an increasing interest of late in the use of more brittle materials, such as ceramics and intermetallics, for structural applications where cyclic loading is critical [e.g., 1]. For intermetallics, this has been focused at elevated temperature applications, and includes the contemplated use of γ-based titanium aluminides for engine valves and blades in gas turbines. Whereas such these materials offer improved specific strength at high temperatures, they suffer in general from a pronounced lack of damage tolerance in the form of poor crack-growth resistance and a consequent sensitivity to flaws. Moreover, it has become apparent that similar to metals, they display a marked susceptibility to premature failure under cyclic fatigue loading [e.g., 2].

Intrinsic and Extrinsic Mechanisms

The mechanisms associated with fatigue-crack propagation in brittle materials such as monolithic and composite intermetallics can be quite distinct from those commonly encountered in metal fatigue; moreover, their crack-growth rate (da/dN) behavior displays a markedly higher sensitivity to the applied stress intensity (K) than is observed in most metals [3]. This behavior, and indeed the critical and subcritical extension of cracks in general, may be understood by considering crack growth as a mutual competition between two distinct classes of mechanisms: *intrinsic* microstructural damage mechanisms, which promote crack extension *ahead* of the tip, and *extrinsic* crack-tip shielding mechanisms, which act primarily *behind* the tip to retard crack growth [2]. In metallic materials, intrinsic damage mechanisms typically involve processes which create microcracks or voids, e.g., by dislocation pile-ups or interface decohesion, in the highly stressed region ahead of the tip, leading to classical failure by cleavage, intergranular cracking or microvoid coalescence; comparable mechanisms under cyclic loads involve the repetitive blunting and resharpening of the crack tip. Extrinsic shielding mechanisms, conversely, result from the creation of inelastic zones surrounding the crack wake or from physical contact between the crack surfaces via wedging, bridging, sliding or combinations thereof [2]. Examples of "zone shielding" are transformation and microcrack toughening in ceramics, where the *in situ* dilatant phase transformations or the microcracking of precipitates/particles ahead of the

crack tip can lead to inelastic zones in the crack wake which impart closing tractions on the crack surfaces. Examples of "contact shielding" are the bridging tractions imposed across a crack by unbroken fibers, laminated layers or a particulate phase in composite materials, or the wedging of oxide debris or crack surface asperities during crack closure in fatigue.

It is important to note that the intrinsic mechanisms are an inherent property of the material, and thus are active irrespective of the length of the crack or the geometry of the test specimen; under monotonic loads, for example, they control the driving forces (e.g., the stress intensity) to *initiate* cracking. Extrinsic mechanisms, conversely, act in the crack wake and are thus critically dependent on crack size and (to a lesser extent) geometry; they are responsible for the development of resistance-curve (R-curve) behavior and thus play a prominent role in the driving forces required for continued *growth* of the crack. The implications of this are that where extrinsic shielding mechanisms are active, rising R-curve toughness behavior and "small-crack" effects are to be expected, both phenomena resulting from the crack-growth properties being dependent upon crack size. Moreover, since extrinsic mechanisms can have no effect on crack initiation (since there is no crack wake), the microstructural factors affecting (large) crack growth may be quite different from those affecting crack initiation (or small crack growth).

In general, ductile materials are toughened intrinsically, e.g., via mobile dislocation activity to induce a significant plastic zone, although extrinsic mechanisms play an important role under cyclic loading in the form of crack closure. In contrast, brittle materials are invariably toughened extrinsically [e.g., 4], via such mechanisms as transformation toughening and crack bridging, the latter through interlocking grains in many monolithic ceramics or by uncracked ligaments or reinforcement phases in composites and laminates.

From the perspective of finding any commonality in mechanisms of fatigue-crack growth, *it is the specific nature and relative importance of the intrinsic (damage) versus extrinsic (shielding) mechanisms which distinguishes the cyclic fatigue behavior of ductile and brittle solids.* This in turn governs the specific dependencies of the alternating and maximum stress intensities on crack-growth rates, i.e., how da/dN depends upon ΔK and K_{max} (and thus how the resulting lifetime is a function of the alternating or maximum stresses), and the relationships between the thresholds for fatigue-crack growth (ΔK_{TH}, $K_{max,TH}$) and the crack-initiation (K_o) and steady-state (K_c) fracture toughness values.

With respect to the toughening of brittle materials such as ordered intermetallics, it should be noted that although both approaches are feasible, extrinsic toughening mechanisms, e.g., by ductile-phase toughening, shear ligament bridging, are far easier to induce; however, unlike intrinsic toughening, *extrinsic mechanisms invariably degrade in fatigue.* Thus, it is this author's opinion that the only safe route to achieving damage tolerance in brittle intermetallics, that will remain in effect under both monotonic and cyclic loading, is by intrinsic toughening, e.g., through the activation of additional slip systems. Accordingly, it is believed that there is little hope for structural application of some of the recently proposed intermetallics and Laves phases with highly ordered crystal structures and very large unit cells; while they might possess excellent strength and high-temperature resistance, achieving the required combination of good low-temperature toughness with high-temperature fatigue resistance may be all but impossible.

RESEARCH PROGRESS AND HIGHLIGHTS

Due to their complex, and invariably ordered, crystal structures, intermetallics generally display only very limited mobile dislocation activity at low homologous temperatures (below their brittle-to-ductile transition temperature), and are thus often highly restricted in ductility and toughness. To toughen intermetallics, both intrinsic and extrinsic toughening approaches have to varying degrees been successful [e.g., 5-7]. For example, Nb_3Al can be

toughened through the addition of a ductile phase, e.g., Nb, with the intermetallic matrix cracking preferentially to the metallic reinforcement [8]. In fact, using a high-aspect ratio reinforcement, e.g., a Nb layer in an arrester laminate, the crack-initiation toughness may be enhanced *intrinsically* by the necessity of the crack in the intermetallic matrix renucleating across the metal phase. However, as the crack extends leaving a wake of uncracked Nb ligaments in its wake, the crack-growth (or R-curve) toughness is also enhanced *extrinsically* from the bridging of the zone of intact ductile ligaments behind the crack tip.

With respect to fatigue-crack propagation, intrinsic damage mechanisms associated with crack advance do appear to operate in the more ductile intermetallics as in metals; in contrast, the mechanism by which the crack extends in the cyclic fatigue of brittle intermetallics, such as Ni_3Al and $MoSi_2$, is identical to that occurring under monotonic loads, as in ceramics [e.g., 9,10]. Moreover, whereas the intrinsic toughening mechanisms, such as crack renucleation, do not degrade under cyclic loading, the extrinsic toughening mechanisms, such as crack bridging, can suffer severe degradation. A notable example is ductile-phase reinforced intermetallic composites, which due to extensive crack bridging by the uncracked ductile phase can display significantly higher toughness (i.e., by a factor of 3 or greater) than the constituent matrix [11]. However, the improvement in crack-growth resistance is far less obvious in fatigue simply because the ductile phase fails prematurely; indeed, the fatigue-crack growth properties are rarely much better than that of the unreinforced matrix [11]. Thus, similar to ceramic materials [3], cyclic loading can act to reduce the potency of extrinsic toughening mechanisms in impeding crack advance.

Thus, to achieve good fatigue-crack propagation resistance in intermetallics, it is necessary to develop toughening mechanisms that are more resilient to cyclic loading. Ideally, this means intrinsic toughening, but as this is so difficult to achieve, certain strategies can be conceived to preserve the potency of extrinsic mechanisms. For ductile-phase toughened systems, for example. These may involve the use of:

- *high aspect-ratio reinforcements*; this merely increases the probability of interception by the crack. For example, $MoSi_2$ reinforced with spherical Nb particles displays insignificant toughening and no improvement in fatigue resistance as the crack merely circumvents the ductile phase [8]; in contrast, with Nb laminate or wire-mesh [10] reinforcements, a 3-fold increases in toughness (due to extensive crack bridging) and good fatigue-crack growth resistance (due to crack closure) can be obtained.
- *reinforcements with weakened interfaces with the matrix*; the resulting delamination at the interface acts to delay the inevitable failure of the ductile ligament, as shown by the improved fatigue properties of Nb/γ-TiAl compared to TiNb/γ-TiAl [11].
- *reinforcements with good intrinsic fatigue resistance*; whereas β-TiNb is a useful reinforcement phase for toughening γ-TiAl because of its high strength ($\sigma_o \sim 430$ MPa), its fatigue properties are poor due to its near zero strain hardening which induces rapid shear localization. A better approach is to use monolithic γ-TiAl alloys with lamellar microstructures, where (R-curve) toughening results from uncracked (shear) ligament bridging; here, since the bridge material is the same as the matrix, there is a lower tendency for the bridges to fail preferentially in fatigue [12].
- *reinforcements that promote other extrinsic toughening mechanisms*; since bridging mechanisms invariably fail under fatigue loading, good fatigue-crack growth resistance can be achieved if alternative shielding mechanisms develop. For example, with Nb-wire mesh reinforced $MoSi_2$, the Nb bridging ligaments which provide for R-curve toughening do fail prematurely in fatigue; however, as the crack follows the weakened interfacial reaction layer of the Nb phase, highly tortuous crack paths result which give rise to high levels of roughness-induced crack closure [10].

- *reinforcements that promote intrinsic toughening*; whereas extrinsic shielding mechanisms tend to degrade in fatigue, intrinsic toughening mechanisms do not. Accordingly, the use of laminate reinforcements in the arrester orientation, which require the crack to renucleate across the ductile layer, both increase the crack-*initiation* toughness and remain equally potent under cyclic loading. Such behavior is shown by coarser-scale Nb/Nb_3Al laminated composites (Fig. 15) [8,13].

Similarities between the Fatigue of Ductile and Brittle Materials

Compared to the extensive database and understanding of fatigue failure in metals, intermetallics still require extensive research with respect to fatigue behavior. It is clear that cyclic loading induces a progressive degradation in the toughening (or shielding) mechanisms behind the crack tip that locally elevates the near-tip driving force. It is this cyclic suppression of shielding that is considered to be the principal source for the susceptibility of brittle materials to cyclic fatigue failure. By contrast, the propagation of fatigue cracks in metallic materials involves primarily *intrinsic* damage processes occurring *ahead* of the crack tip, i.e., involving progressive blunting and resharpening of the crack tip, clearly a mechanism distinct from fracture under monotonic loads. Additionally, shielding, in the form of crack closure (wedging) mechanisms, can act in the crack wake.

Since the physical mechanisms of crack advance and crack-tip shielding are quite different in metals and ceramics, the dependencies on the alternating and mean loads, specifically ΔK and K_{max}, the alternating and maximum stress intensities, respectively, are also quite different (Fig. 1). In metals the dominant dependence of ΔK is a consequence of the intrinsic crack-advance mechanism; the smaller K_{max} dependence results primarily from its effect of the crack-opening displacement, which in turn controls the degree of crack wedging due to crack closure in the wake. Thus, for ductile metals, in a modified Paris law, where $da/dN \propto (\Delta K)^p (K_{max})^n$, $n \ll p$. In ceramics, conversely, growth rates are principally a function of K_{max}, since the crack-advance mechanism is identical to that under static loading; the much weaker ΔK dependence here arises from the cyclic-induced degradation in shielding in the wake. Thus, for ceramics, $p \ll n$. In intermetallics, fatigue properties are intermediate between these two extremes, such that generally $p \sim n$. However, in brittle intermetallics such as $MoSi_2$, where there is no intrinsic cycle-dependent crack advance mechanism, $p > n$, whereas in more ductile materials, such as the $(\gamma+\alpha_2)$ TiAl alloys, intrinsic fatigue damage mechanisms, similar to those in metals, clearly exist, and $p < n$.

Such differing dependencies on ΔK and K_{max} also have a marked influence on how the load ratio affects growth rates. In metals where the ΔK term is dominant, characterizing growth rates in terms of ΔK invariably normalizes the load-ratio dependence (at least in the mid-range of growth rates). In ceramics, conversely, this normalization is achieved by characterizing growth rates as a function of K_{max} as this is the dominant term, whereas in intermetallics, the load ratio dependence cannot be normalized by either ΔK or K_{max} [10-13]. Although both intermetallics and ceramics are susceptible to fatigue-crack growth from degradation of shielding under cyclic loads, there are significant differences. At ambient temperatures, there is no intrinsic fatigue damage mechanism in ceramics - the crack tip advances by an identical mechanism under monotonic and cyclic loads; at a given stress intensity, fatigue cracks simply grow faster due to the cyclic suppression in shielding behind the crack tip. Accordingly, the value of maximum stress intensity at the fatigue threshold, $K_{max,TH}$, is comparable with the crack-initiation toughness, K_o, at the start of the R-curve ($K_{max,TH} \sim K_o$). In many intermetallics, conversely, fatigue-crack growth is seen at stress-intensity levels below the crack-initiation toughness, specifically $K_{max,TH} \sim 0.25\text{-}0.4\ K_o$, implying there are additional *intrinsic* microstructural damage mechanisms associated with fatigue failure; however, this effect is more restricted than in metals, where generally $K_{max,TH} \leq 0.1\ K_o$, due to the limited crack-tip plasticity and consequently lower toughness of intermetallic alloys.

SUMMARY AND CONCLUSIONS

Major progress has been made over the last decade in significantly improving the fracture resistance of low-ductility materials such as intermetallics using the extrinsic shielding approach to toughening. This has included the design of microstructures which develop zones of inelasticity, microcracking or most predominantly bridging (by grains, particulate, fibers or layers) that surround the crack. However, it is now evident that cyclic fatigue loading can severely degrade such toughening; in fact, this provides the critical mechanism promoting fatigue-crack growth, even in materials such as $MoSi_2$ that display no intrinsic mechanism of cyclic crack advance.

Although the mechanisms of cyclic fatigue in brittle materials are conceptually different from the well known mechanisms of metal fatigue, the central thesis of this work has been that by considering the relative importance of the prevailing intrinsic damage and extrinsic shielding mechanisms, a commonality of behavior can be found for the cyclic fatigue of both ductile and brittle materials. However, as noted above, the respective contributions of each mechanism does result in marked differences in the ΔK and K_{max} dependence of growth rates, the load ratio effect and the relationship of the fatigue threshold to the toughness properties; these are summarized in Table I.

Table I: Fatigue-Crack Growth Properties of Ductile and Brittle Materials

	$da/dN \propto (K_{max})^n(\Delta K)^p$	relationship of $K_{max,TH}$ to K_o*
Metals	$p >> n$	$K_{max,TH} \leq 0.1\ K_o$
Intermetallics	$p \sim n$	$K_{max,TH} \sim 0.25\text{-}0.4\ K_o$
Ceramics	$p << n$	$K_{max,TH} \sim K_o$

* $K_{max,TH}$ and K_o are, respectively, the fatigue threshold and the crack-initiation toughness on the R-curve.

Finally, the marked sensitivity of growth rates to the applied stress intensity in intermetallics implies that projected lifetimes will be a very strong function of stress and crack size; this makes design and life prediction using damage-tolerant methodologies more complex. Accordingly, design approaches based on the definition of a critical level of damage for the *onset* of fatigue cracking must be contemplated, involving either an S-N fatigue limit or crack-propagation threshold, although even these approaches may not be conservative due to the sub-threshold extension of small cracks. Clearly, this is an area that mandates increased attention in the future if these materials are to find structural use.

REFERENCES

1. G. F. Harrison and M. R. Winstone, in *Mechanical Behaviour of Materials at High Temperatures*, C. Moura Branco, R. O. Ritchie and V. Sklenicka, eds., Kluwer Academic, Dordrecht, The Netherlands (1996) 309-325.
2. R. O. Ritchie, *Mater. Sci. Eng.*, **A103** (1988) 15-28.
3. R. O. Ritchie and R. H. Dauskardt, *J. Ceram. Soc. Japan*, **99** (1991) 1047-1062.
4. A. G. Evans, *J. Am. Ceram. Soc.*, **73** (1990) 187-206.
5. C. T. Liu, A. I. Taub, N. S. Stoloff, and C. C. Koch, eds., *High-Temperature Ordered Intermetallic Alloys III*, MRS Symp. Vol. 133, MRS, Pittsburgh (1989).

6. D. P. Pope, C. T. Liu, and S. H. Whang, eds., *High Temperature Intermetallics - Parts 1 & 2*, Elsevier, Lausanne, Switzerland (1995).
7. W. O. Soboyejo, T. S. Srivatsan, and R. O. Ritchie, eds., *Fatigue and Fracture of Ordered Intermetallic Materials II*, TMS, Warrendale (1995).
8. D. R. Bloyer, K. T. Venkateswara Rao, and R. O. Ritchie, *Mater. Sci. Eng.*, **A216** (1996) 80-90.
9. K. T. Venkateswara Rao, W. O. Soboyejo, and R. O. Ritchie, *Metall. Trans. A*, **23A** (1992) 2249-2257.
10. K. Badrinarayanan, A. L. McKelvey, K. T. Venkateswara Rao, and R. O. Ritchie, *Metall. Mater. Trans. A*, **27A** (1996) 3781-3792.
11. K. T. Venkateswara Rao, G. R. Odette, and R.O. Ritchie, *Acta. Metall. Mater.*, **42** (1994) 893-911.
12. J. P. Campbell, K. T. Venkateswara Rao, and R. O. Ritchie, *Metall. Mater. Trans. A*, **30A** (1999) March issue.
13. D. R. Bloyer, K. T. Venkateswara Rao, and R. O. Ritchie, *Metall. Mater. Trans. A*, **30A** (1999) March issue.

ACKNOWLEDGMENTS

This work was supported by the Air Force Office of Scientific Research under Grant No. F49620-96-1-0223. Thanks are due to my research group, in particular Drs. K. T. Venkateswara Rao and D. R. Bloyer, and J. P. Campbell, J. J. Kruzic and A. L. McKelvey, whose research forms the major basis for this manuscript.

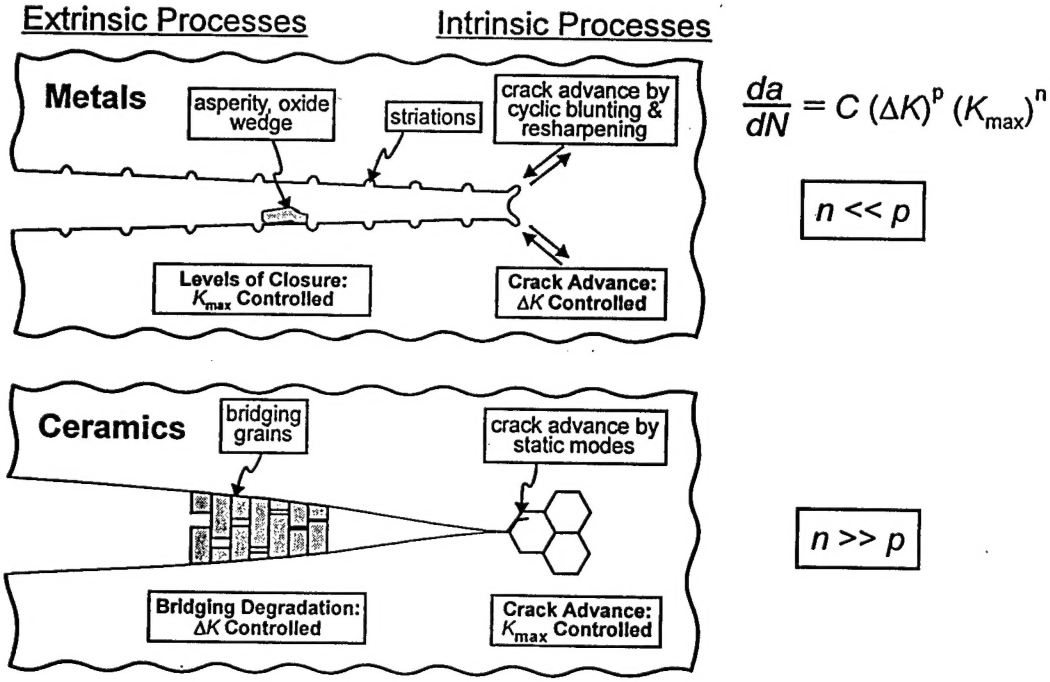

Figure 1: Schematic illustration of the intrinsic damage and extrinsic shielding mechanism involved in the cyclic fatigue-crack growth in (a) ductile and (b) brittle materials, showing the relative dependencies of the growth rates, *da/dN*, on the alternating, ΔK, and maximum, K_{max}, stress intensities.